Miniaturisation of Conductivity Probe Design and Acquisition of Dielectric Properties of Tissues for Catheter Cardiac Ablation Applications

OLLSCOIL NA GAILLIMHE
UNIVERSITY OF GALWAY

Niko Ištuk

Translational Medical Device Lab

College of Science and Engineering

Electrical and Electronic Engineering

University *of* Galway

Submitted to the University *of* Galway for the degree of

PhilosophiæDoctor (PhD)

Supervised by Prof. Martin O'Halloran

Co-supervised by Dr. Emily Porter and Dr. Eoghan Dunne

2023

Contents

Declaration

I, the Candidate Niko Ištuk, certify that this thesis entitled "Miniaturisation of Conductivity Probe Design and Acquisition of Dielectric Properties of Tissues for Catheter Cardiac Ablation Applications":

- ➢ is all my own work;
- ➢ has not been previously submitted for any degree or qualification at this University or any other institution;
- ➢ and where any work in this thesis was conducted in collaboration, appropriate reference to published work by my collaborators has been made and the nature and extent of my contribution has been clearly stated.

The thesis work was conducted from 2018 to 2023 under the supervision of Prof. Martin O'Halloran at the University of Galway.

Galway, 2023

Signature: 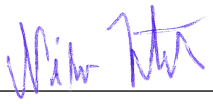

Niko Ištuk

Abstract

Atrial fibrillation, a prevalent cardiac arrhythmia, requires precise and effective treatments such as cardiac ablation. The efficacy of these treatments is closely tied to a comprehensive understanding of the dielectric properties of the heart, including both blood and cardiac tissue. Any inaccuracies or gaps in this information can compromise treatment success, leading to increased health risks and financial burdens.

This thesis identifies several gaps including limited available data on the dielectric properties of specific heart regions, inconsistency in characterising the electrical conductivity of human blood across various frequencies, and the lack of specialised instruments for accurate measurements in small, heterogeneous biological samples. To address these issues, rigorous characterisations of the dielectric properties of cardiac tissues at microwave frequencies ranging from 500 MHz to 20 GHz were performed, along with electrical conductivity measurements of human blood from 100 Hz to 100 kHz.

As well as the contributions to dielectric properties, this research also includes the development and microfabrication of a miniaturised four-electrode probe. This innovative probe is designed to measure the electrical conductivity of biological tissues over a wider frequency range between 10 Hz and 100 kHz and enables accurate measurements in small and heterogeneous samples, such as cardiac tissue.

Overall, the thesis advances the field by enhancing the understanding of the dielectric properties of blood and cardiac tissue. By filling critical gaps in the existing literature, it contributes to improving the reliability and safety of cardiac ablation treatments.

Acknowledgements

I would like to thank Martin for the opportunity and support throughout the years. Your mentorship has been invaluable, and I am deeply grateful for the trust and confidence you have placed in me. A special acknowledgement to Emily, who provided essential support during the initial, most trying days of this endeavour and prepared me for the challenges that lay ahead. I would also like to thank Adnan and Eoghan, who gave me the support and feedback I needed during the thesis writing. Your insights have been invaluable, and I am grateful for your time and effort.

I would like to extend my sincere gratitude to the members of the Graduate Research Committee—Dr. Maeve Duffy, Dr. Peter Corcoran, Dr. Atif Shahzad, and Prof. Martin Glavin—for their invaluable guidance and support throughout the course of this research.

Finally, from the lab, I would like to extend my gratitude to Alessandra, Anna, Laura, Nadia, Camille, Adam, Declan, Barry, Hamza, Nuno, Marcin, Chris, Prateek, and Bilal. Your collective knowledge, camaraderie, and support have made the lab a second home and have greatly contributed to the success of this research project.

Additionally, I would like to extend my deepest gratitude to all the Emerald supervisors and fellows. Your dedication to creating a culture of excellence, innovation, and collaboration has not gone unnoticed. Thank you for making such an enriching and supportive environment possible.

Posvećeno mojoj obitelji, sigurnom utočištu koje mi daje hrabrost da se penjem sve više i više, znajući da najdalje što mogu pasti je u njihov zagrljaj.

List of Figures

LIST OF FIGURES

LIST OF FIGURES

LIST OF FIGURES

List of Tables

LIST OF TABLES

Abbreviations

AC	Alternating Current
AF	Atrial Fibrillation
AV	Atrioventricular
CC	Current Carrying
CE	Counter Electrode
DC	Direct Current
DIW	Deionised Water
EDTA	Ethylenediaminetetraacetic Acid
EIS	Electrical Impedance Spectroscopy
EM	Electromagnetic
IRE	Irreversible Electroporation
LA	Left Atrium
LAA	Left Atrial Appendage
LV	Left Ventricle
MCH	Mean Corpuscular Haemoglobin
MCHC	Mean Corpuscular Haemoglobin Concentration
MCV	Mean Corpuscular Volume
MINDER	Minimum Information for Dielectric Measurements of Biological Tissues
MW	Microwave
PA	Pulmonary Artery
PAF	Paroxysmal Atrial Fibrillation
PEDOT:PSS	poly(3,4-ethylenedioxythiophene) polystyrene sulfonate
PF	Pulsed Field
PU	Pick Up
PV	Pulmonary Vein
PVI	Pulmonary Vein Isolation
RA	Right Atrium
RAA	Right Atrial Appendage
RBC	Red Blood Cell Count
RF	Radiofrequency
RMS	Root Mean Square
RV	Right Ventricle
SA	Sinoatrial
SD	Standard Deviation
SMA	SubMiniature Version A
VNA	Vector Network Analyzers
WCC	White Cell Count
WE	Working Electrode
ZIF	Zero Insertion Force

1

Introduction

1.1 Motivation

The interaction of electromagnetic (EM) fields with the human body is dependent on the inherent dielectric properties of tissues, namely relative permittivity and conductivity [1]. These properties dictate how EM waves are transmitted, absorbed, and reflected by biological tissues in various proportions. A precise understanding of these properties is crucial for dosimetry (safety) calculations and advancing medical diagnostic, monitoring, and therapeutic technologies [2].

Various modalities of cardiac ablation for atrial fibrillation (AF) treatment focus on ablating the cardiac tissue by delivering EM energy into the tissue. To accurately quantify the EM energy being deposited into the tissue, an exact knowledge of the dielectric properties of the cardiac tissue is necessary. This knowledge is utilised in the design and optimisation of cardiac ablation treatment and monitoring devices.

Moreover, the dielectric properties of cardiac tissues, specifically the change in the conductivity of cardiac tissue, can potentially be employed to assess the ablation treatment [3]. Currently, there is no modality to monitor the ablation treatment in real-time, which makes the effectiveness of the treatment heavily dependent on the clinician's experience [4]. While the direction of change in conductivity depends on the ablation modality employed, the conductivity does change during all modalities, meaning conductivity can potentially be a marker for successful ablation. Measuring these changes in the electrical conductivity of

tissues during the ablation treatments could provide a means of monitoring and assessing the ablation treatment in real-time, potentially improving the effectiveness of the treatment and ultimately patient outcome.

This thesis contributes to the field of dielectric properties of tissues relevant for treatment planning and treatment monitoring of different modalities of cardiac ablation. The contributions to treatment planning include the characterisation of cardiac tissue dielectric properties at microwave frequencies and the characterisation of human blood conductivity at frequencies lower than 100 kHz. Contributions to ablation treatment monitoring involve the development of a miniaturised four-electrode probe for the assessment of the conductivity of biological tissue. These contributions are discussed in more detail in the following section.

1.2 Thesis Contributions

This thesis presents several novel and significant contributions in the fields of dielectric properties of tissues, dielectric spectroscopy, and electrical impedance spectroscopy (EIS). The contributions are:

- Recording, reporting, and modelling of the dielectric properties of the heart as a dielectrically heterogeneous organ at the important microwave application frequencies of 915 MHz and 2.45 GHz;
- The design of a simple and low-cost four-electrode probe as a practical tool for measuring the electrical conductivity of human blood in the 100 Hz–100 kHz frequency range.
- The measurement of the conductivity of human whole blood at room temperature and at body temperature over the frequency range of 100 Hz–100 kHz.
- The design and microfabrication of a miniaturised four-electrode probe (900 µm in width) for the measurement of electrical conductivity of small biological samples in the wider 10 Hz–100 kHz frequency range.

1.2.1 Journal and Conference Publications

The work presented in this thesis has been published across a range of peer-reviewed journals and international conference papers. These publications are summarised here for completeness.

Dielectric properties of cardiac tissue:

- **N. Ištuk**, E. Porter, D. O'Loughlin, B. McDermott, A. Santorelli, S. Abedi, N. Joachimowicz, H. Roussel, and M. O'Halloran, "Dielectric Properties of Ovine Heart at Microwave Frequencies," Diagnostics, vol. 11, no. 3, Art. no. 3, Mar. 2021, doi: 10.3390/diagnostics11030531.

- **N. Ištuk** et al., "Detailed Dielectric Characterisation of the Heart and Great Vessels," in 2020 14th European Conference on Antennas and Propagation (EuCAP), Mar. 2020, pp. 1–5. doi: 10.23919/EuCAP48036.2020.9135896.

- **N. Ištuk**, E. Porter, D. O'Loughlin, and M. O'Halloran, "Dielectric Properties Model of the Left Atrium and Left Atrial Appendage for Applications in Cardiac Ablation," in 2021 International Conference on Electromagnetics in Advanced Applications (ICEAA), Aug. 2021, pp. 154–154. doi: 10.1109/ICEAA52647.2021.9539744.

Electrical conductivity of human blood:

- **N. Ištuk**, A. L. Gioia, H. Benchakroun, A. Lowery, B. McDermott, and M. O'Halloran, "Relationship Between the Conductivity of Human Blood and Blood Counts," IEEE J. Electromagn. RF Microw. Med. Biol., pp. 1–7, 2021, doi: 10.1109/JERM.2021.3130788.

- **N. Ištuk**, A. L. Gioia, H. Benchakroun, A. Lowery, E. Porter, and M. O'Halloran, "Measurement of Electrical Conductivity of Human Blood at Frequencies Below 100 kHz with Four-electrode Probe Method," in 2021 XXXIVth General Assembly and Scientific Symposium of the International Union of Radio Science (URSI GASS), Aug. 2021, pp. 1–4. doi: 10.23919/URSIGASS51995.2021.9560424.

Miniaturised four-electrode probe for tissue electrical conductivity measurements:

- **N. Ištuk**, H. Benchakroun, A. Elahi, M. O'Halloran, R. Matta, D. Moreau, R. O'Connor, and E. Dunne, "Reducing Sensing Volume Confounding Effects in Conductivity Measurements: The Use of a Miniaturised Four-Electrode Probe," in ICECOM 2023, Dubrovnik, Croatia: IEEE, Sep. 2023, p. 4.

- **N. Ištuk**, R. Matta, H. Benchakroun, J.M. Baena-Montes, L. Quinlan, D. Moreau, R. O'Connor, E. Dunne, A. M. Elahi, M. O'Halloran, "Miniaturised Four-Electrode Conductivity Probe with PEDOT:PSS Coating," in URSI GASS 2023, Sapporo, Japan: URSI GASS 2023, Aug. 2023.

- **N. Ištuk**, C. DeCaro, H. Benchakroun, E. Dunne, A. Elahi, and M. O'Halloran, "Eliminating the Geometric Error in Tissue Conductivity Measurements by Increasing the Sample Size," in BioEM2022, Nagoya, Japan, Jun. 2022, p. 3.

- H. Benchakroun, D. O'Loughlin, **N. Ištuk**, M. O'Halloran, and A. L. Gioia, "Evaluation of the Feasibility of Three Custom-made Tetrapolar Probes for Electrical Characterization of Cardiac Tissue," in 2021 15th European Conference on Antennas and Propagation (EuCAP), Mar. 2021, pp. 1–5. doi: 10.23919/EuCAP51087.2021.9410978.

Other related research contributions:

- **N. Ištuk**, F. Kienberger, E. Porter, M. O'Halloran, A. Santorelli, I. Alić, M. Ragulskis, A. Moradpour, and M. Kasper, "Fast Measurements of Dielectric Properties with Small Size Microwave Transceiver," in 2020 14th European Conference on Antennas and Propagation (EuCAP), Mar. 2020, pp. 1–5. doi: 10.23919/EuCAP48036.2020.9135361.

- **N. Ištuk**, H. Benchakroun, E. Dunne, and M. O'Halloran, "Pressure Dependency of Conductivity Measurements: The Specific Case of the Lung,"

in 21st International Conference on Biomedical Applications of Electrical Impedance Tomography (EIT 2021), Jun. 2021. doi: 10.5281/zenodo.5113377.

- **N. Ištuk**, A. Bottiglieri, E. Porter, M. O'Halloran, and L. Farina, "Changes in the Dielectric Properties of ex-vivo Ovine Kidney Before and After Microwave Thermal Ablation," in 2020 XXXIIIrd General Assembly and Scientific Symposium of the International Union of Radio Science, Rome, Italy, Aug. 2020, pp. 1–4. doi: 10.23919/URSIGASS49373.2020.9232147.

- A. La Gioia, A. Elahi, A. Bottiglieri, **N. Ištuk**, C. Dowling, F. D'Arcy, M. O'Halloran, and E. Porter, "Early-stage Dielectric Characterisation of Renal Cell Carcinoma for Positive Surgical Margin Detection," in 2019 13th European Conference on Antennas and Propagation (EuCAP), Mar. 2019, pp. 1–5.

- M. Savazzi, S. Abedi, **N. Ištuk**, N. Joachimowicz, H. Roussel, E. Porter, M. O'Halloran, J. R. Costa, C. A. Fernandes, J. M. Felicio, and R. C. Conceição, "Development of an Anthropomorphic Phantom of the Axillary Region for Microwave Imaging Assessment," Sensors, vol. 20, no. 17, p. 4968, Sep. 2020, doi: 10.3390/s20174968.

1.3 Aims and Objectives

The primary aim of this dissertation is to characterise the dielectric properties of tissues relevant to different modalities of cardiac ablation for AF. The relevant tissues examined in this dissertation include cardiac tissues, where the heart is considered a heterogeneous organ, and blood, which is regarded as homogeneous. The dielectric properties of the tissues were characterised at microwave frequencies (i.e., 500 MHz to 20 GHz) for cardiac tissue and at frequencies from 100 Hz to 100 kHz for blood. These frequency ranges were chosen to correspond to different modalities of cardiac ablation such as microwave (MW) ablation, radiofrequency (RF) ablation, and pulsed-field (PF) ablation, and to address gaps in the understanding of the dielectric properties of cardiac tissues and blood.

This thesis presents its findings and addresses gaps in the literature in the following ways:

- In *Chapter 2*, the aim is to provide a comprehensive overview of the anatomy and physiology of the heart and to address the topic of dielectric properties and impedance measurement. The first part is focusing on the condition of AF. This includes a detailed examination of the electrophysiology of AF, various treatments for the condition, and the applications of dielectric properties in cardiac ablation for AF treatments. The second part aims to provide a clear understanding of the principles behind dielectric properties and impedance measurement, which are integral to the characterisation of tissues relevant to cardiac ablation.

- In *Chapter 3*, the aim is to characterise the dielectric properties of different regions of the heart at MW frequencies, ranging from 500 MHz to 20 GHz. This characterisation will contribute to an understanding of the heterogeneity of the heart in the context of cardiac ablation.

- In *Chapter 4*, the goal is to characterise the impedance properties of human blood relevant for applications in PF ablation. This characterisation covers frequencies from 100 Hz to 100 kHz, contributing to the understanding of the dielectric properties of blood and how these properties might affect this type of ablation therapy.

- In *Chapter 5*, the objective is to present the design and capabilities of a miniaturised four-electrode probe for the measurement of the conductivity of biological tissues. This tool serves as a crucial part of the overall goal to comprehensively characterise tissue properties for improved cardiac ablation strategies. Moreover, it introduces a practical instrument for real-time monitoring of ablation treatment, offering potential improvements in treatment effectiveness and ultimately patient outcomes.

- In *Chapter 6*, the focus is on summarising the key findings of the dissertation, reiterating its contributions to the field of cardiac ablation. This final chapter also discusses potential areas for future work, aiming to identify how

this thesis research can be built upon to further advance the understanding of tissue dielectric properties and improve therapeutic technologies for AF.

In summary, this dissertation seeks to comprehensively investigate the dielectric properties of cardiac tissues and blood, addressing current knowledge gaps and providing actionable insights for the enhancement of AF treatment planning and monitoring.

1.4 Thesis Outline

The remaining chapters of the thesis are:

Chapter 2 provides an overview of the anatomy and physiology of the heart, with a specific focus on AF. The electrophysiology of AF is also discussed, along with various treatments available for the condition. The applications of dielectric properties in cardiac ablation for AF treatments are also examined in this chapter. This chapter also contains a comprehensive review of the dielectric properties and impedance measurement. This chapter explains the theoretical concepts and measurement techniques related to dielectric properties and impedance.

Chapter 3 presents the dielectric characterisation of cardiac tissue, considering the heart as a heterogeneous organ. The dielectric properties of different parts of the heart are characterised at MW frequencies, highlighting their differences and their relevance to cardiac ablation strategies.

Chapter 4 describes the impedance characterisation of human blood, focusing on its applications in pulsed field (PF) ablation. The conductivity of the blood is analysed in the context of frequencies relevant to PF ablation, providing crucial insights for the development of effective ablation techniques.

Chapter 5 presents the design and fabrication of a miniaturised four-electrode probe for the measurement of the conductivity of biological tissues. It demonstrates the potential of this tool for characterising tissue properties and its potential use for real-time monitoring during ablation treatments.

Chapter 6 draws conclusions from the presented studies and evaluates the implications of these findings for the field of cardiac ablation treatments. This

chapter also proposes potential for future work, based on the findings from this dissertation.

2

Background

2.1 Introduction

The topic of dielectric properties for cardiac ablation for the treatment of AF presents significant challenges and complexities. This chapter will provide a context for the research questions addressed in this thesis, focusing specifically on the dielectric properties of blood and cardiac tissue.

This chapter is divided into two distinct parts. The first part of this chapter (*Sections 2.2– 2.3*) provides a background of the anatomy and physiology of the heart, with a focus on AF. This part also discusses the electrophysiology of AF and various treatments for the condition. The second part of the chapter (*Section 2.4*) provides a comprehensive overview of dielectric properties of blood and cardiac tissue, including the theoretical background, the measurement techniques, and the applications in the context of AF ablation.

2.2 Anatomy and Physiology of the Heart

2.2.1 The Heart Anatomy and Regular Cardiac Cycle

The heart is a hollow, muscular organ and is at the centre of the circulatory system. The heart acts as a dual muscular pump. Each "pump" takes blood from low-pressure veins and propels the blood into high-pressure arteries. One pump

supports the systemic circulation throughout the body, and the other manages the circulation to and from the lungs [5].

On the right side of the heart (Fig. 2.1b), carbon dioxide-rich blood from the vena cava enters the right atrium before being pumped out from the right ventricle to the lungs through the pulmonary artery [6]. Oxygen-rich blood from the lungs returns through the pulmonary vein to the left atrium (Fig. 2.1c), before being pumped out from the left ventricle to the entire body via the aorta. Valves in the heart allow blood to flow in one direction only and help maintain the pressure required to pump the blood [5].

From a histological perspective, the parts of the heart are arranged to fit a certain function. The endocardium is the inner lining of the heart, continuous with the endothelium of blood vessels [7]. Inside this layer is the cardiac muscle layer called the myocardium, which is thicker on the left side due to the need for greater force in pumping blood to the entire body as opposed to the right side that serves the lungs [6]. On the exterior surface of the heart is the epicardium, a serous membrane. Finally, a layer of fibrocartilage separates the atria and ventricles supporting the heart valves and forming openings between the chambers [7].

The blood is being pumped through the heart by the contractions that are caused by electrical signals from the nervous system. The heart has a special electrical system called the cardiac conduction system. This system controls the rate and rhythm of the heartbeat.

With each normal heartbeat, an electrical signal travels from the top of the heart to the bottom. As the signal travels, it causes the heart to contract and pump blood. The heartbeat process includes the following steps (Fig. 2.2):

- ➢ The signal begins in a group of cells, called pacemaker cells, located in the sinoatrial (SA) node in the right atrium [9]. The SA node generates the signal through the process of automaticity, which is the property of cardiac tissue to generate spontaneous action potentials [10].

- ➢ The electrical signal travels through the atria, depolarising the tissue and causing it to pump blood into the ventricles [9].

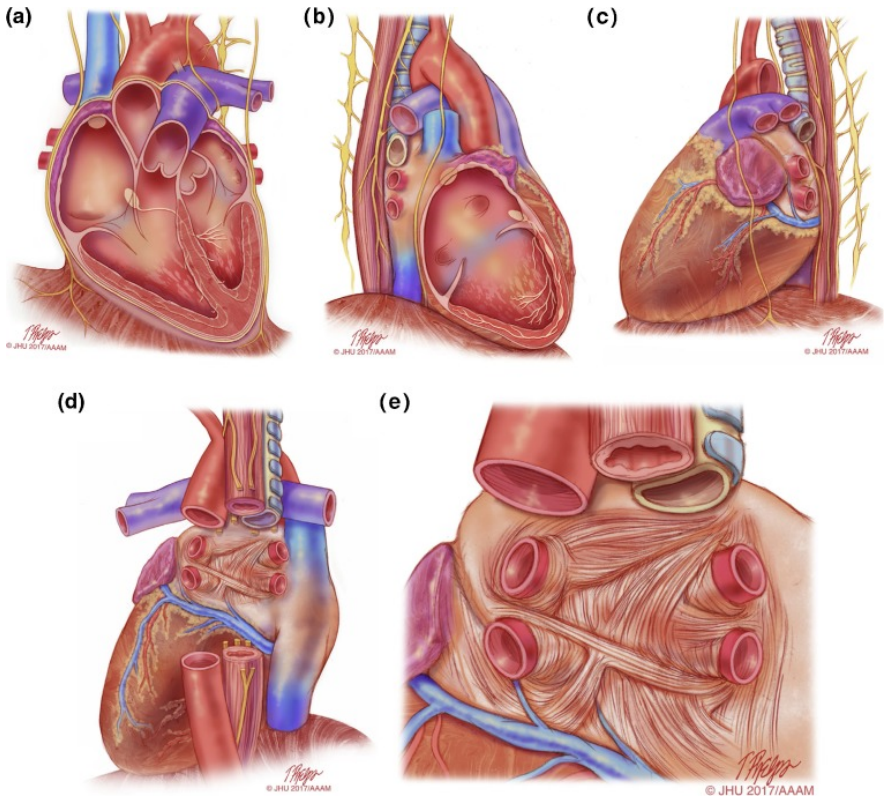

Figure 2.1: Anatomical drawings of the heart relevant to AF ablation. This series of drawings shows the heart and associated relevant structures from four different perspectives relevant to AF ablation. This drawing includes the phrenic nerves and the esophagus. a) The heart viewed from the anterior perspective. b) The heart viewed from the right lateral perspective. c) The heart viewed from the left lateral perspective. d) The heart viewed from the posterior perspective. e) The left atrium viewed from the posterior perspective. Illustration: Tim Phelps © 2017 Johns Hopkins University, AAM, reproduced with permission from [8].

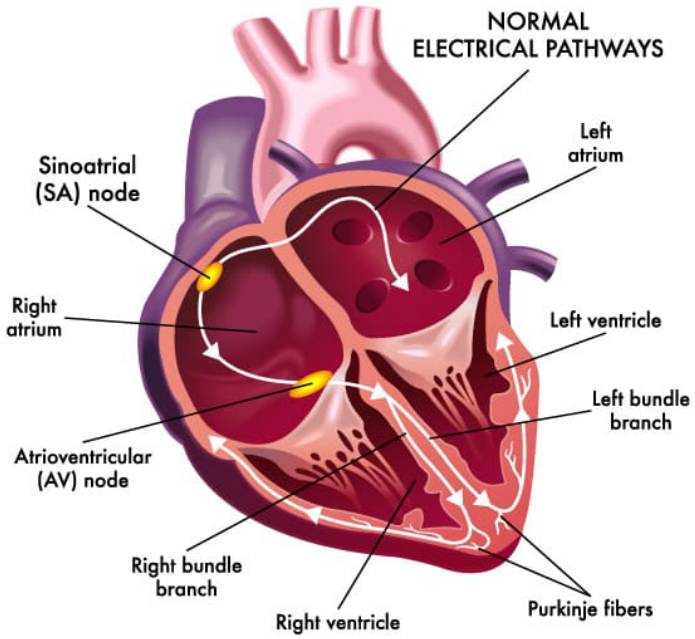

Figure 2.2: The conduction system of the heart. Normal excitation originates in the sinoatrial (SA) node and then propagates through both atria. The atrial depolarisation spreads to the atrioventricular (AV) node, passes through the bundle of His (not labelled), and then to the Purkinje fibres, which make up the left and right bundle branches; subsequently, all ventricular muscle becomes activated [9]. Illustration: Vejthani Hospital ©, reproduced under Creative Commons Attribution 3.0 License.

- ➢ The electrical signal then moves down to a group of pacemaker cells called the atrioventricular (AV) node, located at the floor of the right atrium, between the atria and the ventricles [9]. Here the signal is delayed, allowing the ventricles time to finish filling with blood [11].
- ➢ Following the AV node excitation, the depolarisation proceeds through to the bundle of His [9], which is the physical link that electrically bridges the atria and ventricles of the heart [12].
- ➢ After leaving the bundle of His, the depolarisation spreads to both the left and the right bundle branches [9]. These pathways carry depolarisation to the left and right ventricles, respectively [9].
- ➢ The signal then travels through the remainder of the Purkinje fibres, which are specialised cardiac muscle cells that conduct electrical impulses that allow coordinated contraction of cardiac muscle [13], and ventricular myocardial depolarisation spreads [9], causing the ventricles to contract and pump blood out of the heart [11].
- ➢ The ventricles relax, and the heartbeat process starts all over again in the SA node.

This entire process, called the cardiac cycle, relies on coordinated electrical signals. Each of these steps happens in a single normal heartbeat, with this entire cycle normally happening 60–100 times per minute [14].

A heart arrhythmia is an irregular heartbeat [10, 15]. Heart arrhythmias occur when the electrical signals that coordinate the heartbeat do not work properly [10, 15]. Atrial fibrillation is the most common type of arrhythmia [16]and is discussed in detail in the next section.

2.3 Atrial Fibrillation: What is it? Prevalence, How Does it Occur? And What are the Current Treatment Options?

Atrial fibrillation is a clinically prevalent cardiac arrhythmia characterised by rapid and irregular contractions of the atria (Fig. 2.3). The resulting effect is inadequate blood flow from the atria to the ventricles [17, 18]. Potential complications caused by AF include stroke and heart failure [16, 19, 20]. Despite the high incidence, accounting for approximately one-third of hospitalisations related to cardiac rhythm disturbances [21], the optimal management strategy for AF remains uncertain [16, 22–25].

Atrial fibrillation has a number of sub-classifications. By temporal classification, AF can be classified as follows: If the event is the first instance of the arrhythmia being ever detected, or if the event is a recurrence of a previously recognised arrhythmia, the event is considered an incident episode [26]. Depending on the outcome, this episode may be further classified [26]. If the arrhythmia self-terminates, the AF is termed paroxysmal [26]. If the arrhythmia continues until medical intervention, the AF is described as persistent [26]. If the arrhythmia lasts for more than a year or resists medical interventions, the AF is designated as longstanding persistent [8]. Finally, if a decision is made not to pursue further action to restore or maintain sinus rhythm, AF is designated as permanent [27].

The mechanisms underlying AF are thought to involve enhanced automaticity (the property of cardiac cells to generate spontaneous action potentials) [10, 28, 29] and self-sustaining re-entrant propagation, where the action potential propagates in a circus-like closed loop manner [30, 31]. Multiple risk factors have been identified for AF, including advanced age, male sex, European ancestry, sedentary lifestyle, smoking, obesity, diabetes, obstructive sleep apnea, elevated blood pressure [32], hypertension, valvular heart disease, and congestive heart failure [33]. Additionally, there is a feed-forward loop between AF and heart failure and myocardial infarction [32].

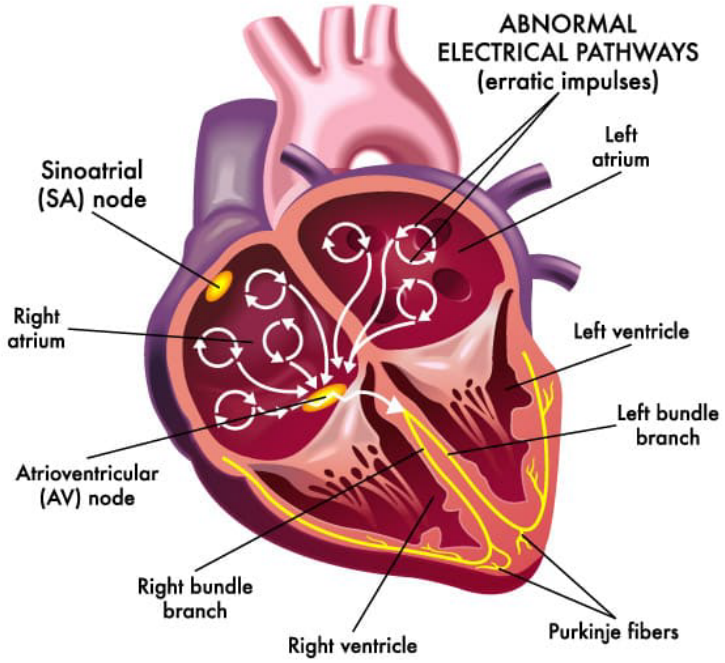

Figure 2.3: Atrial fibrillation is characterised by rapid and irregular contractions of the atria. Illustration: Vejthani Hospital ©, reproduced under Creative Commons Attribution 3.0 License.

2.3.1 Epidemiology

Atrial fibrillation is the most common clinically significant cardiac arrhythmia [16]. In Australia, Europe, and the USA, the current estimated prevalence of AF ranges between 1–4% [31]. A systematic review by Chugh et al. (2014) [34] estimated the global number of individuals with AF in 2010 to be 33.5 million [35], with an age-adjusted prevalence rate of 569.5 per 100000 population for men and 359.9 per 100000 population for women in 1990 [35]. The prevalence of AF is projected to increase drastically in Europe, with an estimated 2.3-fold increase by 2060 [36, 37]. In the UK, projections from the Clinical Practice Research Database suggest that AF will affect between 1.3 and 1.8 million people by 2060 [38]. In the USA, the number of individuals affected by AF is expected to increase to greater than 8 million by 2050 [39].

The age-specific prevalence is higher in men than in women. However, in the older age groups, there is no gender difference. This finding was presented in the Cardiovascular Health Study [40, 41]: the prevalence in the age group 65–69 years was 5.8% and 2.8% in men and women, respectively; and in the age group 70–79 years, the prevalence was almost equal in men and women: 5.9% and 5.8%, respectively [42]. Because of longer life expectancy in women, the absolute number of men and women with AF is about equal. In fact, after age 75 years, about 60% of the people with AF are women [43]. Therefore, although male gender is a risk factor for AF, from a public health perspective, it should not only be regarded as predominantly a male health problem [44]. Lifetime risks for the development of AF are 1 in 4 for men and women 40 years of age and older [45].

Having an understanding of the classification, risk factors, and epidemiology of AF, the following subsection presents an overview of the electrophysiology of AF, including the causes of atrial AF as well as the underlying mechanisms.

2.3.2 Electrophysiology

The mechanisms underlying AF are believed to involve enhanced automaticity and self-sustaining re-entrant propagation, as reported by various studies [28–31, 44]. Enhanced automaticity refers to the rapid depolarisation of aberrant

foci, leading to fibrillatory conduction in other parts of the atria [28, 29, 46]. Self-sustaining re-entrant propagation refers to the continuous circulation of waves of excitation around stationary or spatiotemporally varying circuits [30, 31, 47–49]. The involvement of the pulmonary veins, structural and histopathological changes in the atria, and nonuniform conduction and reentrant circuits have also been observed to play a role in the perpetuation of AF [31, 32, 50].

All theories proposed to explain AF are variations of the circus movement (a continuous repetitive propagation of an excitatory wave travelling in a circular path) and ectopic focus theories [31]. Moe et al. proposed that continuous propagation of multiple wavelets in the atria, which are considered to be offspring of atrial re-entry circuits, perpetuates AF without continuous focal discharge [31]. Allessie et al. [44] reported that there are two major underlying mechanisms of AF, namely random wavelet re-entry and leading circle re-entry. A study conducted by Haissaguerre et al. [29] in humans demonstrated that ectopic impulses originating from the pulmonary veins can initiate AF, which can be eliminated by catheter ablation of these ectopic foci. It is likely that most cases of AF in humans are caused by more than one mechanism [44].

J. Cox et al. [50] conducted a study on AF in animals and humans. They surgically created chronic mitral regurgitation in dogs, leading to enlarged atria and sustained AF. Activation maps of the atria revealed a spectrum of rhythm abnormalities, including atrial flutter and AF, caused by macroreentrant circuits. In human patients with paroxysmal AF, nonuniform conduction and bidirectional block were observed in both atria. While anatomic obstacles like the pulmonary veins and vena cavae may contribute to reentrant circuits, functional conduction block and inhomogeneities in the refractory period also play a role. These findings highlight the presence of multiple wave fronts and reentrant circuits during AF.

As this section has highlighted the complicated nature of AF, the following subsection discusses the various treatments available for atrial fibrillation, including EM energy-based ablation treatments: RF ablation, MW ablation, and PF ablation.

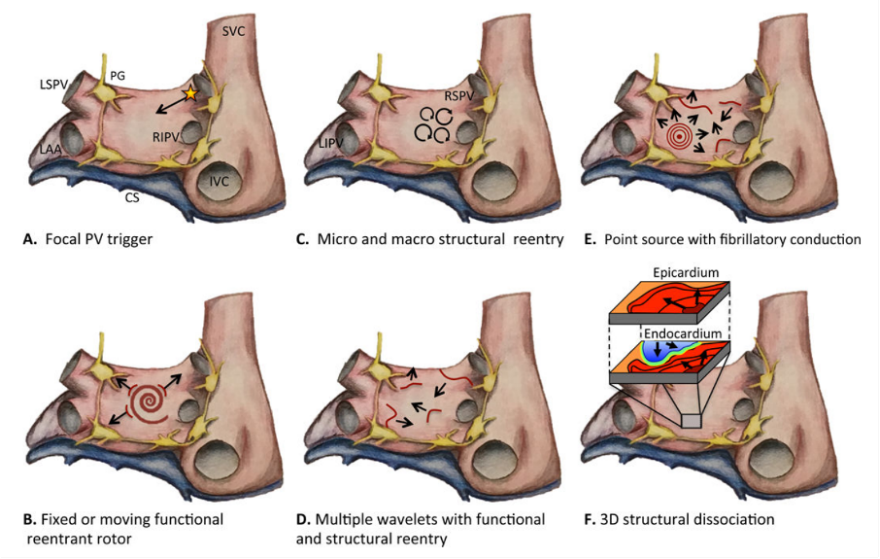

Figure 2.4: Proposed mechanisms of AF. (a) Focal trigger arising from muscle sleeve of PV propagating into the left atrium and initiating AF in the vulnerable substrate. (b) Fixed or moving spiral rotor, a result of functional re-entry, acts as a driver for AF. (c) Circus movement around anatomic structures or scars generates micro and macro re-entrant circuits. (d) Perpetual propagation of multiple simultaneous wavelets mediated by both functional and structural re-entry. (e) Point source with fibrillatory conduction acting as the driver for the persistence of AF. (f) Electrical dissociation between myocardial layers enables re-entry in a three-dimensional construct. [32]. Used with permission of Wolters Kluwer Health, Inc., from [32]; permission conveyed through Copyright Clearance Center, Inc.

2.3.3 Treatments

The management of patients with AF involves three main objectives: rate control, prevention of thromboembolism, and correction of the rhythm disturbance [27, 51]. These objectives are not mutually exclusive and often require a combination of approaches to achieve optimal outcomes [27, 51]. In this section, the various treatment options available for AF, including pharmacological and non-pharmacological interventions are discussed. The indications, benefits, and risks associated with each treatment option are reviewed to provide a brief overview of the management of AF, with a focus on EM energy-based ablation treatments.

2.3.3.1 Pharmacological and Nonpharmacological Treatments

Pharmacological treatment options for AF include cardioversion (use of electric shock to restore the heart rhythm [52]) and the use of antiarrhythmic drugs to maintain sinus rhythm, or the use of rate-controlling drugs, allowing AF to persist [22]. In both cases, anticoagulant therapy is recommended to prevent thromboembolism [22, 53–55]. Treatment with antiarrhythmic drugs and anticoagulation has been considered first-line therapy in patients with symptomatic AF [56, 57]. However, anticoagulation is suboptimal in many cases, and antiarrhythmic drugs are frequently ineffective and have serious potential adverse effects [22, 51, 57–59].

Surgical approaches to the treatment of AF are based on the hypothesis that reentrant activity is the primary mechanism underlying the development and maintenance of AF [60]. Studies by Cox et al. [61] suggest that the presence of macroreentrant circuits and the absence of either microreentrant circuits or evidence of atrial automaticity suggests that AF is amenable to surgical ablation. The proposed mechanism is that atrial incisions made at critical locations create barriers to conduction, thus preventing sustained AF. The procedure, known as the "maze" procedure, is based on the concept of creating a geographical maze within the atria and was developed to achieve this goal [62]. Despite the high success rate, the maze procedure has not been widely adopted, primarily due to the requirement of cardiopulmonary bypass [63–67]. In an effort to simplify and shorten the procedure, groups around the world have used various alternative

energy sources to create lesions with ablation to replace most of the incisions of the original cut and sew Cox "maze" procedure less invasive. At the present time, the interventional treatment of choice for patients with symptomatic and drug-refractory lone AF is catheter ablation, based principally on isolating the pulmonary veins [29, 63, 68–70]. Given that catheter ablation is considered a less invasive option compared to the surgical maze procedure, any surgical approach must now demonstrate favourable outcomes when compared with percutaneous catheter ablation to be considered a viable alternative for treating lone AF [63].

2.3.3.2 Catheter Ablation for Atrial Fibrillation

Since the initial description of triggers in the pulmonary veins that initiate paroxysmal AF, catheter ablation of AF has developed from a specialised and experimental procedure to a common treatment for preventing recurrent AF [8, 71–73]. Catheter ablation is an approach whereby a well-localised region of the endocardial tissue mediating the arrhythmias is destroyed via energy applied through a catheter [74]. The catheter is inserted into the heart through a vein [74]. Pulmonary vein isolation (PVI), requiring complete isolation for full effectiveness, along with additional ablation in the posterior left atrial wall (Fig. 2.5), primarily achieves the desired result [75].

The PVI has the greatest efficacy as a stand-alone procedure in patients with paroxysmal AF [77]. The techniques for PVI have undergone a profound evolution over the years, moving from focal PV ablation of AF triggers to empirical ostial isolation of the PVs and, more recently, to wide circumferential isolation of the PVs, which includes a large portion of the left atrial posterior wall, the so-called PV antrum [78].

PVI may be effective in curing AF, potentially eliminating the need for antiarrhythmic drugs and anticoagulation in many patients. However, due to the invasive nature of the procedure, AF ablation therapy carries potential risks. These risks include procedural stroke and pulmonary vein stenosis. As a result, in current clinical practice, AF ablation therapy is typically considered only after drugs have failed. [16, 51, 56, 57]. However, based on Wazni *et al.* 2005 study [56], PVI is a feasible first-line approach for the treatment of selected patients with

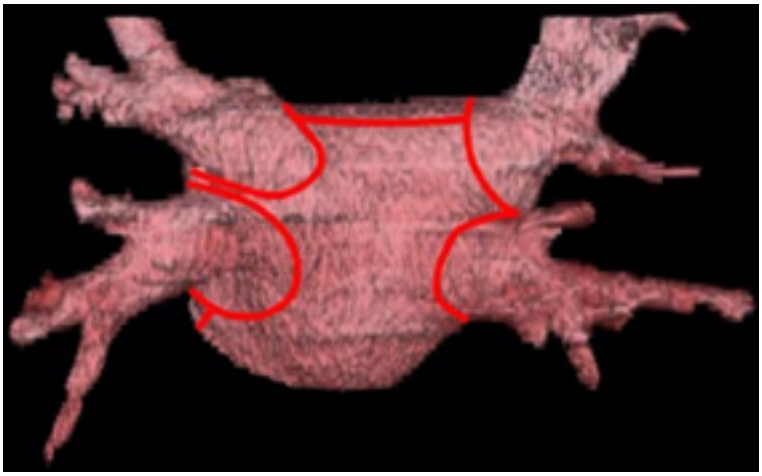

Figure 2.5: Location of linear lesions made during PVI. Posterosuperior three-dimensional computer tomography image of a segmented left atrium with the approximate location of linear lesions [76]. Used with permission of Springer Nature, reproduced from [76]; permission conveyed through Copyright Clearance Center, Inc.

symptomatic AF. Despite the effectiveness of PVI, AF still tends to reoccur after the procedure [79–82].

According to several studies [83–85], AF ablation, when performed in experienced centres by adequately trained teams, is more effective than antiarrhythmic drug therapy in maintaining sinus rhythm. Studies of RF ablation for the treatment of AF report higher efficacy rates and lower complication rates compared to studies of antiarrhythmic drug therapy [86]. Early RF catheter ablation techniques emulated the surgical maze procedure by introducing linear scars in the atrial endocardium [87]. However, while the success rate was approximately 40–50%, a relatively high complication rate diminished enthusiasm for this approach [28]. Despite the advances in catheter ablation, the long-term efficacy of catheter ablation to prevent recurrent AF is still a subject for further study.

Depending on the source of energy used, there are various modalities of catheter ablation [67]. These modalities include:

- RF Ablation is the most common type of cardiac ablation. RF energy is used to generate heat that targets and ablates the problematic heart tissue [8, 67, 88, 89].

- ➢ Cryoablation uses extremely cold temperatures to freeze the tissue, creating a scar that disrupts the abnormal electrical pathway [8].
- ➢ Laser Ablation is the technique that uses laser energy to create controlled scars in the heart tissue, effectively treating the abnormal pathways [8, 67].
- ➢ MW Ablation uses microwave energy to generate controlled heat that ablates the targeted tissue [67, 90].
- ➢ Ultrasound Ablation applies high-intensity focused ultrasound energy to the heart tissue to cause controlled thermal damage, interrupting the abnormal electrical signals [8, 67].
- ➢ PF Ablation, also known as Irreversible Electroporation (IRE) ablation. Though primarily used for cancer treatment, PF ablation has been investigated in cardiac ablation as well. PF ablation uses short, intense electrical pulses to create permanent defects in the cell membrane, leading to cell death without generating heat [91–94].

In some cases, combinations of the above energy modalities may be used to tailor the treatment to the specific condition and anatomy of the patient.

In this thesis, the focus is on improving EM energy-based treatment modalities, specifically RF ablation, MW ablation, and PF ablation. Detailed explanations of these modalities are provided in the subsequent subsections.

2.3.3.3 EM Energy-based Cardiac Ablation Modalities

Radiofrequency ablation is a technique where alternating electrical current with frequencies of 350 kHz to 1 MHz is delivered through electrode catheters to myocardial tissue creating a thermal lesion [88]. The use of RF energy for cardiac ablation was introduced in the late 1980s and rapidly gained supremacy in the field because of the ability to place a controlled lesion at any site within reach of a catheter tip with no risk of barotrauma and greatly reduced risk of collateral injury [95]. When the tip of the catheter is placed against cardiac tissue and an RF current is applied, a 3 to 5 mm circular area of localised cardiac necrosis is created within 10 to 30 seconds, mainly through the effect of local heating [96].

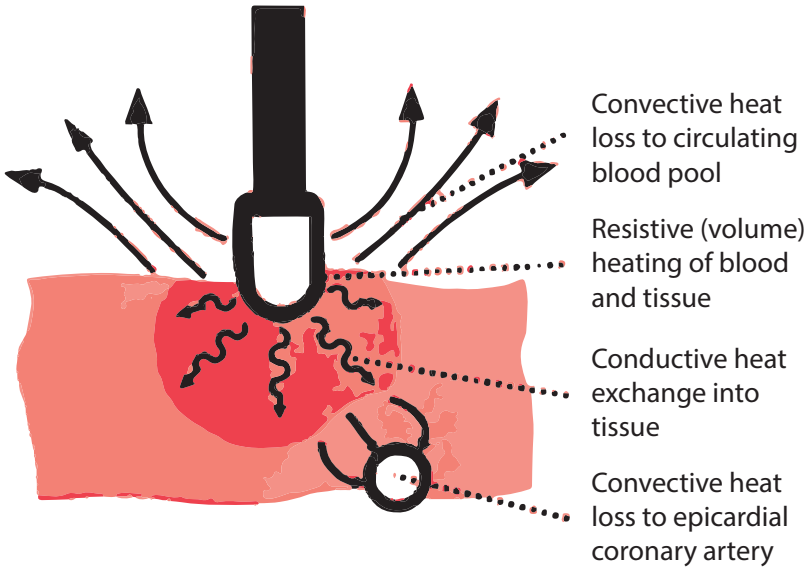

Figure 2.6: Schematic representation of RF catheter ablation. The drawing demonstrates the narrow rim of resistive (volume) heating and the much larger region of conductive heating. The diagram also illustrates the convective heat loss into the circulating blood pool and epicardial coronary arteries. Used with permission of John Wiley & Sons - Books, from [88]; permission conveyed through Copyright Clearance Center, Inc.

The mechanism by which RF current heats tissue is resistive heating of a narrow rim (< 1 mm) of tissue that is in direct contact with the ablation electrode [97]. Deeper tissue heating occurs as a result of passive heat conduction from this small region of volume heating. Lesion size is proportional to the temperature at the electrode-tissue interface and the size of the ablation electrode [97]. Temperatures above 50°C are required for irreversible myocardial injury, but temperatures above 100°C result in coagulum formation on the ablation electrode, a rapid rise in electrical impedance, and loss of effective tissue heating [97].

Lesion formation is also dependent on optimal electrode-tissue contact and duration of RF delivery. Contact force is a major determinant of lesion size and depth and, importantly, can predict procedure-related complications such as steam pop, perforation and thrombus formation[77].

Microwave ablation is an alternative modality in which microwave energy generates heat within the tissue by inducing oscillation of dielectric molecules such as water [67]. The kinetic energy produced in these molecules by the microwave EM field is imparted to the tissue as heat [90]. This form of heat production is known as dielectric heating [90]. The depth of the microwave lesions is dependent on the power, the duration of application, and the type of microwave antennae [90]. In MW ablation, the EM field is radiated by an antenna typically powered at 915 MHz or 2.45 GHz [98–101].

While it is often stated that microwave energy can create deeper lesions with uniform penetration and minimal surface heating [102], this warrants further explanation. In theory, higher frequencies such as those used in microwave ablation could be expected to have greater attenuation than RF energy, potentially leading to shallower penetration. However, the advantage of microwave energy lies in its ability to generate an electromagnetic field that propagates more effectively through desiccated tissue, allowing for the maintenance of energy delivery and deeper lesion formation without significant heating at the surface [102]. This results in tissue temperatures reaching above 50°C but staying below 100°C, thus minimizing the risk of tissue charring and thromboembolism [103, 104]. It is important to note that, while current MW ablation technology does not offer real-time tissue feedback like RF ablation [105], advancements in imaging and monitoring are expected to improve this aspect. Additionally, the concern regarding the focus of MW energy is based on the perception that higher frequencies should lead to more localised effects. Nevertheless, the practical application shows that MW ablation can affect a broader area due to the way the energy disperses, raising considerations about the potential impact on surrounding healthy tissues [105].

Pulsed-field ablation, also known as Pulsed Electric Field ablation or Irreversible Electroporation ablation, is a relatively newer modality of catheter ablation for the treatment of AF [91]. PF ablation utilises brief, high-energy electric pulses to create lesions in the cardiac tissue [91, 93, 94, 94]. PF stands out because it induces cell death through permanent membrane permeabilisation, unlike other technologies that typically rely on thermal damage [106].

One of the main advantages of PF ablation is that PF ablation can produce deeper lesions than RF or MW ablation with much less thermal injury to surrounding tissue, based on the mechanism of PF ablation causes cell death [92, 94, 107–118]. Additionally, PF ablation has been shown to have a lower risk of the induction of vessel stenosis, particularly of the PVs, compared to the current thermal techniques [92, 119–122].

However, PF ablation is still considered an experimental technique and is not widely available. Further research is needed to determine the long-term efficacy and safety of using PF in the treatment of AF.

2.3.4 Treatment Outcomes

The impact of different types of AF and ablation techniques on long-term outcomes is discussed in this subsection. The effectiveness of ablation procedures varies depending on whether patients have paroxysmal (PAF), persistent, or longstanding persistent AF [123].

Published data in the literature suggest that while success rates following ablation of AF are generally favourable, with reported rates between 50-70%, these figures also highlight the challenges associated with the procedure, which can contribute to the perception of a relatively low success rate [123–126]. PVI is the mainstay therapy of paroxysmal AF, but the success of PVI is suboptimal in the persistent population [125, 126].

For PAF, the success rates of single procedures were found to be 68.6% at 1 year, 61.1% at 3 years, and 62.3% at 5 years, with improved success rates after multiple procedures [127]. In contrast, patients with persistent and longstanding persistent AF had lower success rates after a single procedure (50.8% at 1 year, 41.6% at 3 years) but improved success rates after multiple procedures (77.8% in the long term) [127]. Persistent AF was identified as an independent risk factor for recurrence [128].

Long-term follow-up studies have shown that the majority of AF patients do well over time, with sustainable ablation results [123, 124, 129, 130]. Ablation procedures were also found to be more effective than pharmacologic therapy in

preventing AF progression from paroxysmal to persistent form [123, 124, 131, 132].

For persistent and longstanding persistent AF, various strategies have been developed to target the atrial substrate, such as ablation of complex fractionated atrial electrograms, linear lesions, high dominant frequency spots, and rotor ablation [133–136]. The success rates of these techniques vary, and a uniform strategy is yet to be established.

Overall, while ablation procedures show promise in treating AF, the outcomes are influenced by the type of AF and the chosen ablation technique. Further research is needed to determine the long-term efficacy and optimal approach for different patient populations.

2.3.5 Treatment Challenges

The relatively low success rate of AF ablation therapy can be attributed to many different challenges, including:

- Heterogeneity of AF: AF is a complex arrhythmia with diverse underlying mechanisms and substrates. The nature of AF can vary significantly between patients, making it challenging to develop a one-size-fits-all approach to ablation therapy [123, 136, 137]. The success of the procedure depends on accurately identifying and targeting the specific mechanisms causing AF in each individual.

- Electrical remodelling: AF can lead to changes in the electrical properties of the heart tissue, known as electrical remodeling [26, 138]. These changes can result in the perpetuation and recurrence of AF even after ablation [139]. Electrical remodelling can affect the efficacy of the procedure and contribute to lower success rates.

- Procedural complexity: AF ablation is a complex procedure that requires precise mapping and ablation of abnormal electrical pathways in the heart [137]. The procedure involves navigating intricate anatomical structures and targeting specific areas with catheters or other ablative techniques. The technical challenges and the steep learning curve associated with the procedure

can influence success rates, particularly in less experienced centers [140, 141].

- ➢ Recurrence and reconnection: Despite successful ablation, AF can recur in some patients [142]. The formation of new or reconnected electrical pathways in the heart tissue can contribute to the recurrence of arrhythmia [142–144]. These reconnections may occur due to incomplete ablation, tissue healing, or progressive disease processes [145–147].

- ➢ Lack of standardisation: There is a lack of consensus on the optimal ablation strategies and techniques for different types of AF [148–150]. Variations in energy sources, lesion sets, and endpoint definitions among different centres and operators can affect the success rates and comparability of outcomes [64, 65, 67, 151–157].

- ➢ Limitations in imaging and mapping technologies: The accuracy of mapping and imaging technologies used during ablation procedures can influence the success rates [158–162]. Limitations in spatial resolution [162], registration errors [163] may impact the effectiveness of targeting and ablating the affected areas.

Addressing these challenges requires ongoing research, technological advancements, and an improved understanding of the underlying mechanisms of AF. The development of personalised treatment approaches, integration of advanced imaging and mapping techniques, optimisation of ablation strategies, and standardised outcome assessments can contribute to improving the success rates and long-term outcomes of AF ablation therapy.

While the existing literature primarily focuses on clinical interventions and hard outcomes, such as success rates and recurrence of AF, there is a gap in the understanding of the sources of uncertainties and errors related to the basic science of EM-based ablation modalities [164–166]. Specifically, what are the dielectric properties of cardiac tissue and blood, how do the properties vary inter-individually, as well as how do the properties change during the course of treatment?

2.4 Dielectric Properties of Blood and Cardiac Tissue

This section explores the significant role that the dielectric properties of blood and cardiac tissues play in cardiac ablation for AF treatments. Starting with an overview of the fundamental dielectric properties of materials, the text explains how these properties govern the interaction between EM fields and materials. Following this introduction, the section illustrates how dielectric properties relate to impedance measurements and then moves on to describe the dielectric properties specific to biological tissues. A detailed review of the dielectric properties of blood and cardiac tissue in the literature is given, focusing on RFs (below 1 MHz) and MW (500 MHz – 20 GHz) frequencies[1]. The section concludes with an analysis of how these dielectric properties can be applied to optimise ablation strategies through careful treatment planning and monitoring.

2.4.1 The Fundamentals of the Dielectric Properties of Materials

The fundamental behaviour of electric and magnetic fields, whether in cases of electrostatics, magnetostatics, or electrodynamics (electromagnetic fields), is governed by Maxwell's equations [167]. Maxwell's equations of classical electromagnetism [167] are presented (2.1, 2.2, 2.3, 2.4) as:

$$\nabla \times \mathbf{E} = -\frac{\partial \mathbf{B}}{\partial t}, \tag{2.1}$$

$$\nabla \times \mathbf{H} = \mathbf{J} + \frac{\partial \mathbf{D}}{\partial t}, \tag{2.2}$$

$$\nabla \cdot \mathbf{D} = \rho, \tag{2.3}$$

$$\nabla \cdot \mathbf{B} = 0, \tag{2.4}$$

where $\nabla\cdot$ and $\nabla\times$ denote divergence and curl respectively. $\mathbf{E}$ is the electric field, in volts per meter (V/m). $\mathbf{H}$ is the magnetic field, in amperes per meter

[1]Various organisations, including ITU, IEEE, EU, NATO, and US ECM, use different frequency band designations. However, in this thesis, frequencies below 1 MHz are categorised as radiofrequencies, and those between 500 MHz and 20 GHz are defined as microwave frequencies.

(A/m). **D** is the electric flux density, in coulombs per meter squared (Coul/m^2). **B** is the magnetic flux density, in webers per meter squared (Wb/m^2). **J** is the electric current density, in amperes per meter squared (A/m^2). ρ is the electric charge density, in coulombs per meter cubed (Coul/m^3). $\frac{\partial}{\partial t}$ denotes the time derivative.

Equations 2.1–2.4 are linear but are not independent of each other.

In free space, the following simple relations hold between the electric and magnetic field intensities and flux densities [168]:

$$\mathbf{B} = \mu_0 \mathbf{H} \tag{2.5}$$

$$\mathbf{D} = \varepsilon_0 \mathbf{E} \tag{2.6}$$

where $\mu_0 = 4\pi \times 10^{-7}$ henry/m is the permeability of free-space, and $\varepsilon_0 = 8.854 \times 10^{-12}$ farad/m is the permittivity of free-space.

When electromagnetic fields exist in material media, the field vectors are related to each other by constitutive relations. For a dielectric material, an applied electric field **E** causes the polarisation of the atoms or molecules of the material to create electric dipole moments that augment the total displacement flux, **D**. This additional polarisation vector is called $\mathbf{P}_e$, the electric polarisation, where

$$\mathbf{D} = \varepsilon_0 \mathbf{E} + \mathbf{P}_e. \tag{2.7}$$

In a linear medium, the electric polarisation is linearly related to the applied electric field as

$$\mathbf{P}_e = \varepsilon_0 \chi_e \mathbf{E}, \tag{2.8}$$

where χ_e, which may be complex, is called the electric susceptibility. Then,

$$\mathbf{D} = \varepsilon_0 \mathbf{E} + \mathbf{P}_e = \varepsilon_0 (1 + \chi_e) \mathbf{E} = \varepsilon \mathbf{E}, \tag{2.9}$$

where

$$\varepsilon = \varepsilon' - j\varepsilon'' = \varepsilon_0 (1 + \chi_e) \tag{2.10}$$

is the complex permittivity of the medium.

The imaginary part of ε accounts for the loss in the medium (heat) due to damping of the vibrating dipole moments [168]. Free space, having a real ε, is lossless [168]. Due to energy conservation, the imaginary part of ε must be negative (ε'' positive) [168].

The loss of a dielectric material may also be considered an equivalent conductor loss. In a material with conductivity σ, a conduction current density will exist:

$$\mathbf{J} = \sigma\mathbf{E} \tag{2.11}$$

which is Ohm's law from an EM field point of view [168].

The above equations are valid for arbitrary time dependence. If the fields have a sinusoidal, or harmonic, time dependence, with steady-state conditions assumed, phasor notation can be used. With phasor notation in place, all field quantities will be assumed to be complex vectors with an implied $e^{j\omega t}$ time dependence. Assuming an $e^{j\omega t}$ time dependence, the time derivatives in 2.1–2.4 can be replaced with $j\omega$. Maxwell's equations in phasor form then become

$$\begin{aligned}
\nabla \times \mathbf{E} &= -j\omega\mathbf{B}, && (2.12)\\
\nabla \times \mathbf{H} &= j\omega\mathbf{D} + \mathbf{J}, && (2.13)\\
\nabla \cdot \mathbf{D} &= \rho, && (2.14)\\
\nabla \cdot \mathbf{B} &= 0. && (2.15)
\end{aligned}$$

If Ohm's law from 2.11 is applied then $\mathbf{H}$ in 2.13 becomes

$$\begin{aligned}
\nabla \times \mathbf{H} &= j\omega\mathbf{D} + \mathbf{J}\\
&= j\omega\varepsilon\mathbf{E} + \sigma\mathbf{E}\\
&= j\omega\varepsilon'\mathbf{E} + (\omega\varepsilon'' + \sigma)\mathbf{E}\\
&= j\omega(\varepsilon' - j\varepsilon'' - j\frac{\sigma}{\omega})\mathbf{E},
\end{aligned} \tag{2.16}$$

where it is seen that loss due to dielectric damping ($\omega\varepsilon''$) is indistinguishable from conductivity loss (σ). The term $\omega\varepsilon'' + \sigma$ can then be considered as the total effective conductivity [168].

Typically for the purpose of analysing the behaviour of biological tissues in the EM field, the tissues are characterised by defining two key parameters: the real part of the relative permittivity (also known as the dielectric constant, although the real part is often incorrectly referred to as relative permittivity ε_r), represented as ε' and the effective conductivity (simply called conductivity within the scope of this thesis). These two parameters are generally recognised as the dielectric properties of tissues and they are frequency dependant meaning the values of these parameters change with the frequency of the EM field. The measurements of these dielectric properties, namely the real part of relative permittivity and conductivity of blood and cardiac tissue at different frequencies relevant to various modalities of cardiac ablation are the focus of this thesis.

To comprehend the variations in relative permittivity and conductivity with the frequency of the EM field, and to discern what these changes reveal about the material, the next section explores the polarisation mechanisms responsible for the change in the dielectric properties across different frequencies.

2.4.1.1 Polarisation Mechanisms and Dielectric Dispersion

Dielectric materials respond to an applied electric field through various polarisation mechanisms, dependent on the size, shape, and interactions of bound charges [169]. Electronic polarisation is a rapid process involving the redistribution of the electron cloud around the nucleus of the atom, with effects observed in the ultraviolet spectrum [170, 171]. Atomic or ionic polarisation, another mechanism, shifts the distribution of ions in a crystal structure of the material, causing an alternating dipole moment typically seen in the infrared spectrum [171, 172]. Both mechanisms have very short relaxation times of 10^{-15} s for the electronic polarisation and 10^{-13} s to 10^{-12} s for the ionic polarisation.

Moving to the molecular level, orientation polarisation occurs when polar molecules align their permanent dipolar moments with the electric field, contributing to the material's overall polarisation. The duration of this process varies with the size of the molecule and is generally observed within the microwave region ($\tau \approx 10^{-12}$ s to 10^{-10} s) [171, 173, 174].

Two other mechanisms, interfacial and counterion polarisation, manifest in heterogeneous media. Interfacial polarisation arises from the electrical boundary between two media with different conductivities and permittivities, leading to an accumulation of charges [175–177]. Counterion polarisation is a process where counterions (the ions that accompany an ionic species in order to maintain electric neutrality) in an electric double-layer structure of the electrolyte solution are redistributed under an applied electric field [178]. The extent of polarisation from this mechanism heavily relies on the size and shape of the particles [179].

Biological tissues are heterogeneous materials usually consisting of mostly water with dissolved ions, organic molecules and insoluble matter. These constituting elements are organised in cellular and subcellular structures. Biological tissues interact with electromagnetic fields due to the presence of electrical charge, namely ions, polar molecules and polarisable molecules.

As frequency increases, the net polarisation of the material drops as each polarisation mechanism ceases to contribute, and hence its dielectric constant drops. The frequency dependence of the polarisation mechanisms gives rise to the frequency dependence of the dielectric constant. The frequency dependence of the dielectric constant is known as dielectric dispersion. In other words, the dielectric constant (or permittivity) of a material may vary depending on the frequency of the applied electric field. It is closely related to the process of polarisation within the material and can reveal information about the molecular dynamics of a system.

In the next section, the mathematical formulations that have been developed to capture the dielectric behaviour of biological tissues and other polar materials are discussed.

2.4.1.2 Dielectric Models and Multiple Relaxation

Differential equations have been developed to model the dielectric dispersions of biological tissues and other polar materials. A dispersion region is generally described by first-order differential equations that lead to single-time constant responses [180]. However, given the multiple relaxation processes in biological

materials, the overall tissue response may be characterised by multiple time constants. These time constants characterise the poles of the differential equations constituting the dielectric model [181], of which there is one per relaxation process.

Dielectric models find their primary use in fitting dielectric data, thereby reducing measurement data points to closed-form equations and convenient graphical representations [181, 182]. These models enable the calculation of relative permittivity and conductivity (or the imaginary part of the complex permittivity) at any desired frequency within the valid range of the model [181, 183] and they offer an easy way to transfer information that can be used in simulations. Common models used for fitting dielectric data of aqueous electrolytic solutions and tissues include the Debye, Cole-Cole, and Cole-Davidson models [184].

The Debye model, which denotes the dielectric relaxation response of an ideal, non-interacting dielectric material to an alternating external electric field, can express the dielectric response of a first-order system in the frequency domain as:

$$\varepsilon(\omega) = \varepsilon_\infty + \frac{\varepsilon_s - \varepsilon_\infty}{1 + j\omega\tau}, \tag{2.17}$$

where ε_∞ is the permittivity at infinite frequencies due to electronic polarisability, and ε_s is the static (low-frequency) permittivity. However, this equation does not consider the static conductivity σ_s and can be expanded:

$$\varepsilon^*(\omega) = \varepsilon_\infty + \frac{\varepsilon_s - \varepsilon_\infty}{1 + j\omega\tau} + \frac{\sigma_s}{j\omega\varepsilon_0}. \tag{2.18}$$

In 1941, Cole *et al.* [185] introduced the Cole-Cole equation as an empirical model for the dielectric relaxation of materials. As an extension of the Debye model, the Cole-Cole model serves as a physics-based representation of wideband frequency-dependent dielectric properties. The first-order Cole-Cole equation introduces the empirical variable α to account for the relaxation time distribution:

$$\varepsilon(\omega) = \varepsilon_\infty + \frac{\varepsilon_s - \varepsilon_\infty}{1 + (j\omega\tau)^{1-\alpha}}. \tag{2.19}$$

where ε denotes the complex permittivity, ε_∞ the permittivity at infinite frequency, ε_s the static permittivity, τ the relaxation time constant, ω the angular

frequency and α an empirical parameter that ranges from 0 to 1 to facilitate the modelling of different spectral shapes. Although the Cole-Cole equation is effective for non-lossy materials [180, 186, 187], for lossy materials like biological tissues, a conductivity term for accurate representation of tissue relaxation is necessary [180, 186, 187]. The Cole-Cole model for biological tissues thus expands to:

$$\varepsilon(\omega) = \varepsilon_\infty + \frac{\varepsilon_s - \varepsilon_\infty}{1 + (j\omega\tau)^{1-\alpha}} + \frac{\sigma_i}{j\omega\varepsilon_0}, \tag{2.20}$$

where σ_i signifies the static ionic conductivity and ε_0 the permittivity of free space.

The dielectric spectrum of biological tissues is typically characterised by three major relaxation regions, each defined by a unique time constant, τ. However, due to the complexity of both the composition and the structure of biological tissues, there are multiple relaxation processes, resulting in a distribution of relaxation time constants and a consequent broadening of the dispersion region [181].

To address the broadening of the dispersion region, Gabriel *et al.* [181] proposed the decomposition of relaxation into a sum of single time constant components, known as poles, in 1996. Each pole characterises a unique dispersion region. The resulting multi-pole Cole-Cole model is expressed as:

$$\varepsilon(\omega) = \varepsilon_\infty + \sum_{p=1}^{n} \frac{\Delta\varepsilon_p}{1 + (j\omega\tau_p)(1 - \alpha_p)} + \frac{\sigma_i}{j\omega\epsilon_0}, \tag{2.21}$$

where n represents the total number of poles and $\Delta\varepsilon_p = \varepsilon_s - \varepsilon_\infty$.

The Havriliak–Negami relaxation is a collective representation of the Debye, Cole-Cole, and Cole-Davidson models, which is an empirical modification of the Debye relaxation model, factoring in the asymmetry and broadness of the dielectric dispersion curve:

$$\varepsilon(\omega) = \varepsilon_\infty + \frac{\varepsilon_s - \varepsilon_\infty}{[1 + (j\omega\tau)^{1-\alpha}]^\beta}. \tag{2.22}$$

Here, when $\alpha = 0$ and $\beta = 1$, the equation is equivalent to the Debye model. For $0 < \alpha < 1$ and $\beta = 1$, it results in the Cole-Cole equation. And for $\alpha = 0$ and $0 < \beta < 1$, it corresponds to the Cole-Davidson equation, characterised by

an asymmetrically broadened distribution of relaxation times. While all these models find use in fitting polar aqueous solutions, the dielectric data of biological tissues are generally fitted with Debye and Cole-Cole models [181, 182]. These models enable the straightforward incorporation of the dielectric properties of biological tissues into advanced computational models.

Considering that the dielectric behaviour of a material across a wide frequency range involves multiple relaxation processes, more poles corresponding to the different relaxation times of the material must be introduced to accurately represent the material properties [180]. Biological tissues are typically described in terms of multiple Cole-Cole dispersions, which offer a compact, physics-based representation of wideband frequency-dependent dielectric properties [181].

Having understood the relationship between fields and materials as governed by Maxwell's equations, the next section will discuss how dielectric properties correlate with impedance and the methodologies for measurement of both impedance and dielectric properties.

2.4.2 Relationship Between Dielectric Properties and Impedance

The extraction of dielectric properties typically involves interpreting impedance, conventionally described as the voltage-current ratio within an electrical circuit [188]. However, at microwave frequencies, direct measurement of impedance presents practical challenges, necessitating indirect methods or specialised techniques for accurate characterisation. /par

This section aims to provide a fundamental understanding of impedance, the key characteristics of impedance, and how impedance serves as a vital link connecting the dielectric properties of materials with practical applications. Through this exploration, the endeavour is to bridge the gap between the theoretical concepts and their tangible applications, offering a comprehensive understanding of the subject at hand.

The impedance Z can be represented in complex form as

$$Z = R + jX \tag{2.23}$$

and in polar form as

$$Z = |Z|\angle\theta. \tag{2.24}$$

The admittance Y, which is the inverse of impedance, is

$$Y = \frac{1}{Z} = G + jB, \tag{2.25}$$

where G is conductance and B is susceptance. Impedance is measured in Ohm (Ω) while admittance is measured in Siemens (S). When the real (R) and imaginary (jX) components are connected in series, the impedance $Z = R + jX$. Conversely, when these components are connected in parallel, the impedance is

$$Z = \frac{jRX}{R + jX}, \tag{2.26}$$

or it could be represented using the admittance as in 2.25. Reactance comes in two forms: inductive reactance (X_L) and capacitive reactance (X_C), defined as

$$X_L = 2\pi f L = \omega L \tag{2.27}$$

$$X_C = \frac{1}{2\pi f C} = \frac{1}{\omega C}, \tag{2.28}$$

where f is the frequency, ℓ is the inductance, and C is the capacitance. Here, $\omega = 2\pi f$ is known as the angular frequency.

Impedance and related properties such as admittance, resistance, reactance, conductance and susceptance are extensive properties, in the sense that these properties not only depends on the electrical properties of the sample but also on the geometry of the measurement system (the measurement *cell*) [188]. In contrast, relative permittivity and conductivity are examples of intensive properties, which retain constancy and are dependent only on the electrical properties of the sample and are not influenced by the geometry or dimensions [188].

Based on their ability to transmit electrical current when exposed to an electric field, materials can generally be categorised as either conductors or dielectrics [3]. Conductors contain charges that under the action of an electric field can move

relatively freely within the material. In contrast, the charges in dielectrics can only shift a small distance from their equilibrium position.

Bioimpedance deals with passive electrical properties of tissue and is defined as the ability to oppose (impede) electric current flow [188]. In the case of biological tissues, there is a duality in the electrical properties. Tissue may be regarded as a conductor (i.e. offers little or no resistance to the flow of electric current) or a dielectric (i.e. insulating material or a very poor conductor of electric current). At frequencies of 100 kHz or less, most tissues primarily function as electrolytic conductors, with electrolytes serving as the main charge carriers [188]. At higher frequencies the dielectric properties of tissue start to dominate. At the highest frequencies, tissue properties become more and more equal to that of water [188].

Most conductive materials follow Ohm's law which states a linear relationship between the electric current and the applied voltage according to the resistance, R, which is expressed in ohms (Ω). The resistance of a piece of material depends on the intrinsic resistivity, ρ, of the material and on its geometry.

$$R = \rho \frac{\ell}{A}, \tag{2.29}$$

$$G = \sigma \frac{A}{\ell}\,. \tag{2.30}$$

If a geometrical constant, k is designated as the ratio of A and ℓ then the resistance and the resistivity or conductivity will be related by k, expressed in m [3, 189–191] [1]:

$$R = \frac{1}{k}\rho = \frac{1}{k\sigma} \tag{2.31}$$

From 2.31 and given that $G = 1/R$ it follows

$$k = \frac{1}{\sigma R} = G/\sigma. \tag{2.32}$$

[1] In different studies cell constant can be defined slightly differently and can be expressed in m, m^{-1} and cm^{-1}. In this thesis all the definitions and equations are adjusted for the definition of the cell constant in m.

Similarly to resistance R in 2.31, and in the case of material not being a good conductor, the capacitance C depends on an intrinsic property of the dielectric material, the electric permittivity ε and the geometry of the capacitor

$$C = \varepsilon \frac{A}{\ell}, \tag{2.33}$$

$$C = k\varepsilon. \tag{2.34}$$

or

$$C = k\varepsilon = k\varepsilon_r\varepsilon_0. \tag{2.35}$$

Not unlike the parallel plate capacitor, in the standard form, the measurement cell consists of two metallic flat electrodes, with area A, and a gap ℓ between them, in which the material is confined ($k = A/\ell$).

However, most materials are not ideal conductors nor ideal dielectrics so any real material, including biological tissues, placed in the measurement cell (or between the parallel plates) will act as a combination of a resistor and a capacitor (Fig. 2.7). This combination of a resistor and a capacitor is the simplest equivalent circuit mimicking the impedance found in tissue measurements [188, 192]. While this model is the simplest, it is also the most important model because every measurement on a specific frequency is reduced to such a circuit [188].

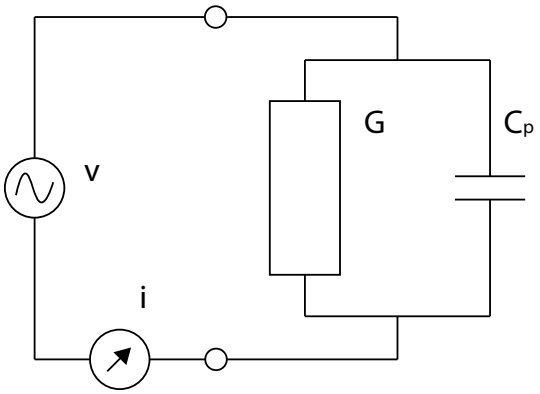

Figure 2.7: Parallel resistor and capacitor is the most simple model of biological tissue [188, 192].

While parallel plates are the most simple geometry to analyse, a more realistic measurement cell would be comprised of two-needle electrodes inserted into a living tissue (two-electrode probe). For more general electrode geometries (i.e. two-electrode probe, four-electrode probe), it will be necessary to compute the cell constant by numerical methods [193] or to find it by measuring the resistance of a sample with a well-known conductivity [191, 194]. For instance, in the field of bioimpedance, the 0.9% aqueous sodium chloride (NaCl) solution is typically used because its composition and conductivity (1.44 S/m at 20°C) are similar to those of blood plasma [3].

The cell constant is typically determined during the calibration process of the conductivity measurement system. It can be determined experimentally by using a sample with a known conductivity or by performing simulations or calculations based on the electrode geometry and sample dimensions. In the standard canonical form, the measurement cell consists of two metallic flat electrodes, with area A, and a gap ℓ between them, in which the material is confined ($k = A/\ell$).

It is worth noting that scaling the measurement cell by a factor will result in the change of the cell constant by that same factor, as the area A of the measurement cell will scale by the square of the factor, while the gap ℓ is proportional with the factor.

The volume (V) of the sample changes with the third power of the scaling factor. For example, if the dimensions of the measurement cell are increased by a factor of s, the cell constant would also increase by the same factor. The volume of the sample that would fit inside the cell would be s^3 times that of the original cell. Conversely, if the cell size is scaled down by a factor of s, the cell constant would decrease by the same factor and the volume would be $(1/s)^3$ of the original.

The relationship between the cell constant (k), the electrode area (A), and the gap distance (ℓ) can be expressed as:

$$k = \frac{A}{\ell} \tag{2.36}$$

When scaling the measurement cell by a factor s, the new cell constant (k'), area (A'), and gap distance (ℓ') can be calculated as follows:

$$k' = \frac{A'}{\ell'} = \frac{s^2 A}{s\ell} = \frac{sA}{\ell} = sk \tag{2.37}$$

Therefore, the cell constant changes proportionally with the scaling factor. This change of the cell constant also extends to the electrode configurations other than standard parallel plates, as is shown in the following subsection for the case of a four-electrode probe.

Impedance is a complex magnitude that establishes a relation between the sinusoidal voltage and the current for each frequency taking into account the contribution of both, the resistive and the capacitive components. Therefore, from impedance measurements performed with an electrode setup of known cell constant k, it is possible to extract both σ and ε [188].

$$Z = R - j\frac{1}{2\pi f C} = \frac{1}{k}\left(\frac{1}{\sigma + j2\pi f\varepsilon}\right) \tag{2.38}$$

It is important to note that both σ and ε may depend on the frequency [3]. While it can be argued that k is constant for a given geometry, parasitic capacitances and frequency-dependent distribution of field lines can yield a frequency-dependent complex k [194].

2.4.2.1 Electrode Polarisation and Four-electrode Probe Cell Constant

Water is one of the main constituents of any biological tissue. Water is a good solvent for ions and other molecules found in biological tissues. Electrolytes such as sodium, potassium, calcium, magnesium, chloride and others play an important role in the functioning of biological systems. These ions produce ohmic current and energy loss under the applied electric field. In addition, because of the cellular structure of biological tissues, these ions produce polarisation due to charge accumulation at the cell membrane.

Under the influence of an electric field, the ions tend to move towards the electrode/sample interface, leading to the development of ionic double layers in such regions (Fig. 2.8) [195]. The applied voltage drops rapidly in these layers, which implies a huge electrical polarisation of the material and a near-absence of the electric field in the bulk sample at low frequencies [196–198].

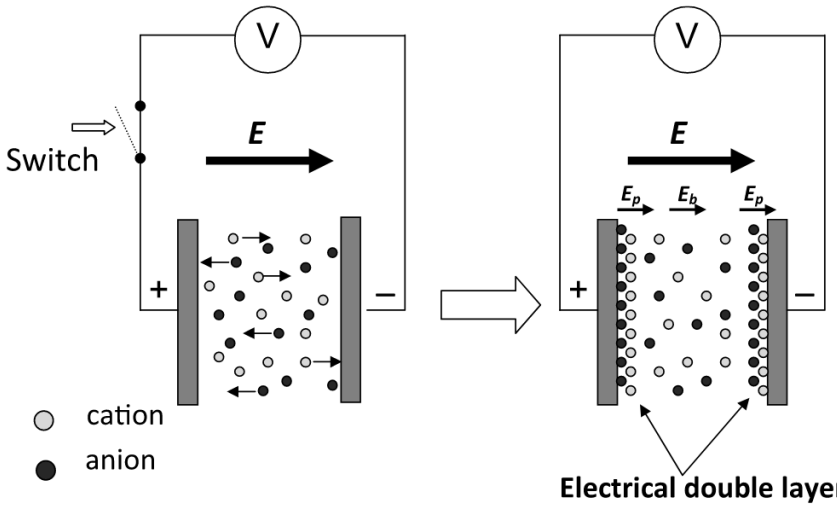

Figure 2.8: This schematic illustrates the formation of ionic double layers at the electrode/sample interfaces. The electric field, represented as E, is influenced by the development of these double layers, resulting in $\mathbf{E} = \mathbf{E_b} + 2\mathbf{E_p}$, where $\mathbf{E_p}$ is generally greater than $\mathbf{E_b}$ [195]. Used with permission of IOP Publishing, reproduced from [195]; permission conveyed through Copyright Clearance Center, Inc.

The two most commonly used methods of mitigating electrode polarisation (EP) are the electrode coating technique and the four-electrode method [195, 196].

In terms of a correction method to change the measured data to conductivity and relative permittivity (i.e., the cell constant), Jakosky [189, 199] solved Laplace's equation to show that the potential at any point in an infinite isotropic homogeneous medium caused by a small source of current is given by $V = I/4\rho\pi r$, where σ is the conductivity of the medium and r is the distance from the current source to the point of measurement [189].

Fig. 2.9 identifies the potential V_e at a point P between a pair of current-carrying electrodes A, B in a volume conductor of conductivity σ. The potential V_v is given by

$$V_P = \frac{I}{\sigma 4\pi}\left(\frac{1}{r_1} - \frac{1}{r_2}\right) \tag{2.39}$$

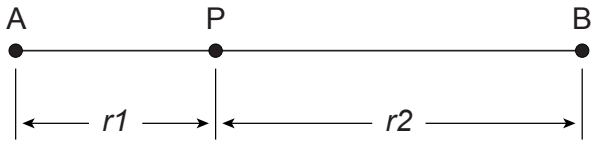

Figure 2.9: A point P between a pair of current-carrying electrodes A, B in a volume conductor of conductivity σ.

If a second electrode Q is placed symmetrically at a distance d from electrode P on the line AB as shown in Fig. 2.10, it is possible to determine the potential $(V_P - V_Q)$ appearing between electrodes P and Q. This difference in potential is given by

$$\begin{aligned} V_{PQ} &= V_P - V_Q \\ &= \frac{I}{\sigma 4\pi}\left(\frac{1}{r} - \frac{1}{r+d} - \frac{1}{r+d} + \frac{1}{r}\right) \\ &= \frac{I}{\sigma 2\pi}\left(\frac{1}{r} - \frac{1}{r+d}\right) \end{aligned} \tag{2.40}$$

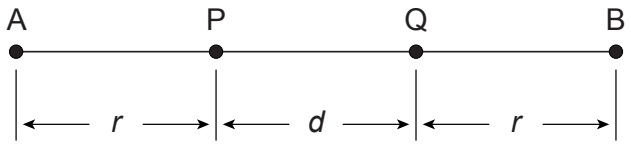

Figure 2.10: Two point P and Q between a pair of current-carrying electrodes A, B in a volume conductor of conductivity σ.

The resistance R, appearing between the potential measuring electrodes P, Q is given by

$$\begin{aligned} R &= \frac{V_P - V_Q}{I} \\ &= \frac{1}{\sigma 2\pi}\left(\frac{1}{r} - \frac{1}{r+d}\right) \end{aligned} \tag{2.41}$$

For a symmetrical probe as in Fig. 2.10

$$\begin{aligned} 2r &= d - L \\ r &= \frac{L-d}{2} \end{aligned} \tag{2.42}$$

where L is the length of the probe.

Substituting r in 2.41 with 2.42

$$R = \frac{1}{\sigma\pi}\left(\frac{1}{L-d} - \frac{1}{L+d}\right). \tag{2.43}$$

If ratio of distance d over the length of the probe L is introduced as $\alpha = d/L$ then

$$\begin{aligned} R &= \frac{1}{\sigma\pi L}\left(\frac{1}{1-\alpha} - \frac{1}{1+\alpha}\right) \\ &= \frac{2}{\sigma\pi L}\left(\frac{\alpha}{1-\alpha^2}\right). \end{aligned} \tag{2.44}$$

And finally combined with 2.32 the cell constant is

$$k = \frac{\pi L}{2}\left(\frac{1-\alpha^2}{\alpha}\right). \tag{2.45}$$

If the same size/scaling analysis as in the previous section is conducted then when scaling the four-electrode probe by a factor s, the new cell constant (k') can be calculated from the scaled length (L'), and distance (d')

$$L' = sL \tag{2.46}$$
$$d' = sd \tag{2.47}$$
$$\tag{2.48}$$

and the ratio α'

$$\alpha' = \frac{d'}{L'} = \frac{sd}{sL} = \alpha \tag{2.49}$$

as

$$\begin{aligned} k' &= \frac{\pi L'}{2}\left(\frac{1-\alpha'^2}{\alpha'}\right) \\ &= s\frac{\pi L}{2}\left(\frac{1-\alpha^2}{\alpha}\right) \\ &= sk. \end{aligned} \tag{2.50}$$

The cell constant of the four-electrode probe changes proportionally with the scaling factor.

It is important to note here that while the resistance R in 2.31 is inversely proportional to the cell constant k, the conductance C is proportional to k. Typically, materials are neither perfect conductors nor perfect dielectrics [3]. That is, it will be possible to define a conductivity value σ, and also a permittivity value ε. These two values are typically referred to as the passive electrical properties of the material [3].

Given that the measured impedance increases as the cell constant decreases, it can be inferred that a smaller volume of the sample is engaged by the electric

current. Thus, it can be concluded that a lower cell constant implies the requirement for a smaller sample volume. In essence, the sample size is proportional to the cell constant, which in turn is proportional to the size of the probe.

Following on from a method to convert measured data to conductivity, the specific methods to measure conductivity at RF as well as dielectric properties at MW frequencies are discussed in the next subsection.

2.4.3 Impedance Measurement Methods

There are a number of measurement methods to choose from when measuring impedance, each of which has advantages and disadvantages. Measurement requirements and conditions must be considered, and then the most appropriate method has to be chosen while considering such factors as frequency coverage, measurement range, measurement accuracy, and ease of operation. The choice requires tradeoffs as there is not a single measurement method that includes all measurement capabilities.

Table 2.1 lists the advantages and disadvantages of six commonly used impedance measurement methods, the applicable frequency range of the instrument, and the typical applications for each method.

Dielectric spectroscopy, as defined in [200], involves the measurement of the dielectric properties of a medium across varying frequencies. It is often discussed within the broader context of impedance spectroscopy, which encompasses the study of the impedance of a system as a function of frequency. There is a nuanced overlap between the two methods, as each provides insights into the frequency-dependent electrical properties of materials.

2.4.3.1 Open-ended Coaxial Probe Method for Measurement of Dielectric Properties at Microwave Frequencies

In order to address the research questions from *Chapter 1* the following approach was taken. For the characterisation of dielectric properties of cardiac tissues in *Chapter 3*, dielectric spectroscopy using an open-ended coaxial probe method was performed.

Table 2.1: Common impedance measurement methods (from Keysight, "Application Note 5950:3000 - Impedance Measurement Handbook: A Guide to Measurement Technology and Techniques, 6th Edition" [201])

Method	Advantages	Disadvantages	Applicable frequency range	Common applications
Bridge method	High accuracy (0.1% typ.), Wide frequency coverage, Low cost	Needs to be manually balanced, Narrow frequency coverage with a single instrument	DC to 300 MHz	Standard lab
Resonant method	Good Q accuracy up to high Q	Needs to be tuned to resonance, Low impedance measurement accuracy	10 kHz to 70 MHz	High Q device measurement
I-V method	Grounded device measurement, Suitable for probe-type test needs	Operating frequency range is limited by transformer used in probe	10 kHz to 100 MHz	Grounded device measurement
RF I-V method	High accuracy (1% typ.) and wide impedance range at high frequencies	Operating frequency range is limited by transformer used in test head	1 MHz to 3 GHz	RF component measurement
Network analysis method	Wide frequency coverage from LF to RF, Good accuracy when the unknown impedance is close to characteristic impedance	Recalibration required when the measurement frequency is changed, Narrow impedance measurement range	5 Hz and above	RF component measurement
Auto-balancing bridge method	Wide frequency coverage from LF to HF, High accuracy over a wide impedance measurement range, Grounded device measurement	High frequency range not available	20 Hz to 120 MHz	Generic component measurement

The open-ended coaxial probe technique consists of placing a tissue sample in contact with the probe and measuring the signal reflected to the port of a vector network analyser (VNA). The open-ended coaxial probe method is based on the theoretical assumption that the sample interrogated by the probe occupies a semi-infinite volume so that the acquired signal is only due to the impedance mismatch between the system and the sample [202–204].

A coaxial probe, generally, consists of an inner conductor of radius a, an insulator of width c having low relative permittivity ε_r (i.e., relative permittivity close to that of air), and an outer conductor having an inner radius b. Ideally, in order to minimise EM signal attenuation, the probe insulator is low-loss and the inner and outer conductors are high conductivity. An illustration of the top view of a coaxial probe, with its dimensions a, b and c, and the illustrations of the EM propagation across the probe and the sample are shown in Fig. 2.11 [202].

In historical context, the fabrication of open-ended coaxial probe was tailored to the needs of diverse studies [205–213]. In order to convert the measured complex reflection coefficient into complex permittivity, different methods to model the probe have been developed [203, 204, 211, 214–216]. These methods can be divided into two categories: full wave formulation techniques and lumped equivalent circuit models [216, 217].

Over the last decade, a growing number of dielectric studies have been conducted using commercial probes, predominantly those manufactured by Keysight Technologies (Keysight, Santa Rosa, CA, USA) [202]. The Keysight probes have been used in most of the recent tissue dielectric studies [218–222]. The slim form probe, because of the small diameter, is a common choice for tissue measurements. The ability to steam-sterilise the probe allows for the use of the probe in vivo. [218–220].

The slim form probe is typically used in conjunction with the Materials Measurement Suite from Keysight Technologies (Keysight, Santa Rosa, CA, USA) [223], which has been designed to automate the complex process of permittivity measurements. The Materials Measurement Suite is equipped with a proprietary model of the probe and employs this model to yield relative permittivity values automatically, thereby eliminating the need for conversion from the reflection coefficient to permittivity.

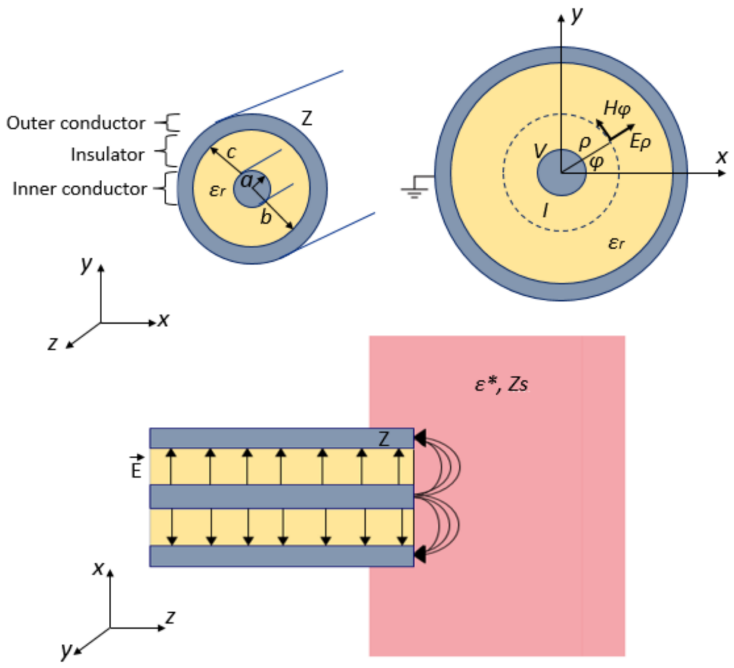

Figure 2.11: Diagrams illustrating the EM transmission along an open-ended coaxial probe and the electric probe-sample interaction: on the top, views of the top cross-section of a coaxial probe with probe dimensions indicated on the left, and generated EM signals on the right; on the bottom, side cross-section of a coaxial probe placed in contact with a sample. In particular, the top left picture illustrates the inner and outer conductors, and the insulator characterised by the relative permittivity ε_r, of a coaxial probe with dimensions a, b and c, which, specifically, are inner conductor radius, outer conductor inner radius and insulator width, respectively. Due to the TEM propagation mode generated by the application of a voltage signal V between the two conductors, the top right picture depicts an electric field component E_ρ along the radial direction ρ, and a magnetic field component H_ϕ along the azimuthal direction Φ. In the top right diagram, the resulting generated current I encircling the probe is also labelled. In the bottom picture, the side-view cross-section of the interaction between the probe and the sample is illustrated by highlighting the radial electric field within the probe and the fringing electric field across the sample, due to the impedance mismatch between the probe and the sample, which have impedances of Z and Z_S, respectively. When the electric field fringes, part of the signal is transmitted into the sample and the rest of the signal is reflected back to the probe. Note that the diagrams are not to scale [202].

The study presented in *Chapter 3* utilised the Keysight slim form probe in conjunction with the Materials Measurement Suite.

2.4.3.2 Four-electrode Probe Method for Electrical Impedance Spectroscopy

For the characterisation of the electrical conductivity of human blood in *Chapter 4*, an electrical impedance spectroscopy was performed using a custom-made four-electrode probe. In *Chapter 5*, a miniaturised version of the four-electrode probe working in the same configuration is detailed and utilised. In this subsection, the four-electrode method basics are presented. The custom-made probes and the measurement methods used in *Chapter 4* and *Chapter 5* are detailed within the chapters.

In the simplest two-electrode measurement setup the stimulus is applied and the measurement is done using the same two electrodes, named the working electrode (WE) and the counter electrode (CE) [224]. In this case, the measured impedance Z includes contributions due to the sample interface at both electrodes [224]. If the effect of the zones proximal to the current-carrying (CC) electrodes (WE and CE) and the polarisation impedance of the electrodes themselves are to be reduced, the four-electrode system is preferred. In addition to CC electrodes, the four-electrode system has a separate circuit for measuring the voltage. This circuit is connected by a separate pair of electrodes. These electrodes are sensing electrode (SE) and reference electrode (RE) and as a pair of electrodes are referred to as the pick-up (PU) electrodes. Such four-electrode systems correspond to a two-port, four-terminal network equivalent. Because there are two ports in these systems, they measure transfer parameters between the ports. If, for instance, impedance is measured to be 0 Ω, it doesn't convey that there is high-conductivity tissue present. Instead, it may imply that there is no signal transfer from the CC electrodes (WE and CE) to the PU electrodes (SE and RE) [188].

Since no current is drawn at both SE and RE, the measured impedance is independent of the electrode–sample interfaces [224].

Different types of four-electrode probes exist, and they typically fall into two main categories: needle-type probes [225, 226] and planar-type probes [227–230].

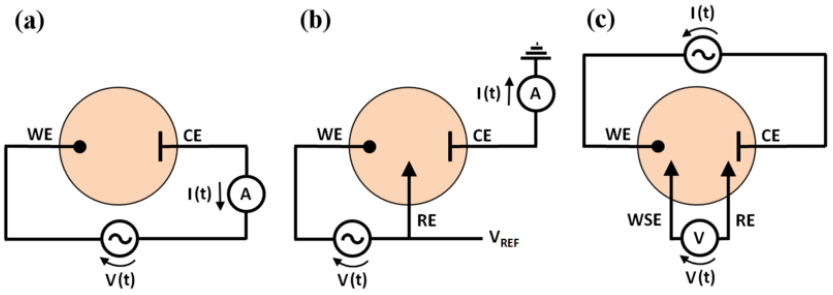

Figure 2.12: Measurement setup configurations featuring (a) two electrodes, (b) three electrodes and (c) four electrodes. Reproduced from [224] under Creative Commons Attribution 3.0 License.

While needle-type probes are more appropriate for measuring liquid samples, this type of probe has also been utilised for assessing soft tissue conductivity [225, 226]. However, the impact of piercing the tissue on the structure and, subsequently, on measurement results remains uncertain. For this reason, planar-type probes are generally considered better suited for soft tissue conductivity measurements, while needle-type probes remain an option for measurements on liquid samples.

2.4.4 Dielectric Properties of Blood and Cardiac Tissue

In this work, the dielectric properties of cardiac tissue and blood are of interest at different frequencies relevant to various modalities of cardiac ablation. To understand the state of the art, this section discusses the conductivity of cardiac tissue at radiofrequencies, the dielectric properties of cardiac tissue at microwave frequencies, the dielectric properties of blood at microwave frequencies, and the conductivity of blood at radiofrequencies.

2.4.4.1 Conductivity of Cardiac Tissue at Radiofrequencies

The electrical conductivity of cardiac tissues at frequencies below 1 MHz has been extensively studied with a variety of animal models and methodologies. A 1957 study by Schwan and Kay [231] was conducted on dogs in situ, measuring the conductivity of the heart muscle across the 10 Hz to 10 kHz range using a

two-electrode method. More recent studies listed in Table 2.2 have expanded on this initial methodology and used the four-electrode method.

Fallert et al. 1993 study [232] and Ellenby et al. 1987 study [233] utilised a four-electrode method to map the impedance of ischemic sheep hearts and left ventricle myocardium of mongrel dogs, respectively. Cinca et al. 1997 study [234] also conducted in vivo studies on the left ventricle myocardium of pig, employing a four-electrode method. Their research was specialised towards understanding the changes in myocardial electrical impedance induced by coronary artery occlusion. Tsai et al. 2002 study [235] also conducted in vivo studies on pigs but focused their research on the left ventricle myocardium. Gabriel et al. in 2009 study [191] conducted in vivo studies on pigs, employing a four-electrode method to measure the dielectric properties of the atrium, providing significant data in the 40 Hz to 1 MHz frequency range.

Table 2.2: Summary of animal studies measuring the dielectric properties of the heart.

Source	Animal (N)	Tissue	T [°C]	Measurement Method	Frequency
Schwan 1957 [231]	Dog (In situ)	Heart (muscle)	37	Two electrodes	10 Hz–10 kHz
Ellenby 1987 [233]	Mongrel dogs (In vitro) (N=21)	Left ventricle myocardium	37	Four electrodes	1 kHz
Fallert 1993 [232]	Sheep (In vivo) (N=39)	Left ventricle myocardium	Body	Four electrodes	1 kHz–15 kHz
Cinca 1997 [234]	Pig (In vivo) (N=26)	Left ventricle myocardium	Body	Four electrodes	1110 Hz
Tsai 2002 [235]	Pig (In vivo) (N=8)	Left ventricle myocardium	38	Four electrodes	1 Hz–1 MHz
Gabriel 2009 [191]	Pig (In vivo) (N=3+)	Heart (atrium)	37	Four electrodes	40 Hz–1 MHz

2.4.4.2 Dielectric Properties of Cardiac Tissue at Microwave Frequencies

A number of previous studies have reported on the dielectric properties of the heart (Table 2.3).

Table 2.3: Summary of studies measuring the dielectric properties of the heart at microwave frequencies.

Source	Animal	Tissue	T [°C]	Measurement Method	Frequency
Gabriel 1996 [236]	Human, Ovine (Ex vivo)	Heart	37	Open ended coaxial probe	300 kHz–20 GHz
Schwartz 1985 [237]	Bullfrog (In vivo)	Heart		Open-ended coaxial probe	200 MHz–8 GHz
Xu 1987 [238]	Canine (In vitro, Immersed in saline)	Heart	20	Open ended coaxial probe	100 MHz–11 GHz
Fornes-Leal 2019 [239]	Porcine (In vivo)	Heart (Epicardium)	37.2–38.5	Open ended coaxial probe	500 MHz–26.5 GHz
Salahuddin 2018 [240]	Porcine (Ex vivo)	Heart (LA, LV, RA, RV, and PA)		Open ended coaxial probe	400 MHz–20 GHz

The Gabriel *et al.* parametric model for the heart tissue is based on the data gathered from the literature [236] as well as data from their experimental study [207]. In their experimental study, Gabriel *et al.* measured dielectric properties ex vivo on excised animal tissue and human autopsy material. The dielectric properties of the heart were measured ex vivo on human tissues obtained from an autopsy performed between 24 and 48 h after death at frequencies between 300 kHz to 20 GHz, and ovine heart at frequencies between 10 Hz and 20 GHz, within 2 h of death. Both the human and ovine heart tissues were measured at 37 °C. Part of the data gathered from the literature that was measured over the microwave frequency range includes data from in vivo experiments on bullfrog [237] and in vitro experiments on canine tissue [238].

In their study from 1987, Xu *et al.* measured canine tissues in vitro [238]. The tissues were immersed in saline for up to 12 h, which is not considered best practice by today's standards since such immersion can modify the dielectric properties [2]. While the room temperature is reported, the temperature of the tissue is not.

In a more recent study by Fornes-Leal *et al.* from 2019 [239], dielectric properties of the porcine heart, among other porcine thoracic tissues, were measured in vivo at the frequency range from 500 MHz to 26.5 GHz. In this study, the heart

was treated as a homogeneous organ and while the measurements were made at five different locations on each organ that was measured, the anatomical part of the heart that was measured is not specified.

However, further work is needed to accurately characterise the dielectric properties of the heart. Challenges include the inherent variation in all tissues (both within the patient and between patients) [241], well as the anatomical and functional heterogeneity of the organ [6, 7]. Indeed in a recent study, Salahuddin *et al.* experimentally demonstrated that treating the heart as a homogeneous organ may not provide an accurate dielectric representation of the entire organ [240].

2.4.4.3 Dielectric Properties of Blood at Microwave Frequencies

There are a number of studies examining the dielectric properties of blood at microwave frequencies. Alison and Sheppard [242] characterised human blood dielectric properties at frequencies from 29 GHz to 90 GHz in a 1993 study. Wolf *et al.* [243] measured dielectric spectra of human blood over a broad frequency range from 1 Hz to 40 GHz using several different techniques across the frequency range. In the frequency range from 1 Hz to 10 MHz, they applied the AC voltage to a parallel plate capacitor made of platinum, containing the sample material [243]. In a more recent study from 2018 Santorelli *et al.* [244] found that at microwave frequencies (i.e. 500 MHz–8.5 GHz) haemoglobin is the biggest predictor of changes in complex permittivity of blood. They demonstrated that blood permittivity at a single microwave frequency (i.e. 1 GHz) can detect anaemia with high sensitivity and specificity [244].

All studies at microwave frequencies that are included in this review were conducted by using the open-ended coaxial probe method [242–245]. This comprehensive understanding of dielectric properties of blood at microwave frequencies highlights the depth and breadth of the current knowledge base and was not further explored within this thesis.

2.4.4.4 Conductivity of Blood at Radiofrequencies

An overview of studies investigating blood conductivity is presented in Table 2.4. The fields in the table are highlighted where the corresponding study has fulfilled

one or more of the following criteria, which ensure the best practice:

- ➢ measured the conductivity of human blood;
- ➢ at body temperature (37°C);
- ➢ at frequencies below 1 MHz; and
- ➢ using the four-electrode technique.

It is worth noting here that none of the studies in the table fulfils all four criteria.

Fricke *et al.* [246] in their 1925 study measured electrical resistance and capacity of calf blood at the frequency range from 800 Hz to 4.5 MHz using a custom two-electrode electrolytic cell [246, 247]. The effect of polarisation was mitigated by the use of the platinum electrodes coated in platinum black [246]. They found that at lower frequencies, which they specified as being from 3.6 kHz to 8.7 kHz, the resistance and the capacity of blood are frequency independent [246]. At frequencies from 8.7 kHz to 4.5 MHz however, they found that both resistance and capacity begin to decrease [246]. Hirsch *et al.* [248] and Texter *et al.* [249] used a similar two-electrode electrolytic cell with platinised platinum electrodes in their 1950 studies. They found that the conductivity of blood can be used to measure red cell counts [249]. They used a variable frequency oscillator operating at approximately 1 kHz, 5 kHz, 11 kHz and 19 kHz as their alternating current source [248].

Both Fricke *et al.* [246] and Hirsch *et al.* [248] stressed the importance of stirring blood samples before measuring the conductivity to ensure the homogeneity, as letting blood settle can increase conductivity.

In 1973, Geddes and Sandler [250] measured the specific resistance of human, canine, bovine and equine blood at 25 kHz, at body temperature with a Hct range extending from 0 to 0.7 l/l. They eliminated the electrode impedance errors by varying the length of their two-electrode measurement cell. They found the resistivity of blood increases with increasing haematocrit [250]. In a 1975 study by Mohapatra and Hill [251] it was confirmed that the resistivity of blood

Table 2.4: Overview of studies on the conductivity of blood: Highlighted fields fulfil one of the four criteria: a) human blood, b) at body temperature, c) at frequencies below 1 MHz and d) using the four-electrode technique. No study satisfies all four criteria.

Year	Study	Method	Frequency	Electrode polarisation	Species	Temperature [°C]	Blood count dependency
1925	Fricke and Morse [15]	Two-electrode electrolytic cell	(800 HZ) 87 kHz–4.5 MHz	Platinised platinum	Calf	21.6	
1950	Hirsch *et al.* [17]	Two-electrode glass conductivity cell	1075 Hz, 5.2 kHz, 11 kHz, 19 kHz	Platinised platinum, 5 kHz results reported	Human	30	Conductance decreasing with increase in red cell count
1973	Geddes and Sadler [19]	Two-electrode conductivity cell	25 kHz	Variable length	Human Canine Bovine Equine	37	Resistivity increasing with percentage haematocrit
1975	Mohapatra and Hill [20]	Two-electrode conductivity cell	100 kHz	Variable length	Human	22–40	Resistivity increasing with percentage haematocrit
1980	Hahn *et al.* [28]	Nine needle probe, two-electrode configuration	(0.1 MHz) 1 MHz–110 MHz (100 MHz)		Pig	34–36	
1993	Alison and Sheppard [24]	Waveguide system	29 GHz–90 GHz	N/A	Human	25, 37	
1993	Bevinget *al.* [21]	Four-electrode	200 kHz–10 MHz	Four-electrode technique	Human	25	
2002	Chelidze *et al.* [22]	Two-electrode	30 Hz–30 MHz	Platinised platinum Variable length	Human	22–28 (15–75)	

Table 2.4: Overview of studies on the conductivity of blood: Highlighted fields fulfil one of the four criteria: a) human blood, b) at body temperature, c) at frequencies below 1 MHz and d) using the four-electrode technique. No study satisfies all four criteria.

Year	Study	Method	Frequency	Electrode polarisation	Species	Temperature [°C]	Blood count dependency
2003	Jaspard *et al.* [23]	Open-ended coaxial probe	1 MHz–1 GHz	N/A	Cow Sheep	37	The conductivity increases in the whole frequency range when the haematocrit decreases
2008	Chang *et al.* [12]	Two-electrode (12 MHz - 100 MHz) Four-electrode (100 Hz–20 kHz)	100 Hz - 100 MHz	Four-electrode technique	Human	24	
2009	Gabriel *et al.* [13]	Four-electrode probe	40 Hz - 1 MHz	Four-electrode technique	Pig	37	
2011	Wolf *et al.* [25]	Parallel plate capacitor (1 Hz–10 MHz) Open-ended coaxial probe	1 Hz–40 GHz	Platinum coating	Human	37	
2017	Constantinou *et al.* [14]	Four-electrode technique	30 kHz–300 kHz	Four-electrode technique	Human	22	
2017	Salahuddin *et al.* [27]	Open-ended coaxial probe	400 MHz–20 GHz	N/A	Human	37	
2018	Santorelli *et al.* [26]	Open-ended coaxial probe	500 MHz–8.5 GHz	N/A	Human	24.1	Haemoglobin is the biggest predictor of changes in complex permittivity of blood

increases with an increase in haematocrit. The same study also shows resistivity increases with a decrease in temperature [251].

Beving *et al.* [252] in 1994 measured the dielectric properties of human blood at radiofrequencies (200 kHz–10 MHz) and investigated the dependence of the properties on cell volume fraction. Beving *et al.* [252] were using a four-electrode technique with the four electrodes being made of solid 24-carat gold pins in order to mitigate the effect of electrode polarisation. In 2002, Chelidze *et al.* [253] covered the frequency range from 30 Hz to 30 MHz. Chelidze *et al.* [253] used a two-electrode technique at lower frequencies. They excluded the effects of electrode impedance by using the platinised platinum electrodes and varying the distance between the electrodes [253]. Jaspard *et al.* [254] performed measurements on bovine and ovine blood at body temperature at frequencies from 1 MHz to 1 GHz in 2003. They used an open-ended coaxial probe method. They found that the dielectric properties of blood are strongly dependent on haematocrit [254]. The conductivity was found to decrease with the increase of haematocrit while the relative permittivity would increase with the increase of haematocrit [254].

In a 2008 study, Chang *et al.* [255] find the four-electrode technique superior to the two-electrode technique for accurate characterisation of blood impedance in the low-frequency range (100 Hz up to 20 kHz). The four-electrode technique also has been used to characterise the blood impedance by Gabriel *et al.* [191] in 2009 and Constantinou *et al.* [256] in 2017.

The study presented in *Chapter 4* employs the method that was used by Gabriel *et al.* in their 2009 study [191]. However, Gabriel *et al.* measured porcine blood in vivo while in this study the measurement was performed on human blood samples in vitro. This study, as far as existing knowledge suggests, is the first to measure the conductivity of:

- human blood,
- at body temperature (37°C),
- at frequencies below 1 MHz, and
- using the four-electrode technique.

2.5 Conclusion

AF is a prevalent medical condition frequently managed through electromagnetic-based catheter ablation techniques. The success of these treatments hinges on a deep understanding of the electrical properties of tissues. However, the current literature reveals notable gaps, which could compromise the accuracy and efficacy of these interventions. In this chapter, we have identified specific gaps in the areas of tissue conductivity, electrode-tissue interaction, and mathematical modelling of electrical properties. Consequently, we formulated the following research questions aimed at bridging these knowledge gaps:

- What are the dielectric properties of different regions of the heart at microwave frequencies ranging from 500 MHz to 20 GHz, and how does this knowledge contribute to the understanding of heart heterogeneity in the context of cardiac ablation?
- What is the conductivity of human blood across frequencies from 100 Hz to 100 kHz?
- What are the design features and capabilities of a miniaturised four-electrode probe for measuring the conductivity of biological tissues?

In the next chapter, the first research question is investigated.

3

Dielectric Characterisation of Cardiac Tissue as a Heterogeneous Organ

3.1 Introduction

In *Chapter 2*, the importance of obtaining accurate knowledge of the dielectric properties of biological tissues in dosimetry and medical applications was highlighted, particularly in the context of numerical simulations of radiofrequency and microwave ablation of the heart. Despite this need for accurate dielectric properties of tissue, previous studies have largely treated the heart as a homogeneous organ, neglecting variations in dielectric properties between different parts of the heart. To address this matter, this work aims to characterise the dielectric properties of different parts of the heart, both within and external to the heart across the frequency range of 500 MHz to 20 GHz. By utilising anatomical landmarks, specific parts such as the epicardium, endocardium, myocardium, exterior and interior surfaces of the atrial appendage, and the luminal surface of the great vessels were identified. Next, the relative permittivity and conductivity of these parts of

This chapter is based on a published journal paper [257] N. Ištuk et al., "Dielectric Properties of Ovine Heart at Microwave Frequencies," Diagnostics, vol. 11, no. 3, Art. no. 3, Mar. 2021, doi: 10.3390/diagnostics11030531. For consistency with the rest of this thesis, parts of the content are modified, and equations, figures, references, and tables are updated.

the heart were measured and compared to determine the presence of statistically significant variations between these parts of the heart. The obtained dielectric properties for each region were reported at two specific frequencies (915 MHz and 2.45 GHz) relevant to microwave medical applications, as well as in the form of parameters of a broadband Debye model [200].

3.2 Experimental Setup for Measurement of Dielectric Properties of the Heart at Microwave Frequencies

In this section, the method for measuring the dielectric properties of the heart at microwave frequencies is outlined. The procedure for calibrating and validating the setup is also described. Additionally, the preparation of the samples and the measurement procedure are documented.

3.2.1 Open-Ended Coaxial Probe Measurement Method

In line with best practices for dielectric characterisation of biological tissues, as was previously discussed in *Chapter 2*, all measurements in this work were collected using the open-ended coaxial probe method. The method is simple, requires minimum sample handling and is non-destructive [2]. The slim form open-ended coaxial probes from 85070E Dielectric Probe Kit (Keysight, Santa Rosa, CA, USA) were used in this study. The probes are suitable for both ex vivo and in vivo measurements over the frequency range of interest [2, 211, 258]. The open-ended coaxial probe method has been shown to be the most suitable method for measuring the dielectric properties of biological tissues in the microwave frequency range, with consideration given to factors such as temperature control of the tissue, time since excision, and measurement uncertainties [2]. The following sections describe the experimental setup, sample preparation, and data collection procedures.

3.2.1.1 Experimental Setup

Two VNAs were used to record the scattering parameter S_{11}: E8362B PNA (Agilent, now Keysight, Santa Rosa, CA, USA) (VNA1) and 5063A ENA (Keysight, Santa Rosa, CA, USA) (VNA2).

Scattering parameters, which are commonly referred to as S-parameters, are a parameter set that relates to the travelling power waves that are scattered or reflected by an n-port network [259]. For a one-port network, the concept of scattering parameters simplifies as it involves only the relationship between the incident and reflected power waves at a single port. S-parameters describe how power waves are scattered or reflected by an n-port network, and in the case of a one-port network, this relationship can be represented by a single S-parameter, S_{11}, which is known as the reflection coefficient. It relates the amplitude of the reflected wave (b_1) to the amplitude of the incident wave (a_1) at the port of the network as follows:

$$b_1 = S_{11} \cdot a_1, \tag{3.1}$$

where:

- a_1 is the amplitude of the incident power wave,
- b_1 is the amplitude of the reflected power wave,
- S_{11} is the reflection coefficient, indicating the proportion of the incident wave that is reflected by the network.

The S_{11} parameter of a network is equal to the ratio of the output voltage of the port to the voltage going into the port. The physical meaning of S_{11} is the input reflection coefficient with the output of the network terminated by a matched load ($a2 = 0$). The S_{11} represents how much power is reflected from the open-ended coaxial probe back to the Port 1 of the VNA when the probe is connected to the Port 1 of the VNA.

The S_{11} parameters were measured at different frequencies and then converted into complex permittivity values [2]. The two VNAs and two probes were used

to increase the measurement throughput by simultaneously conducting measurements on two heart samples, thus minimising the time between the excision and the measurements.

Both VNAs were set to record the S_{11} parameters at 101 discrete frequency points. The frequency points were distributed logarithmically over the frequency range from 200 MHz to 20 GHz for measurements performed with VNA1, and over the frequency range from 200 MHz to 8.5 GHz for VNA2. The logarithmic distribution of frequency points results in more accurate modelling of the measured data, especially at lower frequencies [260]. The frequency ranges were determined by the respective VNA operating frequencies and they both cover the most commonly used frequencies for MW ablation (915 MHz and 2.45 GHz [261]).

While data was acquired starting at 200 MHz, it has been reported that the operating frequency range of the open-ended coaxial probe starts at 500 MHz [262]. To overcome this mismatch, the results were filtered to exclude the measurements at frequencies from 200 MHz to 500 MHz. Therefore the final frequency range was 500 MHz–20 GHz in the case of VNA1 (81 points) and 500 MHz–8.5 GHz in the case of VNA2 (77 points). Despite the reduced number of points, it is believed there is still a sufficient number of points and that a Debye model could be fitted. Also, measurements at the key frequencies of 915 MHz and 2.45 GHz were not affected.

To eliminate noise from cable movement and reduce measurement uncertainty, both of the slim form open-ended coaxial probes from 85070E Dielectric Probe Kit (Keysight, Santa Rosa, CA, USA) were connected directly to the VNAs using a right-angle SubMiniature Version A (SMA) connector. The measurement setup with an open-ended coaxial probe connected to VNA2 can be seen in Fig. 3.1. To reduce movement of the measurement setup, tissues were placed on top of a lift table and brought into contact with the probe. While this method does exert some pressure on the VNA ports, it is a recommended compromise that has been validated by previous studies [2].

While the manufacturer recommends the probe should be inserted 5 mm into the material under test, this penetration depth was avoided in this study as it would cause damage to the tissue, resulting in the dielectric properties of the structurally damaged tissue. Instead, a direct contact between the tissue and the

probe has been considered to be adequate in numerous studies on dielectric properties of biological tissues [2, 239–241, 263, 264]. In these cases, direct contact was considered when the entire surface of the probe was in contact with the tissue sample. In order to make the entire surface of the probe contact the tissue sample some pressure needs to be applied between the probe and the tissue sample. Excessive probe-sample pressure can cause inaccurate measurements [2]. Therefore, a direct observation confirmed adequate probe contact. However, future work may consider improvements to assessing direct contact, such as pressure measurements.

The measured S_{11} parameters were converted to the dielectric properties using the N1500A Materials Measurement Suite (Keysight, Santa Rosa, CA, USA).

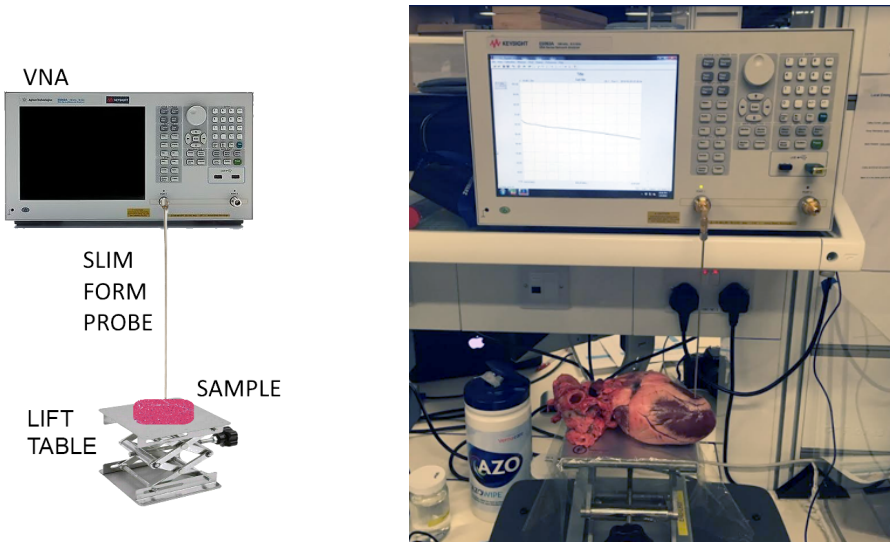

(a) **(b)**

Figure 3.1: Measurement setup showing a schematic (a) and a photo (b) of the measurement setup. VNA2 is directly connected to the slim form probe. The sample is brought in contact with the probe by lifting the lift table, which helps bring the sample into direct contact with the probe. The exclusion of the cable from the setup eliminates one source of measurement uncertainty.

3.2.1.2 Calibration and Validation

In order to correctly calculate the dielectric properties of the sample from the S_{11} parameter, we need the S_{11} value at the reference plane of the sample, which in this case is the open end of the probe. However, the VNA measures the S_{11} parameter at the port of the VNA. Therefore, to obtain the S_{11} parameter at the sample reference plane we need to do the de-embedding of the probe.

The measured S_{11} parameter also suffers from the instrument's systematic (repeatable) errors which should be corrected in the error correction procedure. Both the de-embedding of the probe and the error correction are done by the one-port calibration procedure [259].

In Fig. 3.2, Γ_m represents the measured value of S_{11} while the true value of S_{11} is represented by Γ. The four error coefficients are organised as S parameters of a fictitious network called the error matrix. The error matrix is represented by the error box which includes both the difference caused by measurements being made in the VNA plane instead of the plane of the sample and the instrument's systematic errors. The error coefficients can be written as [259]:

$$\begin{bmatrix} b_{m1} \\ a_1 \end{bmatrix} = \begin{bmatrix} e_{11} & e_{12} \\ e_{21} & e_{22} \end{bmatrix} \begin{bmatrix} a_{m1} \\ b_1 \end{bmatrix}, \tag{3.2}$$

From (3.2) we calculate the error-corrected reflection coefficient at the VNA plane as [259]:

$$\Gamma = \frac{\Gamma_m - e_{11}}{e_{22}\Gamma_m - \Delta}, \tag{3.3}$$

where Δ is $e_{11}e_{22} - e_{12}e_{21}$.

The error coefficients e_{11}, e_{22} and Δ are calculated from [259]:

$$\begin{bmatrix} 1 & -\Gamma_1\Gamma_{m1} & -\Gamma_1 \\ 1 & -\Gamma_2\Gamma_{m2} & -\Gamma_2 \\ 1 & -\Gamma_3\Gamma_{m3} & -\Gamma_3 \end{bmatrix} \begin{bmatrix} e_{11} \\ e_{22} \\ \Delta \end{bmatrix} = \begin{bmatrix} \Gamma_{m1} \\ \Gamma_{m2} \\ \Gamma_{m3} \end{bmatrix}. \tag{3.4}$$

This calibration process is completed by measuring materials with known or partially known characteristics and using these measurements to establish the measurement reference planes [265]. Calibration also corrects the imperfections

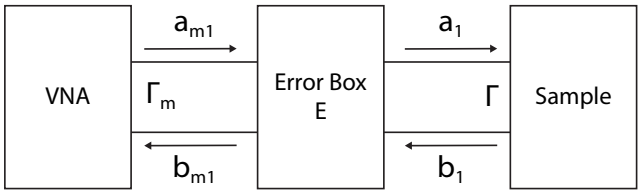

Figure 3.2: One-port calibration error box. Γ_m corresponds to the measured S_{11} and Γ is the true reflection coefficient at the sample reference plane [259].

of the measurement system, which include the nonideal nature of cables and probes as well as the internal characteristics of the VNA [265].

One-port calibration method [259] was used to correct the systematic errors of the instrument. The calibration was performed before the first measurement on each heart sample and was repeated approximately every 35 minutes to prevent any system drift affecting the subsequent measurements. The three standard loads used in the calibration procedure were open circuit, short circuit, and deionised water (DIW), which are commonly used in the literature [2]. The temperature of DIW was measured for every calibration using a digital thermometer. The temperature varied during the entire experiment from 23.5°C to 26.5°C.

Following calibration, a validation of the measurement system is typically performed [18]. In order to validate that the calibration was successful, dielectric measurements of a sample with known material properties are recorded [220, 266]. Then, the recorded data can be compared to the property values of the known material in the literature and the accuracy of the measurement can be calculated. If the accuracy is satisfactory (the exact required accuracy is study-dependent and evaluated on a case-to-case basis), then the sample under investigation can be measured with the confidence that the measurement equipment is performing accurately.

The validation was performed after each calibration. The validation was also performed each time the part of the heart that was being measured was changed. Typical material/solutions used for validation are standard liquids, such as deionised water, saline solution, or methanol [2, 220].

Table 3.1: The mean and the maximum value of the validation error across all frequency points, in percentage. The mean error is the mean across all 99 validation measurements (with 81 or 77 frequency points per measurement, 99×81 points in the case of VNA 1 and 99×77 points in the case of VNA 2). Similarly, the maximum error is the maximum taken across all validation measurements.

	Mean Error (±SD) [%]	**Maximum Error [%]**
Relative permittivity	1.36 ± 0.83	4.92
Conductivity	1.78 ± 0.65	3.64

In this study, the standard liquid used was 0.9% sodium chloride (NaCl) in aqueous solution. The 0.9% aqueous NaCl solution has similar dielectric properties as high water content tissues [267]. Heart tissue was considered to be a high-water tissue in this work. The dielectric properties and the temperature of the NaCl solution were measured. Recorded temperatures during validation experiments exhibited a narrow range from 23.6°to 25.7°, suggesting a minimal thermal influence on dielectric measurements.

The dielectric model for the NaCl solution was obtained from the literature [268] and was calculated for the given concentration and temperature over the desired frequency range. The mean error over all frequencies between the results of the validation measurement and values obtained from the model was considered the validation error for that particular validation measurement. The validation error was calculated separately for the relative permittivity and conductivity. The mean and maximum validation errors across 99 validations are reported in Table 3.1. The difference between the validation measurement and the model was on average 1.36% in relative permittivity and 1.78% in conductivity resulting in a high degree of confidence in accurate measurement of the dielectric properties with the experimental setup.

3.2.2 Preparation of Cardiac Tissue Samples

To obtain samples for measurement, thoracic contents were collected from four sheep (labelled A1-A4). The thoracic contents were collected immediately after humane euthanasia, which was performed using a captive bolt and carotid artery dissection. All animal tissues were sourced from a commercial abattoir in

compliance with Irish and EU law, and the study was conducted in accordance with ethical guidelines at the University of Galway. The use of ex-vivo tissues in place of live animals is considered a replacement method in accordance with the 3Rs principles for humane research (Replace, Reduce, Refine) [269]. The excised thoracic contents were placed in an airtight container to limit tissue dehydration. The hearts were then dissected and the blood was drained by dissecting the carotid artery. The times of excision, dissection, and measurement were recorded. The time from excision to the first measurement was approximately 4 hours and the time from excision to the last measurement was approximately 8.5 hours. The hearts were dissected from the rest of the thoracic contents directly before the beginning of the measurements. The time of heart dissection from the thoracic content was considered to be the same as the time of the first measurement, as the measurement occurred within one minute of dissection.

The blood was drained to mitigate the potential impact of blood perfusion on dielectric properties.

In Fig. 3.3, two hearts (A1 on the left, A2 on the right) are shown to illustrate differences in the size and shape of the heart and the amount of pericardial fat. Heart A2 has notably less fat, and parts of the epicardium may be covered with a thin layer of fat that can be difficult to discern. Care must be taken to avoid measuring a combination of epicardium and fat, as dielectric measurements can be highly sensitive to tissue heterogeneity [264].

3.2.3 Measurement Procedure

A total of 19 distinct locations on the heart were identified by a veterinarian, based on the anatomy and function of the heart. Measurements were conducted at each location by moving the probe slightly (2-5 mm) between each measurement in order to obtain repeatable results for a given region. However, measurements performed on the mitral and tricuspid valves did not yield consistent results, possibly due to the small size of the valves, and thus were omitted from the analysis.

The measurement results from the remaining 17 locations were grouped into six categories according to the part of the heart they belonged to epicardium,

Figure 3.3: Two heart samples from A1 (**left**) and A2 (**right**). The hearts differ in size, shape, and amount of pericardial fat covering the epicardium. The pericardial fat extends around the whole heart, presenting a challenge when measuring the dielectric properties of the tissues on the exterior surface.

myocardium, endocardium, the exterior surface of the atrial appendage, the interior surface of the atrial appendage, and the luminal surface of the great vessels. Fig. 3.4 provides a schematic of the 17 measurement locations, each belonging to one of the six categories based on the location and nature of the cardiac tissue. The total number of measurements on a specific part of the heart was determined by multiplying the number of repeated measurements on each location (15 measurements per location) by the number of locations that corresponded to that part of the heart.

After measurements on the exterior of the heart samples were completed, a series of transverse sections of the heart were performed to access the endocardium of the ventricles and the myocardium. Fifteen measurements were conducted on the interior surface of the left atrium and 15 measurements were conducted on the interior surface of the right atrium. The dielectric properties of the myocardium were measured on the septum of the heart sample (15 measurements).

Further transverse sections were performed at the level of the atria and 15 measurements were conducted on the endocardium of the left atria and 15 mea-

surements were conducted on the endocardium of the right atria. The measurements on the vessels were performed on the luminal surface of the four great vessels of the heart: the aorta, pulmonary artery, pulmonary vein, and the vena cava (15 measurements on each for a total of 60 measurements). The luminal surfaces were accessed using longitudinal cuts across vessel walls. This procedure was repeated for each of the four heart samples, resulting in a total of 1,020 measurements with 17 locations on the four heart samples measured 15 times each. Table 3.2 provides an overview of the distribution of measurements across different parts of the heart.

The temperature of the tissue was recorded at the point of contact with the probe before the first measurement and after the last measurement for that particular location. A Fluke 62 MAX+ (Fluke, Everett, WA, USA) infrared thermometer was used to measure the temperature. The minimum temperature of the tissue measured was 23.7°C and the maximum temperature was 25.6°C. The temperature of the room was controlled during the measurements at 25°C. The observed marginal temperature variation implies a negligible effect on measurement outcomes.

3.2.4 Data Collection, Modelling, and Statistical Analysis

In this study, the data collected from the vector network analyzers (VNAs) were analysed to determine the complex permittivity of the samples at each frequency point. The data collection and analysis adhered to the Minimum information for dielectric measurements of biological tissues (MINDER) guidelines for reporting of dielectric data of biological tissues [266]. The dielectric properties data and metadata were made available online following the FAIR principles [270] and can be accessed through the online dielectric properties database [271].

To facilitate the incorporation of the dielectric data in the simulation of exposure situations and the calculation of internal fields within the human body, it is convenient to express frequency dependence of dielectric properties as parametric mathematical models [181]. The two most commonly used parametric models of dielectric properties are the Cole-Cole model and Debye model [185, 200, 272, 273]. The Cole-Cole model is considered the most reliable fitting tool to describe

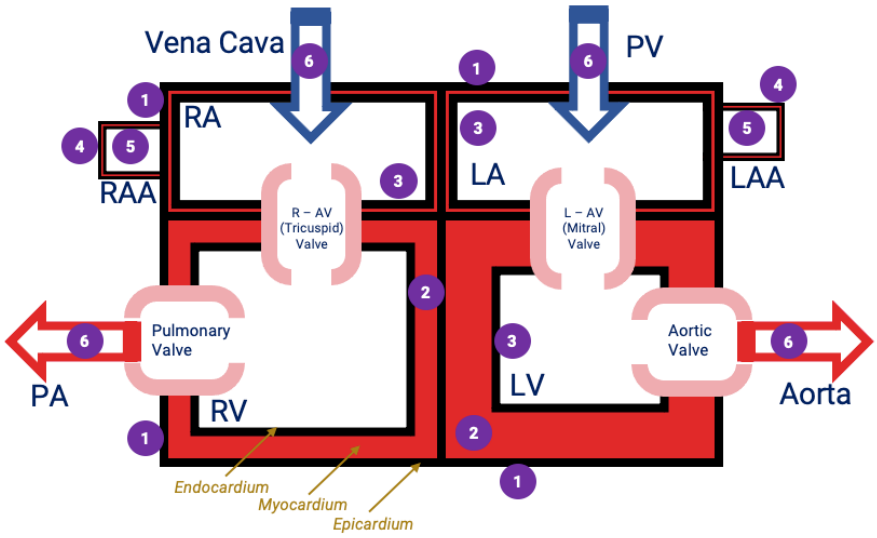

Figure 3.4: Schematic of measurement locations. Seventeen distinct locations were selected on the ovine heart, with 15 measurements taken at each location. These locations were divided into 6 groups: (1) epicardium, (2) endocardium of the right atrium, (3) endocardium of the left atrium, (4) the exterior surface of the left atrial appendage, (5) the interior surface of the left atrial appendage and (6) the luminal surface of the great vessels. These groupings 1-6 are shown in the figure, with each group represented by a different colour. The locations include the right atrium (RA), left atrium (LA), right ventricle (RV), left ventricle (LV), right atrioventricular valve (R–AV Valve), left atrioventricular valve (L–AV Valve), pulmonary artery (PA), pulmonary vein (PV), right atrial appendage (RAA), and left atrial appendage (LAA). The aim of measuring at different locations was to study the variations in dielectric properties across different parts of the heart, in order to gain a more accurate understanding of the dielectric characteristics of the organ.

Table 3.2: The number of measurements taken on various parts of the heart. The measurements were taken at seventeen locations (listed in regular text) that were grouped into six groups (listed in bold). The table provides an overview of the distribution of measurements across different parts of the heart.

	A1	**A2**	**A3**	**A4**	**Total**
Epicardium	**60**	**60**	**60**	**60**	**240**
Epicardium (Left Ventricle)	15	15	15	15	60
Epicardium (Right Ventricle)	15	15	15	15	60
Epicardium (Left Atrium)	15	15	15	15	60
Epicardium (Right Atrium)	15	15	15	15	60
Myocardium	**15**	**15**	**15**	**15**	**60**
Endocardium	**60**	**60**	**60**	**60**	**240**
Endocardium (Left Ventricle)	15	15	15	15	60
Endocardium (Right Ventricle)	15	15	15	15	60
Endocardium (Left Atrium)	15	15	15	15	60
Endocardium (Right Atrium)	15	15	15	15	60
Atrial Appendage Exterior Surface	**30**	**30**	**30**	**30**	**120**
Left Atrial Appendage Exterior Surface	15	15	15	15	60
Right Atrial Appendage Exterior Surface	15	15	15	15	60
Atrial Appendage Interior Surface	**30**	**30**	**30**	**30**	**120**
Left Atrial Appendage Interior Surface	15	15	15	15	60
Right Atrial Appendage Interior Surface	15	15	15	15	60
Great Vessels	**60**	**60**	**60**	**60**	**240**
Pulmonary Artery	15	15	15	15	60
Pulmonary Vein	15	15	15	15	60
Vena Cava	15	15	15	15	60
Aorta	15	15	15	15	60
Total	**225**	**225**	**225**	**225**	**1020**

tissue dielectric properties, but it is not the most ideal for efficient numerical computation of EM fields [274]. On the contrary, the Debye model permits very fast computation and can easily be expressed in both time and frequency domains, but it is not adequate to describe the tissue dispersion in the whole frequency spectrum [272, 274]. However, it has been demonstrated that for a large class

of actual wideband sources, the Debye model is sufficiently accurate by retaining fast time and efficiency for EM field calculations [274] and therefore, it was used in this study.

The Debye model [200] is defined as:

$$\hat{\varepsilon} = \varepsilon_\infty + \sum_{p=1}^{n} \frac{\Delta\varepsilon_p}{1 + j\omega\tau_p} + \frac{\sigma_s}{j\omega\varepsilon_0}, \tag{3.5}$$

where τ_p is the relaxation constant of pth dispersion, ω is angular frequency, ε_∞ is the permittivity at frequencies where $\omega\tau_p \gg 1$, σ_s is the static ionic conductivity, ε_p is the magnitude of pth dispersion and ε_0 is the permittivity of free space.

In this study, the mean of the measurements of all measured parts of the heart for each of the four heart samples in this study was fitted to a three-pole Debye model using the least squares method [187]. This approach is the most common one to obtain the best parameters for the model [181]. The fit error between the mean of the measured data and the resulting Debye model for each region of the heart was calculated and is reported with the results in the Results and Discussion section.

The results for relative permittivity and conductivity at selected single frequencies (915 MHz and 2.45 GHz) are presented with mean and standard deviation (SD). One-way analysis of variance test (one-way ANOVA) was used to compare the mean permittivity and mean conductivity values for each part of the heart. This was repeated for each of the four hearts. A separate test was performed for each of the 4 heart samples for a total of 4 tests. The one-way ANOVA compares the means between the groups and determines whether any of those means are significantly different from each other. Specifically, the one-way ANOVA tests the null hypothesis:

$$H_0 : \mu_1 = \mu_2 = \mu_3 = ... = \mu_k \tag{3.6}$$

where μ is group mean and k is number of groups. If, however, the one-way ANOVA returns a statistically significant result, the null hypothesis (H_A) is rejected, which means that not all means are statistically significantly different from each other. A p value of <0.01 was considered statistically significant [275].

3.3 Results and Discussion

3.3.1 Dielectric Properties of the Heart as a Heterogeneous Organ and Comparison with the Literature

In this study, the dielectric properties of ovine heart samples were measured and analysed. Fig. 3.5 displays the results of the measurements, which were performed on four ovine heart samples and six different parts of the heart. The results are presented as the mean of individual measurements on each part of the heart. The shaded area represents the mean ± two standard deviations, defined as the confidence interval. The average temperature of the tissue during the measurements was 23.5°C (±0.9°C). For comparison, a model from Gabriel et al. [273, 276, 277] and data from Gabriel et al. for human tissue at 37°C are also shown in the figure. We compared the data with the dielectric properties of the heart reported by Gabriel *et al.* [273], which forms the basis of two most widely used literature databases on the dielectric properties of tissues [277, 278].

The differences between the data measured in this study and the data from Gabriel et al. [207] can be attributed to several factors, including variations between species, temperature of the tissue, level of hydration, and variability between different parts of the organ.

Firstly, the data in this study were acquired at room temperature (between 21.7 and 25.6°C), whereas all measurements reported by Gabriel *et al.* [273] were acquired at body temperature (37°C). In historical dielectric studies, to measure tissue at body temperatures, the same is normally heated. The exact method used in Gabriel *et al.*[273] is not reported. In this study the decision was made to avoid heating the tissue, which could impact tissue dehydration and lead to non-representative measurements, despite the fact that dielectric properties are temperature-dependent and measuring at body temperature would be more representative [186, 279–281]. Consequently, it must be noted that the dielectric properties reported herein reflect room temperature conditions and may not correspond precisely to physiological temperatures within the human body. Further quantitative analysis is required to assess the temperature-dependence of dielectric properties to extrapolate these findings to clinical settings accurately.

Measuring at room temperature was chosen to avoid the need to reheat the tissue. Secondly, it is possible that there is inter-species variation in the dielectric properties of the heart, but the differences between animal and human species are not systematic and the variation in tissue properties within a species may exceed variations between species [236]. Thirdly, the time from excision to measurements was approximately 4 hours in this study, while the Gabriel *et al.* study did not specify the time from excision to measurements. However, despite these factors that could have impacted the differences between the measurements, this study still provides valuable insights into the comparison of dielectric properties variation in heart tissue at room temperature. The focus of this research is to examine the variability of the heart, with the expectation that the observed trends would persist across a spectrum of temperatures, encompassing both room and physiological conditions. However, without quantitative analysis of temperature effects, further research is needed to clarify the temperature effect and ensure accurate modelling.

In order to evaluate the impact of tissue dehydration on the measurement results, Fig. 3.6 presents the measurements of relative permittivity at 2.45 GHz, a frequency commonly used for microwave thermal ablation [261]. The data points are plotted against the time elapsed from tissue excision in minutes, as tissue dehydration could potentially lead to a decrease in relative permittivity over time [282]. However, the analysis revealed that there was no noticeable trend in the changes in dielectric properties with respect to time from excision. The data points are closely grouped together without many outliers. The data analysed suggests a minimal influence of tissue dehydration on the outcomes, although this claim would benefit from further quantitative substantiation to ascertain its validity across different experimental conditions.

Table 3.3 and Table 3.4 show the relative permittivity and conductivity for each part of the heart for all four ovine heart samples at 915 MHz and 2.45 GHz respectively. The results at these particular frequencies are suitable for modelling MW ablative technologies, which often operate at 915 MHz and 2.45 GHz [98–101]. These results as presented in Table 3.3 and Table 3.4 are suitable for use in single-frequency numerical simulations, where each part of the heart dielectric properties can be set using single frequency values for relative permittivity and

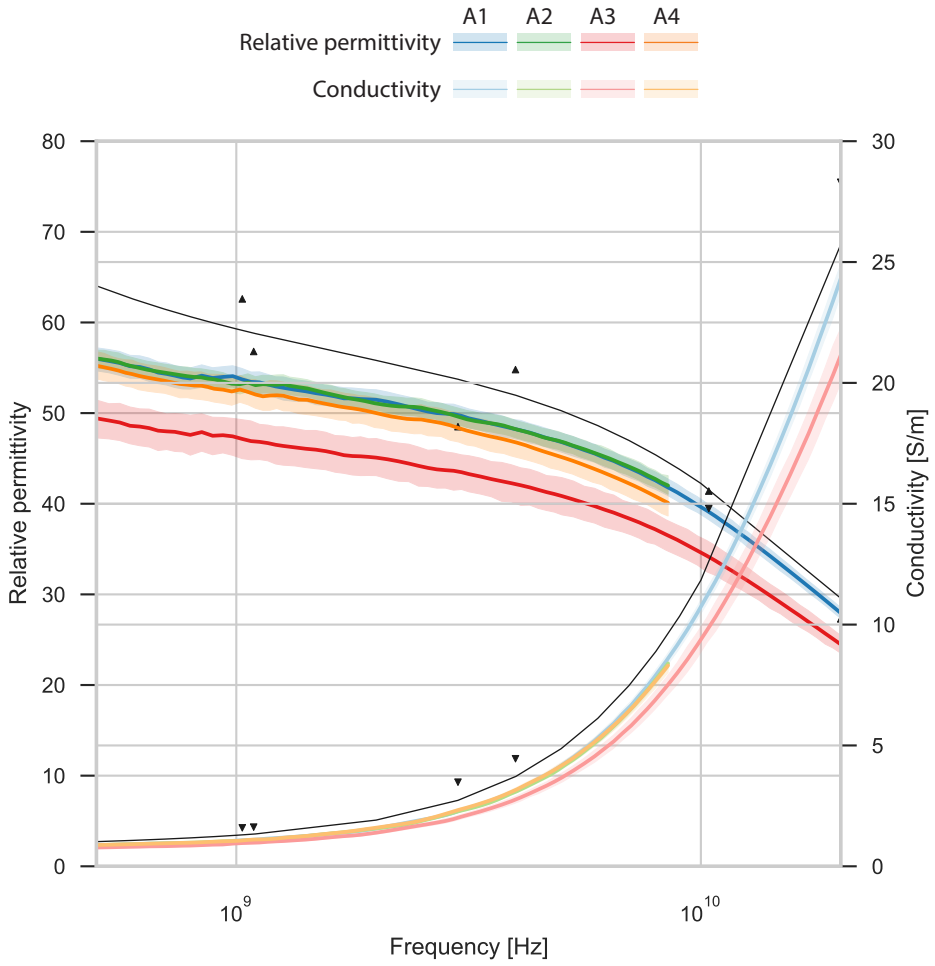

a) Epicardium

Figure 3.5: Dielectric properties of six parts of the heart in this study. Each plot shows the relative permittivity and conductivity for each part of the heart. Each of the colours corresponds to one of the hearts: A1 is blue, A2 is green, A3 is red and A4 is orange. Darker lines are the relative permittivity and lighter lines are the conductivity. The measurement results plotted with the green and the orange lines are measured with the E5063A VNA. The measurement results plotted with the blue and red lines represent the measurements performed with the E8362B VNA. Each line is plotted with the corresponding mean ± 2 standard deviations confidence interval. The thin black lines are the model for the relative permittivity and conductivity of the heart muscle from the literature [181, 273, 277]. The model is based on the data from experimental studies on several different species. The triangle markers are the data points from measurements on human tissues from Gabriel *et al.* 1996 study [207], which did not differentiate between different tissue types.

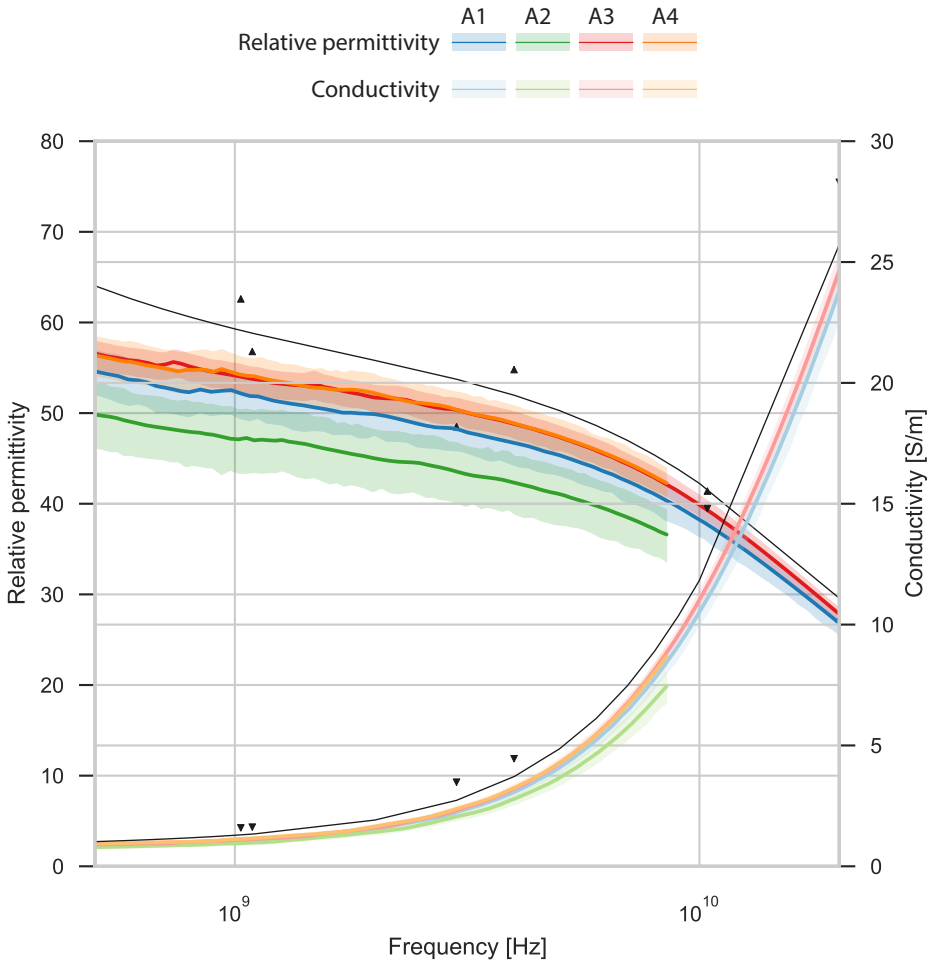

b) Atrial Appendage (Exterior Surface)

Figure 3.5: Dielectric properties of six parts of the heart in this study. Each plot shows the relative permittivity and conductivity for each part of the heart. Each of the colours corresponds to one of the hearts: A1 is blue, A2 is green, A3 is red and A4 is orange. Darker lines are the relative permittivity and lighter lines are the conductivity. The measurement results plotted with the green and the orange lines are measured with the E5063A VNA. The measurement results plotted with the blue and red lines represent the measurements performed with the E8362B VNA. Each line is plotted with the corresponding mean $\pm$ 2 standard deviations confidence interval. The thin black lines are the model for the relative permittivity and conductivity of the heart muscle from the literature [181, 273, 277]. The model is based on the data from experimental studies on several different species. The triangle markers are the data points from measurements on human tissues from Gabriel *et al.* 1996 study [207], which did not differentiate between different tissue types.

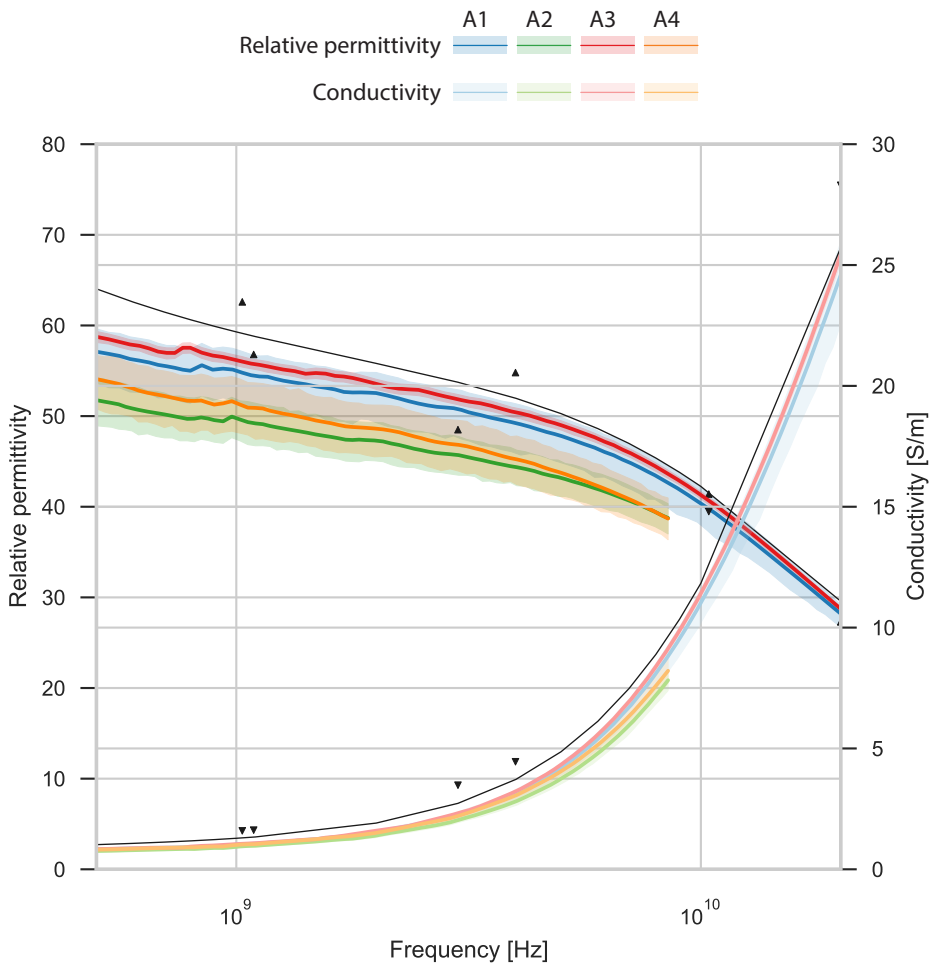

c) Myocardium

Figure 3.5: Dielectric properties of six parts of the heart in this study. Each plot shows the relative permittivity and conductivity for each part of the heart. Each of the colours corresponds to one of the hearts: A1 is blue, A2 is green, A3 is red and A4 is orange. Darker lines are the relative permittivity and lighter lines are the conductivity. The measurement results plotted with the green and the orange lines are measured with the E5063A VNA. The measurement results plotted with the blue and red lines represent the measurements performed with the E8362B VNA. Each line is plotted with the corresponding mean ± 2 standard deviations confidence interval. The thin black lines are the model for the relative permittivity and conductivity of the heart muscle from the literature [181, 273, 277]. The model is based on the data from experimental studies on several different species. The triangle markers are the data points from measurements on human tissues from Gabriel *et al.* 1996 study [207], which did not differentiate between different tissue types.

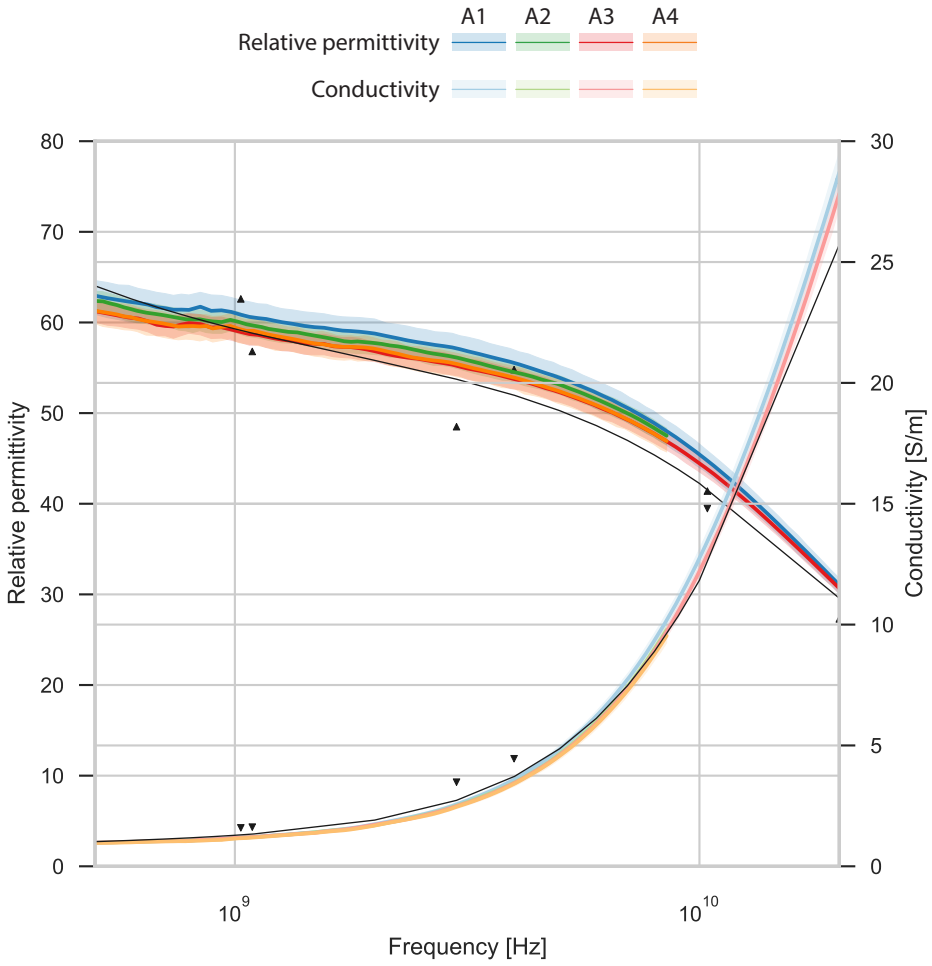

d) Endocardium

Figure 3.5: Dielectric properties of six parts of the heart in this study. Each plot shows the relative permittivity and conductivity for each part of the heart. Each of the colours corresponds to one of the hearts: A1 is blue, A2 is green, A3 is red and A4 is orange. Darker lines are the relative permittivity and lighter lines are the conductivity. The measurement results plotted with the green and the orange lines are measured with the E5063A VNA. The measurement results plotted with the blue and red lines represent the measurements performed with the E8362B VNA. Each line is plotted with the corresponding mean $\pm$ 2 standard deviations confidence interval. The thin black lines are the model for the relative permittivity and conductivity of the heart muscle from the literature [181, 273, 277]. The model is based on the data from experimental studies on several different species. The triangle markers are the data points from measurements on human tissues from Gabriel *et al.* 1996 study [207], which did not differentiate between different tissue types.

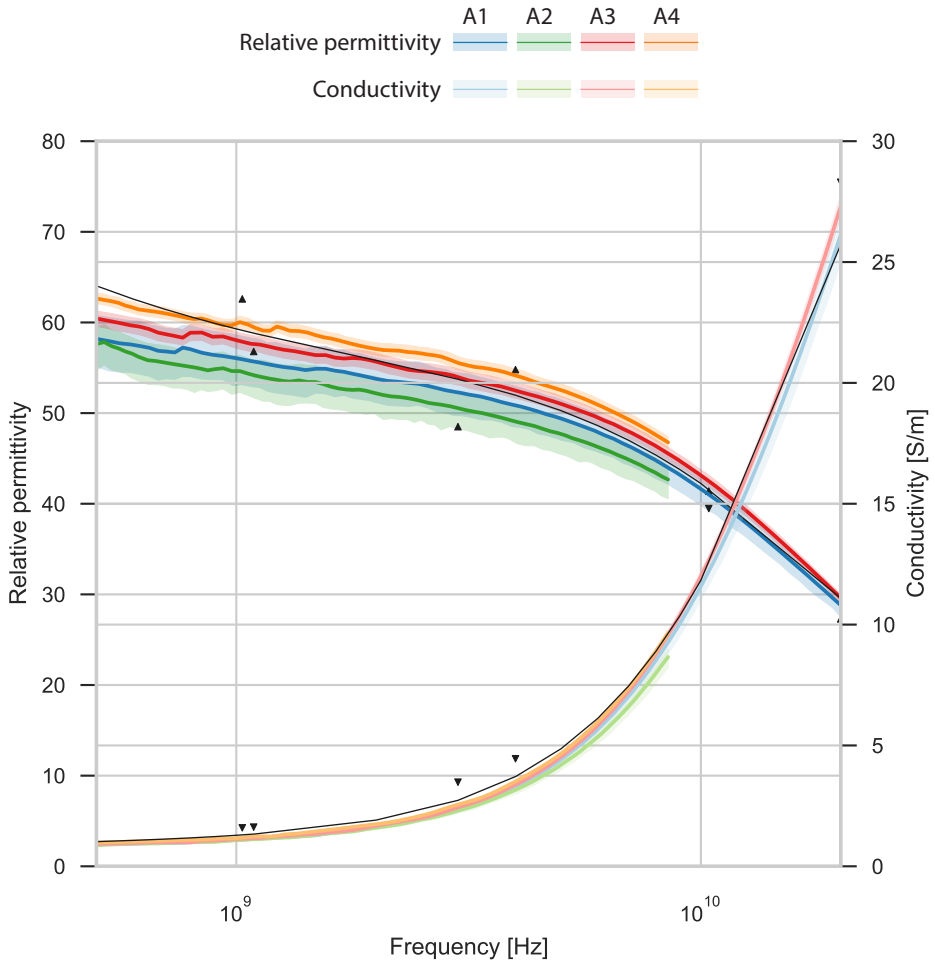

e) Atrial Appendage (Interior Surface)

Figure 3.5: Dielectric properties of six parts of the heart in this study. Each plot shows the relative permittivity and conductivity for each part of the heart. Each of the colours corresponds to one of the hearts: A1 is blue, A2 is green, A3 is red and A4 is orange. Darker lines are the relative permittivity and lighter lines are the conductivity. The measurement results plotted with the green and the orange lines are measured with the E5063A VNA. The measurement results plotted with the blue and red lines represent the measurements performed with the E8362B VNA. Each line is plotted with the corresponding mean ± 2 standard deviations confidence interval. The thin black lines are the model for the relative permittivity and conductivity of the heart muscle from the literature [181, 273, 277]. The model is based on the data from experimental studies on several different species. The triangle markers are the data points from measurements on human tissues from Gabriel *et al.* 1996 study [207], which did not differentiate between different tissue types.

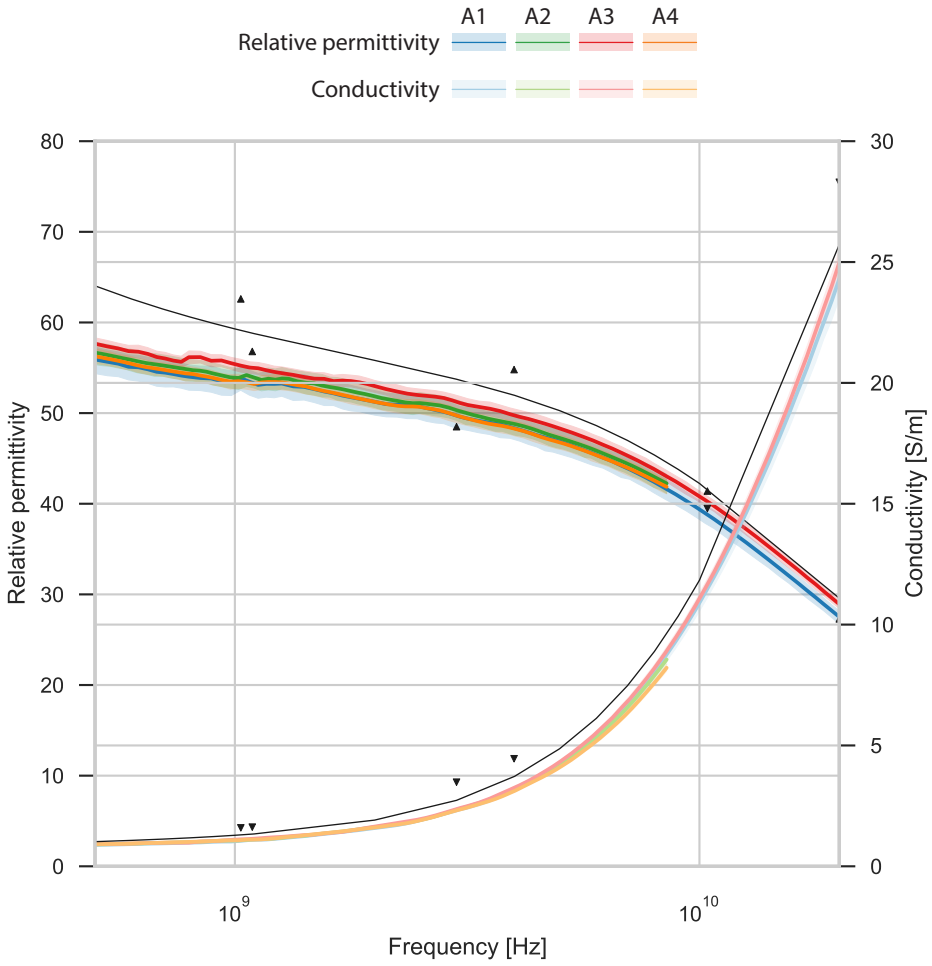

f) Great Vessel (Luminal Surface)

Figure 3.5: Dielectric properties of six parts of the heart in this study. Each plot shows the relative permittivity and conductivity for each part of the heart. Each of the colours corresponds to one of the hearts: A1 is blue, A2 is green, A3 is red and A4 is orange. Darker lines are the relative permittivity and lighter lines are the conductivity. The measurement results plotted with the green and the orange lines are measured with the E5063A VNA. The measurement results plotted with the blue and red lines represent the measurements performed with the E8362B VNA. Each line is plotted with the corresponding mean $\pm$ 2 standard deviations confidence interval. The thin black lines are the model for the relative permittivity and conductivity of the heart muscle from the literature [181, 273, 277]. The model is based on the data from experimental studies on several different species. The triangle markers are the data points from measurements on human tissues from Gabriel *et al.* 1996 study [207], which did not differentiate between different tissue types.

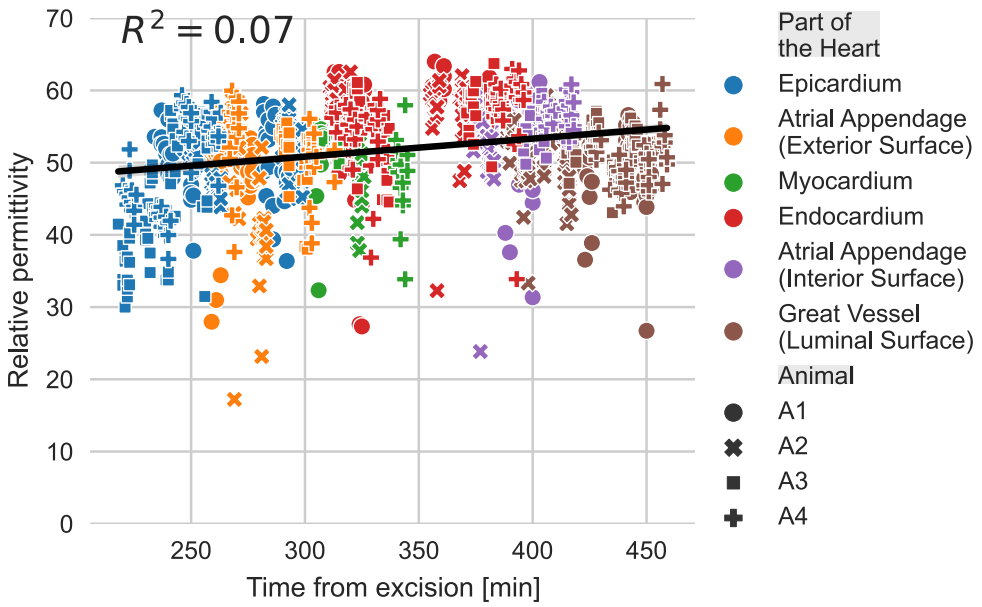

Figure 3.6: Relative permittivity measurements at a single frequency (2.45 GHz) versus time from excision in minutes. Marker colours represent different parts of the heart, while marker shapes denote measurements taken on different hearts. No obvious trend was observed ($R^2 = 0.07$) in the changes of dielectric properties relative to time from excision, suggesting that dehydration of the tissue over time was not considerable enough to affect the dielectric properties of the heart over time.

conductivity. The values are given as the mean of all measurements for each part of each of the hearts.

Table 3.3: The values of the relative permittivity and conductivity of different parts of the heart at 915 MHz. The values are given as mean and SD for a particular part of the heart. These values that are specific to a particular part of the heart can be used in single frequency numerical simulations.

Animal	Part of the Heart	ε_r	SD (ε_r)	σ [S/m]	SD (σ) [S/m]
A1	Atrial Appendage (Interior Surface)	56.30	7.86	1.06	0.15
A2		54.95	6.28	1.04	0.12
A3		58.46	2.54	1.08	0.05
A4		59.71	1.83	1.15	0.06
A1	Atrial Appendage (Exterior Surface)	52.46	7.04	0.99	0.14
A2		47.39	9.92	0.94	0.21
A3		54.40	4.31	1.06	0.07
A4		54.87	6.18	1.08	0.15
A1	Endocardium	61.34	7.27	1.13	0.17
A2		60.05	4.63	1.12	0.10
A3		59.47	4.61	1.13	0.10
A4		59.52	5.46	1.09	0.13
A1	Epicardium	53.99	4.83	1.00	0.10
A2		53.49	3.76	1.03	0.07
A3		47.56	8.33	0.90	0.16
A4		52.58	6.22	1.03	0.10
A1	Myocardium	55.23	6.23	0.97	0.12
A2		49.42	4.80	0.88	0.09
A3		56.52	1.18	1.01	0.02
A4		51.41	6.22	0.94	0.11
A1	Great Vessel (Luminal Surface)	53.50	5.54	1.02	0.10
A2		54.16	4.65	1.06	0.10
A3		55.81	2.69	1.07	0.06
A4		53.66	3.03	1.06	0.07

At 915 MHz, the values for relative permittivity range from 47.39 for the atrial appendage (exterior surface) of A2, to 61.34 for the endocardium of A1 (a 29.4% relative difference). The conductivity values range from 0.88 S/m measured on the myocardium of A2, to 1.15 S/m, as measured on the atrial appendage (interior surface) of A4 (approximately a 30.7% relative difference). All the values in the table are given with the SD. The SD in relative permittivity was between 1.18 and 9.92, and in conductivity between 0.02 S/m and 0.35 S/m. The one-way ANOVA tests the null hypothesis that the mean values of all parts of the heart

Table 3.4: The values of the relative permittivity and conductivity of six measured parts of the heart at 2.45 GHz. The values are given as mean and SD for a particular part of the heart. These values that are specific to a particular part of the heart can be used in single frequency numerical simulations.

Animal	Part of the Heart	ε_r	SD (ε_r)	σ [S/m]	SD (σ) [S/m]
A1	Atrial Appendage (Interior Surface)	53.23	6.80	1.94	0.28
A2		51.51	5.94	1.87	0.22
A3		54.65	2.54	1.98	0.10
A4		56.68	1.98	2.03	0.09
A1	Atrial Appendage (Exterior Surface)	48.84	6.50	1.86	0.27
A2		44.56	9.40	1.64	0.35
A3		51.11	4.11	1.93	0.15
A4		51.19	5.74	1.91	0.24
A1	Endocardium	57.83	6.73	2.10	0.28
A2		57.03	4.42	2.02	0.18
A3		56.01	4.38	2.04	0.18
A4		56.14	5.31	1.99	0.23
A1	Epicardium	50.41	4.39	1.90	0.17
A2		50.69	3.91	1.80	0.12
A3		44.18	8.22	1.68	0.29
A4		49.31	6.28	1.83	0.17
A1	Myocardium	51.38	5.60	1.87	0.23
A2		46.40	4.22	1.67	0.17
A3		52.89	1.13	1.90	0.04
A4		47.76	5.54	1.81	0.19
A1	Great Vessel (Luminal Surface)	50.79	5.29	1.88	0.20
A2		51.10	4.55	1.85	0.17
A3		52.00	2.77	1.93	0.09
A4		50.73	3.08	1.83	0.10

are equal. The hypothesis is rejected with $p < 0.01$ for all tests.

At 2.45 GHz, the values for relative permittivity range from 44.18 for the epicardium of A3, to 57.83 for the endocardium of A1 (26% relative difference). The conductivity values range from 1.64 S/m measured on the exterior surface of the appendage of A2, to 2.10 S/m, as measured on the endocardium of A1 (25% relative difference). The standard deviation in relative permittivity was between 1.13 and 9.40 and in conductivity between 0.04 S/m and 0.35 S/m. The one-way ANOVA tests the null hypothesis is that the mean values of all parts of the heart are equal. The hypothesis is rejected with $p < 0.01$ for all tests.

This analysis shows that at these selected frequencies (915 MHz and 2.45

Table 3.5: The mean and the maximum value of the fit error in percentage. Error for the fit of each of the six parts of the heart for each of the four heart measurements is calculated as the mean value across all frequency points. The mean error is the mean across all parts of each of the hearts. The maximum error is the maximum across all parts of each of the hearts.

	Mean Error [%]	**Maximum Error** [%]
Relative permittivity	0.35	0.51
Conductivity	0.61	0.75

GHz) not all parts of the heart have the same dielectric properties.

3.3.2 Debye Models

To support computer modelling, a broadband three-pole Debye model is fitted to the mean of the measurement data. The parameters of the three-pole Debye model fitted to the mean of the measurement data were obtained using the least squares method and are presented in Table 3.6. The table includes the parameters for each part of the heart, as determined from measurements on four ovine heart samples. These parameters can be used in broadband simulation scenarios, within the frequency range that the models were fitted and verified.

To verify the accuracy of the models, the mean percentage difference between the mean of the measurement data and the model was calculated across all frequency points. This mean difference, referred to as the fit error, is presented in Table 3.5. The results indicate that the fit error is low, with the poorest observed error being 0.51% for relative permittivity and 0.75% for conductivity. These small errors suggest a good fit between the measurement data and the model.

3.4 Conclusions

In *Chapter 3*, the objective was to characterise the dielectric properties across various regions of the heart within the microwave frequency range of 500 MHz to 20 GHz. This analysis aimed to enhance our understanding of the heterogeneity of the heart, particularly in the context of cardiac ablation.

Table 3.6: Three-pole Debye model parameters fitted to the mean permittivity of measurements on different parts of the heart. Each part was measured on four different hearts and is therefore represented by four sets of Debye model parameters. The model parameters for A1 and A3 are verified at frequencies from 500 MHz to 20 GHz. The parameters for A2 and A4 are verified at the frequency range from 500 MHz to 8.5 GHz. These models are suitable for use in broadband numerical simulation scenarios over the respective frequency ranges.

Animal	**Part of the Heart**	ε_∞	σ_s [S/m]	$\Delta\varepsilon_1$	τ_1 [ns]	$\Delta\varepsilon_2$	τ_2 [ns]	$\Delta\varepsilon_3$	τ_3 [ns]
A1	Atrial Appendage (Interior Surface)	6.86	0.741	7.23	0.34	4.79	4.01×10^{-2}	43.27	8.05×10^{-3}
A2		13.02	0.263	137.91	2.15	4.32	1.01×10^{-1}	37.74	1.01×10^{-2}
A3		7.12	0.426	88.09	1.77	4.84	7.89×10^{-2}	46.33	8.38×10^{-3}
A4		12.71	0.210	244.73	3.03	4.59	8.59×10^{-2}	42.98	9.64×10^{-3}
A1	Atrial Appendage (Exterior Surface)	7.00	0.373	72.86	1.39	4.95	6.10×10^{-2}	39.72	8.20×10^{-3}
A2		11.60	0.323	96.24	2.02	4.30	8.44×10^{-2}	31.89	9.96×10^{-3}
A3		7.48	0.690	11.34	0.42	4.78	4.17×10^{-2}	40.64	8.16×10^{-3}
A4		14.40	0.704	19.93	0.97	3.97	8.51×10^{-2}	36.31	1.07×10^{-2}
A1	Endocardium	7.53	0.124	311.85	3.41	4.70	6.24×10^{-2}	48.61	8.41×10^{-3}
A2		13.38	0.626	44.30	1.31	3.51	9.77×10^{-2}	43.37	1.00×10^{-2}
A3		7.36	0.734	17.80	0.74	4.36	6.57×10^{-2}	47.12	8.20×10^{-3}
A4		14.22	0.433	170.62	3.31	3.97	1.06×10^{-1}	41.88	1.02×10^{-2}
A1	Epicardium	7.70	0.439	63.45	1.40	5.13	6.42×10^{-2}	40.64	8.21×10^{-3}
A2		12.71	0.154	254.62	3.34	4.40	8.30×10^{-2}	36.84	9.62×10^{-3}
A3		6.74	0.550	14.43	0.54	4.49	4.97×10^{-2}	34.95	8.06×10^{-3}
A4		14.75	0.141	207.25	2.64	4.27	7.95×10^{-2}	33.65	1.11×10^{-2}
A1	Myocardium	8.34	0.538	25.33	0.86	4.73	6.90×10^{-2}	41.52	8.54×10^{-3}
A2		10.49	0.035	396.00	5.37	4.81	1.03×10^{-1}	35.23	9.50×10^{-3}
A3		8.12	0.533	26.58	0.92	5.21	7.61×10^{-2}	43.11	8.56×10^{-3}
A4		12.75	0.286	112.78	2.15	5.02	9.42×10^{-2}	34.14	1.08×10^{-2}
A1	Great Vessel (Luminal Surface)	8.76	0.369	88.96	1.65	5.00	5.70×10^{-2}	40.53	8.39×10^{-3}
A2		12.75	0.012	376.15	3.97	4.68	7.33×10^{-2}	37.08	9.68×10^{-3}
A3		8.02	0.674	14.78	0.60	5.28	5.42×10^{-2}	41.48	8.15×10^{-3}
A4		14.70	0.319	152.86	2.50	4.75	7.34×10^{-2}	34.59	9.99×10^{-3}

In conclusion, this study has provided the most detailed dielectric characterisation of the heart in the microwave frequency range to date, in terms of measurement of different anatomical locations. The study has shown that not all regions of the heart have the same dielectric properties and therefore a heterogeneous approach to modelling the heart may be necessary for accurate dielectric characterisation.

The study highlights distinct dielectric properties across heart regions at 25°, but the impact and magnitude of these differences at the physiological temperature of 37°remain unclear. Without quantitative analysis of temperature effects, which may vary by region, the implications for cardiac ablation therapies could be significant, potentially altering the dielectric profile used in treatment simulations. Further research is needed to clarify these effects and ensure accurate modelling.

The results of this study have been modelled using a three-pole Debye model, and the parameters of the model have been fitted to the mean of the measurement data. The models were found to have a good fit with the measurement data, indicating they are suitable for use in numerical simulations of cardiac microwave ablation treatment. These models can be used to build an anatomically accurate model of the heart with a fully accurate dielectric profile, ultimately leading to improved patient outcomes in cardiac microwave ablation treatment.

However, it should be noted that this study does not cover the dielectric characterisation of blood and cardiac tissues at frequencies relevant to ablation modalities other than microwaves. This will be addressed in the following chapters as the characterisation of blood dielectric properties at lower frequencies is addressed in *Chapter 4*.

4

Impedance Characterisation of Human Blood for Applications in Pulsed Field Ablation

4.1 Introduction

In *Chapter 2* the lack of knowledge and the gap in the literature regarding the dielectric properties of blood at frequencies below 1 MHz was shown in the context of the three cardiac ablation modalities, RF, MW, and PF ablation. To address this gap in the literature, the following research question was formed: What is the electrical conductivity of human blood at both room and body temperature over the frequency range of 100 Hz to 100 kHz? This question is investigated in this chapter.

Specifically, the gathering of samples, the designing of a custom probe and the experimental procedure are discussed in *Section 4.2*; the results and discussion, including a comparison of the measured data to the literature and the limitations of the data collection, are discussed in *Section 4.3*; and finally, the main findings

This chapter is based on a published journal paper [283] N. Ištuk et al., "Relationship Between the Conductivity of Human Blood and Blood Counts," IEEE J. Electromagn. RF Microw. Med. Biol., pp. 1–7, 2021, doi: 10.1109/JERM.2021.3130788. For consistency with the rest of this thesis, parts of the content are modified, and equations, figures, references, and tables are updated.

and takeaways in this study are summarised in *Section 4.4.*

4.2 Materials and Methods

In this section, the preparation of the blood samples and the methodology used in this study for measuring the conductivity of human blood is described. The design and characterisation of a four-electrode probe, including the determination of the cell constant and the measurement uncertainty are also described.

4.2.1 Human Blood Samples

For this study, blood samples from oncology patients were gathered at the University Hospital Galway after ethical approval was obtained for the study.

Although this study is focused on investigating the electrical conductivity of human blood in the general population, due to the limited availability, a compromise was to utilise blood samples sourced from oncology patients.

A venous blood sample was taken from the antecubital veins of each of the thirteen oncology patients. Whole blood was collected in ethylenediaminetetraacetic acid (EDTA) tubes and transferred directly to the laboratory for measurement.

With the goal of keeping the time gap between sampling and conductivity testing as short as possible to preserve blood composition and maintain consistent electrical conductivity, all blood samples in this study were collected roughly 30 minutes prior to conducting the measurements.

A single well of a 12-well cell culture plate was used as a sample holder. The well of a 12-well cell culture plate was suitable in terms of size, as the well could accommodate the probe with the required blood volume. Out of the thirteen samples that were sourced for this study, ten tubes contained approximately 6 ml of blood, which was sufficient to fill the cell culture well. Hence, ten samples (one per patient) were used in this study for conductivity measurement.

Further, the full blood count was obtained for eight out of ten samples. The full blood count was performed by the Irish National Accreditation Board accredited testing laboratory (Registration Number '239MT'). The counts are given in

Table 4.1. The inclusion of blood counts enabled a comparison with reference values to assess whether the samples from oncology patients adequately represented normal blood characteristics.

The samples were delivered to the laboratory at room temperature. The first measurement on each sample was performed at room temperature (22.6°C, SD = 0.8°C). The second measurement on each sample was performed at close to body temperature (36.6°C, SD = 0.4°C). These two temperature measurements allowed for the data collected in this study to be compared to studies performed in the literature at both room and body temperatures. The experimental equipment setup as well as the measurement procedure is discussed in the next section.

Table 4.1: Mean value and SD of each blood count across the N=8 samples. The mean values of white cell count and lymphocytes are increased. The mean values of other blood counts are within normal.

Test	Mean result	SD	Units	Normal range women	Normal range men
White cell count	13.6 ↑	6.7	10^9/l	4 to 10	4.5 to 11
RBC	4.7	0.9	10^{12}/l	3.8 to 4.8	4.3 to 5.9
Hgb	13.6	2.2	g/dl	12 to 15	13.5 to 17.5
Hct	0.412	0.063	l/l	0.36 to 0.46	0.41 to 0.53
MCV	87.9	7.6	fl	84 to 96	84 to 96
MCH	29.1	3.9	pg	27 to 32	27 to 32
MCHC	32.9	1.8	g/dl	31.5 to 34.5	31.5 to 34.5
Platelet count	317	74	10^9/l	150 to 400	150 to 400
Neutrophils	5.6	3.2	10^9/l	2 to 7	2 to 7
Lymphocytes	4.2	5.7	10^9/l	1 to 4.5	1 to 4.5
Monocytes	0.7	0.4	10^9/l	0.2 to 0.8	0.2 to 0.8
Eosinophils	0.19	0.13	10^9/l	0.04 to 0.4	0.04 to 0.4
Basophils	0.05	0.02	10^9/l	0 to 0.1	0 to 0.1

An INAB accredited testing laboratory Reg.No.'239MT'

4.3 Measurements of Conductivity with Custom Made Four-electrode Probe

4.3.1 Custom Made Four-Electrode Probe

As was discussed in the review of the literature on electrical conductivity measurements in *Chapter 2*, custom-made four-electrode probes are common in conductivity measurement studies. The four-electrode probe used in this study was assembled with the parts from a standard electronics development kit and is shown in Fig. 4.1. Four pins of a gold-plated pin header (Harvin, Portsmouth, United Kingdom) were used as four electrodes in a linear array, as shown in Fig. 4.1. The pin header has a pitch of 2.54 mm, which refers to the uniform distance between the pins measured from centre to centre. Each pin has a square-shaped cross-section with a width of 0.64 mm. The pins are 3 mm in length. Four male-to-female breadboard jumper cables (MikroElektronika, Belgrade, Serbia) were used to connect the pins to the PGSTAT204. The pins were connected to the PGSTAT204 in a four-electrode configuration, as shown in Fig. 4.2.

The custom-made four-electrode probe offered the necessary adaptability and optimisation to meet the specific needs of the conductivity measurement study. Its construction with readily available components ensured cost-effectiveness, while the chosen electrode configuration enabled accurate and reliable measurements within the designated frequency range.

4.3.2 Conductivity Measurements

The conductivity of the human blood samples was extracted from the measured electrical impedance. Measurements of electrical impedance were performed with a four-electrode probe method. Electrical impedance was measured on 10 human blood samples. Electrical impedance data was measured using the PGSTAT204 potentiostat/galvanostat (Metrohm Autolab B.V., Utrecht, The Netherlands) in galvanostatic mode. The electrical conductivity was then determined from the measured data for each sample.

The measurement setup is shown in Fig. 4.2. The measurement setup consisted of the PGSTAT204, connected to a custom-made four-electrode probe

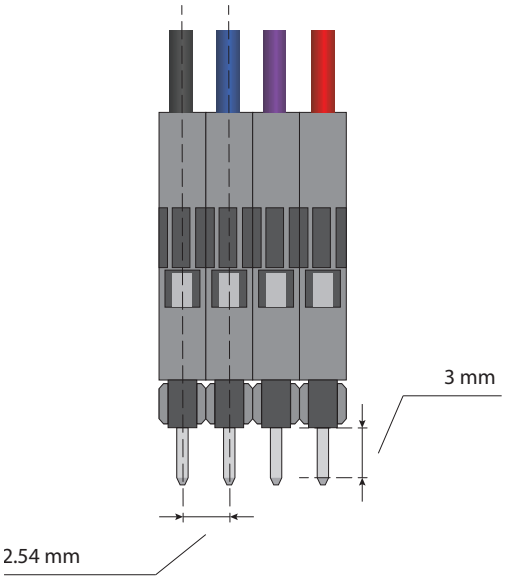

(a) probe schematic

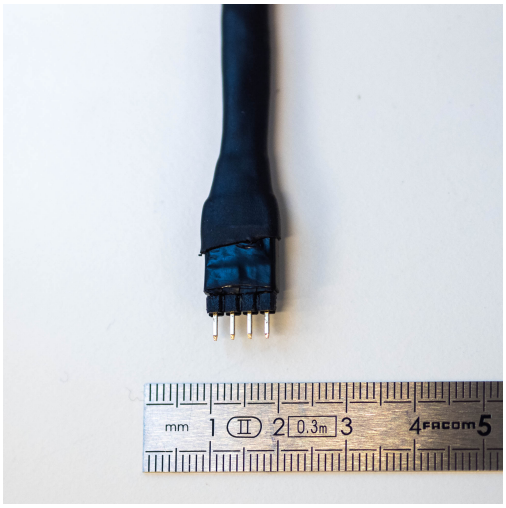

(b) probe

Figure 4.1: The schematic of the probe with the dimensions of the pins (a), and the photo of the probe (b). The probe is designed to be connected to a four-terminal impedance measurement device in a four-electrode configuration shown in Fig. 4.2. The distance between the electrodes is 2.54 mm and the length is 3 mm. The probe is sufficiently small to fit inside a well of a 12-well cell culture tray, is cheap (less than 1.20 EUR per probe), easy to make, and has shown good stability over the 100 Hz–100 kHz frequency range.

(the design of which was discussed in *Subsection 4.2.3*). A personal computer running NOVA 2.1.1 software including FRAM32M impedance analyses module (Metrohm Autolab B.V., Utrecht, The Netherlands) was used to capture the measurement data. A 12-well cell culture tray was used as a sample holder. The temperature of the samples was controlled by the water thermal bath (Fisher Scientific, Isotemp R, Waltham, MA, USA).

Before each measurement, the temperature of the samples was measured using the Checktemp 1 digital stick thermometer (Hanna Instruments, Woonsocket, Rhode Island, United States). The thermometer was also used to stir the sample before the measurement in order to avoid the effects of aggregation and sedimentation of RBCs or any other element of the blood, which can affect the conductivity measurement [246, 248, 284].

When using the four-electrode probe method in galvanostatic mode, a constant current is injected between the two working electrodes. In this study, the value of the constant current was set to 10 mA root mean square (RMS). This value is small enough in order to operate in a pseudo-linear region, where the complex impedance does not depend on the value of current [224]. The voltage drop is measured between the sensing electrode and the reference electrode. The measurements were performed at 51 frequency points with a logarithmic distribution across the range from 1 Hz to 100 kHz (10 frequency points per decade). The logarithmic distribution was chosen as this distribution gives more weight to the lower frequencies, where the most significant changes in impedance are typically observed for biological samples.

4.3.3 Cell Constant and Measurement Uncertainty

While the primary objective of this research is to investigate conductivity, the measurement setup directly measures the impedance. Consequently, it is crucial to establish a relationship between the measured impedance and the conductivity of the sample. By doing so, the impedance data can be accurately interpreted and the conductivity values derived. In this study, impedance data is converted to the electrical conductivity of the samples in two steps. The first step is determining the cell constant, which is the factor that relates measured conductance (inverse

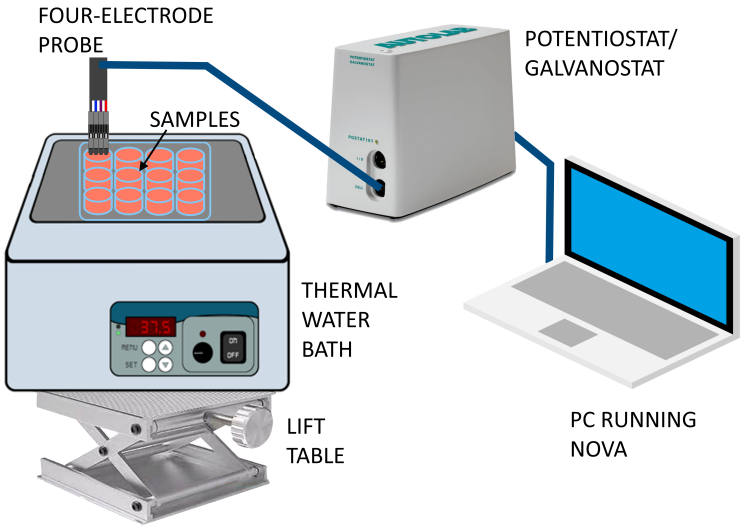

(a) measurement setup schematic

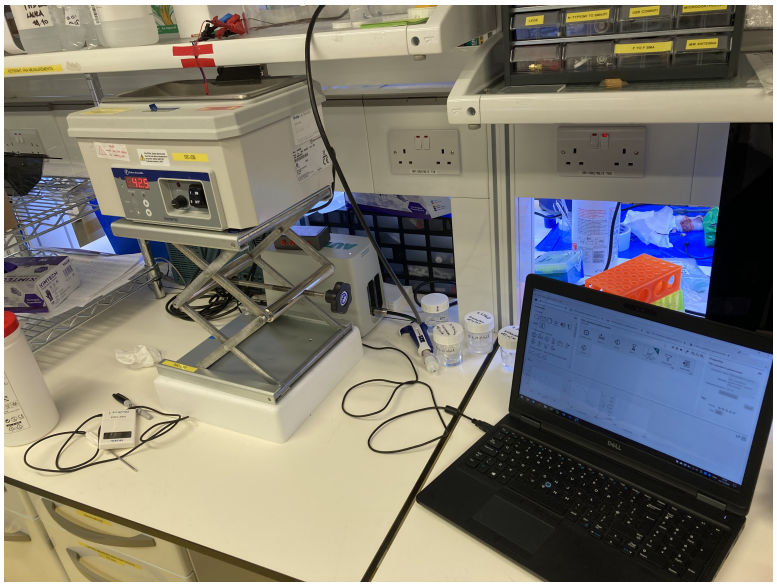

(b) measurement setup

Figure 4.2: Four-electrode configuration measurement setup schematic (a), and photo (b). The connections are the working electrode (red), working sensing electrode (purple), reference electrode (blue), and counter electrode (black).

of the real part of the measured impedance) and the corresponding reference conductivity [191]. The second step is calculating the electrical conductivity from the measured impedance data and the cell constant. The cell constant is determined by measuring the impedance on standard liquids with known electrical conductivity. In this study, the cell constant was determined by using 0.01, 0.05, and 0.1 mol/l aqueous NaCl solutions at room temperature ($T = 20°$) as standard liquids. Fig. 4.4a shows the measured conductance (from the measured impedance) on these three standard liquids. The cell constant k (in m) is calculated as:

$$k = G/\sigma, \tag{4.1}$$

where G is the measured conductance (in S) and σ (in S/m) is electrical conductivity of the standard liquid. The conductance for each of the three aqueous NaCl solutions was measured 10 times (a total of 30 measurements). In theory, there should be no dielectric dispersion in ionic aqueous solutions at frequencies below 1 MHz [65]. Therefore, the conductivity is frequency-independent and only varies with the concentration of the aqueous NaCl solution.

While the measurements were conducted across the range of 1 Hz — 100 kHz, the probe exhibited a degradation in performance at lower frequencies (i.e. below 100 Hz), and the electrode polarisation effect was not completely eliminated. This effect can be seen in Fig. 4.3. To ensure that the performance of the probe meets the acceptable standards (i.e. matching the values from Gabriel *et al.* [191] 2009 study) within this study, the frequency range was narrowed down to 100 Hz – 100 kHz. Over this range, a correlation coefficient relating the measured conductance and conductivity of the standard liquids was maintained at the value reported in the study by Gabriel *et al.* [191], which was 0.993.

Fig. 4.4b shows the relationship between the measured conductance and reference conductivity, obtained from Peyman *et al.* [268]. The cell constant of the probe in this experiment is 2.80×10^{-2} m, which is suitable for measurements of biological tissues and is the same order of magnitude as the cell constant used in the Gabriel *et al.* [191] 2009 study (2.0×10^{-2} m).

These 30 measurements on standard liquids were used to quantify the systematic and random error [191, 285]. In the ideal case, there should be no variation

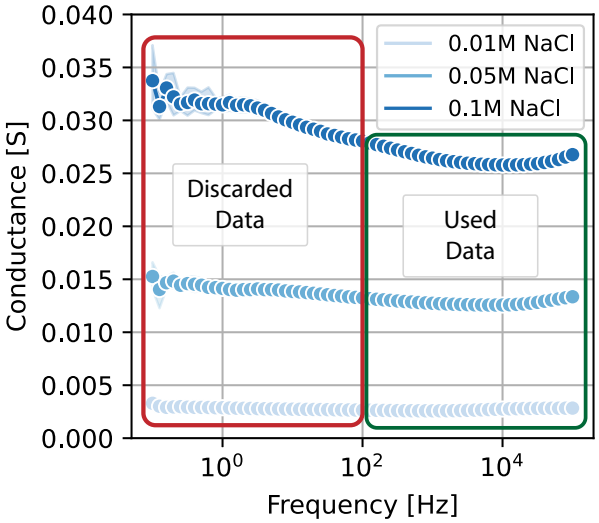

Figure 4.3: Conductance measured on standard liquids over the 1 Hz–100 kHz frequency range. By discarding the data at lower frequencies (i.e. < 100 Hz), where electrode polarisation effects are still present, the acceptable performance of the custom four-electrode probe was ensured.

in the measured conductance over the frequency range [191]. The cell constant and the measured conductance were used to calculate the ionic conductivity of each aqueous saline solution. The standard deviation of the mean represents a random error (Type A). The deviation of the mean calculated conductivity from the actual conductivity of the standards corresponds to systematic error (Type B). The combination of systematic and random errors is expressed as combined uncertainty. The combined uncertainty is calculated as the square root of the linear sum of squared standard uncertainty components [285, 286]:

$$u_{\text{combined}} = \sqrt{u_A^2 + u_B^2} \tag{4.2}$$

where u_A is Type A uncertainty and u_B is Type B uncertainty.

Table 4.2 gives both the random and the systematic error values. If only the values for 0.05 mol/l saline are considered, as it is standard with conductivity closest to that of human blood, the combined uncertainty is 5.90% [285, 287, 288]

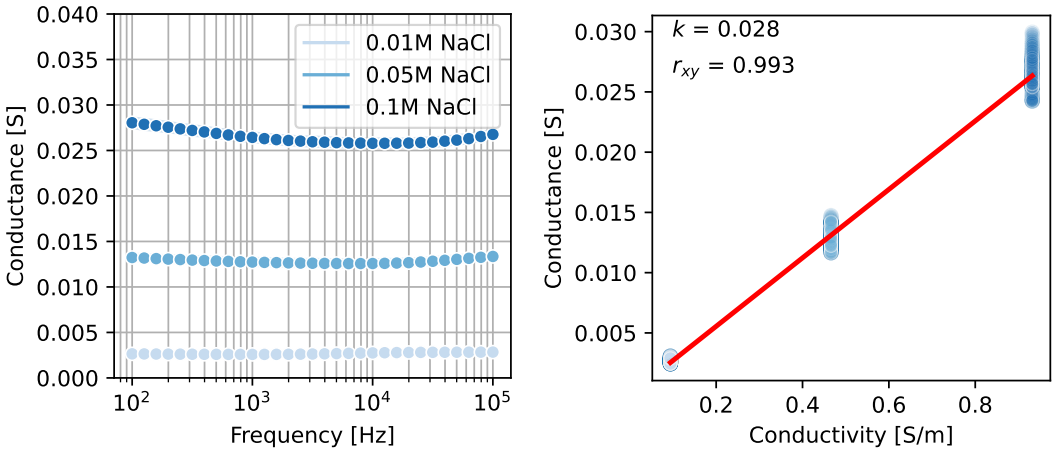

Figure 4.4: Measured a) conductance and b) correlation with reference conductivity. The cell constant, k, relates conductance to conductivity, and r_{xy} represents the Pearson correlation coefficient. The conductance as a function of frequency plot displays a flat pattern, in agreement with the expected behaviour of ionic aqueous solutions at frequencies below 1 MHz [191]. The standard deviation, depicted by the shaded area, is small, indicating a high degree of measurement repeatability. The value of k is appropriate for conducting measurements on biological tissues [191]. The high value of r_{xy} indicates a strong linear relationship between the measured conductances and reference conductivities. The conductance measurements were repeatable and showed a flat pattern consistent with the expected behaviour of ionic aqueous solutions. The correlation between the measured conductance and the reference conductivity was strong, with a high Pearson correlation coefficient value. The cell constant was found to be suitable for conducting measurements on biological tissues.

Table 4.2: Mean conductivity [S/m], standard deviation [S/m], standard deviation as a percentage of the mean [%], reference conductivity [S/m] [268] and the percentage difference between the mean measured conductivity and reference values [%].

NaCl [mol/l]	σ [S/m] average	SD (σ) [S/m]	SD (σ) [%]	σ [S/m] literature [268]	Error [%]
0.01	0.097	0.006	6.05	0.094	3.27
0.05	0.457	0.026	5.79	0.466	-1.98
0.1	0.934	0.032	3.40	0.932	0.24

4.4 Results and Discussion

4.4.1 Blood Counts

The full blood count included the total white cell count (WCC), red blood cell count (RBC), haemoglobin concentration (Hgb), haematocrit (Hct), mean corpuscular volume (MCV), mean corpuscular haemoglobin (MCH), mean corpuscular haemoglobin concentration (MCHC), platelet count, and differential white cell count (as neutrophil, lymphocyte, monocyte, eosinophils and basophils levels). The mean WCC and lymphocyte values were increased. Mean WCC was 13.6×10^9/l, while the normal range is 4×10^9/l to 10×10^9/l. The mean lymphocyte count was 4.2×10^9/l and the normal range is 1×10^9/l to 3×10^9/l. The mean values of other blood counts were within the normal range.

Based on the analysis conducted in this study and the historical studies [248, 249], it was determined that the conductivity measurements were not highly impacted by the increased blood counts of WCC and lymphocytes. This conclusion is supported by the existing literature, which suggests that the electrical conductivity of blood is primarily influenced by blood counts such as Hct, RBC, and haemoglobin levels, which were within normal limits in this study.

By analyzing the correlation between conductivity and different blood counts in this study across the frequency range, the strongest correlation was observed at the lowest frequency ($f = 100$ Hz), indicating a notable association between conductivity and blood counts in that specific frequency range. Furthermore, weak correlations were identified between conductivity and WCC ($R = -0.661$)

as well as lymphocytes ($R = -0.575$). In contrast, a strong correlation was observed between conductivity and Hct ($R = -0.913$), RBC ($R = -0.834$), and haemoglobin levels ($R = -0.825$). These findings are in line with the literature and support the claim that the electrical conductivity of blood is not highly affected by increased blood counts of WCC and lymphocytes.

An important consideration in this study is the completeness of the dataset. Of the intended ten samples, blood counts were only available for eight. This limitation may introduce a degree of uncertainty in the generalisation of the findings. The absence of data for two samples, while not undermining the overall trends observed, does pose a constraint on the robustness of the statistical analyses conducted. This shortfall in sample size could potentially limit the conclusiveness of the findings, particularly in the context of a heterogeneous patient population such as those with cancer. Future studies could benefit from ensuring a more comprehensive data collection to mitigate such limitations and enhance the reliability of the findings.

4.4.2 Measurements and Analysis of the Conductivity of Blood over the 100 Hz–100 kHz Frequency Range

The mean conductivity over the 10 samples measured is presented in Fig. 4.5 along with data from the literature. To provide a comprehensive overview of the studies conducted in the literature, additional literature data at frequencies above 100 kHz were incorporated into this analysis.

The data from this study at body temperature matches well the data from Hirsch *et al.* [248] and Texter *et al.* [249] at 30°C, as well as the data from Rosenthal and Tobias [289] at body temperature. The one SD confidence intervals for these three studies overlap with each other. The average difference between the data from this study and the data from Hirsch *et al.* [248] is 2.55%. The average difference between the data from this study and the data from Texter *et al.* [249] is 13.56%. Rosenthal and Tobias [289] study data was acquired at a single frequency f=1 kHz. The difference between the data from this study at f=1 kHz and the data from Rosenthal and Tobias [289] at f=1 kHz is 12.65%. The data from this study at T=23 °C and at f=79 kHz matches well with the

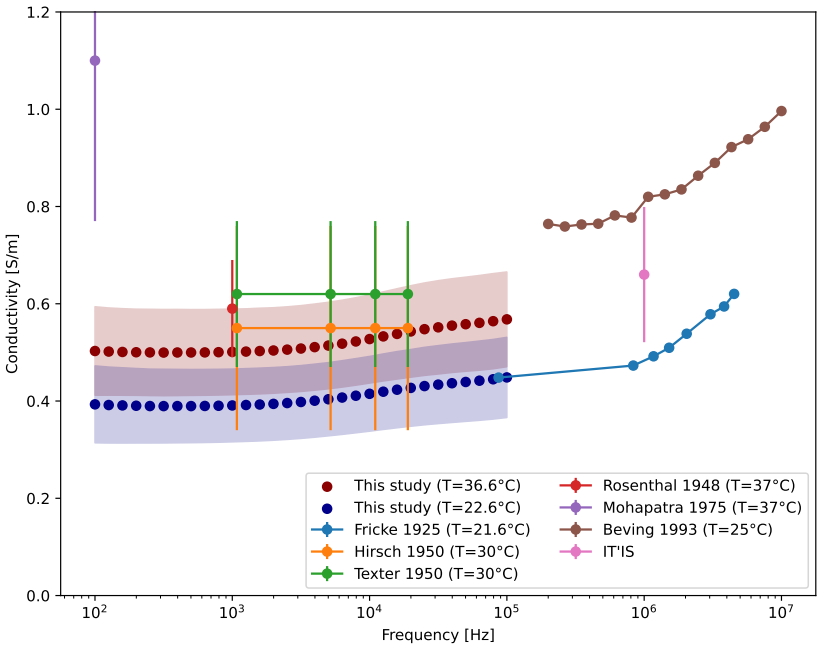

Figure 4.5: Mean conductivity in S/m of human blood samples at room temperature (dark blue is data points, shaded is mean ± SD); human blood samples at body temperature (dark red is data points, shaded is mean ± SD); and blood conductivity value from literature for human blood conductivity (mean ± SD) [246], [248], [249], [251], [252], [277], [289]. The data from this study at body temperature matches very closely the data from Hirsch et al. [248] (orange line) and Texter et al. [249] at 30°C (green line) as well as the data from Rosenthal and Tobias [289] at body temperature (red line). The average difference between the data from this study and the data from Hirsch et al. [248] is 2.55%. The average difference between the data from this study and the data from Texter et al. [249] is 13.56%. The difference between the data from this study at 1 kHz and the data from Rosenthal and Tobias [289] at 1 kHz is 12.65%. The data from this study at T=23°C and at f=79 kHz matches well with the data from Fricke and Morse [246] (blue line) at T=21.6°C and at f=87 kHz, with 1.35% difference between the two values. Other data from the literature are at either higher or lower frequencies and are shown to illustrate the extent of human blood conductivity data available in the literature. Mohapatra *et al.* [251] used the variable-path-length conductivity cell method, which assumes the constancy of the EP impedance, rather than mitigating the effect of EP. The results of this study validate the methodology used and provide valuable additional data to the literature on human blood conductivity. The close match with previous studies highlights the consistency and reliability of the obtained results.

data from Fricke and Morse [246] at T=21.6 °C and at f=87 kHz. The difference between the two values is 1.35%. The chosen comparison is made at the closest frequency available between the two datasets. Other data from the literature is at either higher or lower frequencies, outside of the operating range of the probe used in this study [251], [252].

The measured conductivity is in good agreement with the data from the literature [246], [248], [249], [251], [252], [277], [289]. The mean conductivity measured at room temperature is between 0.11 S/m and 0.12 S/m lower across the frequency range than the mean conductivity measured at body temperature. The difference in percentage is between 23% and 26% and a Student's t-test was conducted, testing if the two means are equal. A p value of <0.05 was considered statistically significant. The hypothesis is rejected at all measurement frequencies. The difference can be explained by blood conductivity increasing with temperature as the mobility of the ions that transport the current increases with temperature and the viscosity of the extracellular fluid decreases [251], [290].

The difference in mean conductivity between measurements taken at room temperature and body temperature was examined using Student's t-test [291]. The Student's t-test was performed at each measurement frequency, and the results were consistent across the frequency range. The t-test yielded a t-statistic value ranging between 0.0075 and 0.01, with degrees of freedom (df) calculated as follows: df = n1 + n2 - 2 = 10 + 10 - 2 = 18 (where n1 and n2 are the sample sizes of each group). The obtained p-value was less than 0.05, indicating a statistically significant difference between the mean conductivities at room temperature and body temperature.

The observed difference in conductivity can be attributed to blood conductivity increasing with temperature, as the mobility of ions transporting the current rises with temperature, and the viscosity of the extracellular fluid decreases [251], [290].

4.4.3 Limitations

One of the challenges in the measurement of the conductivity of human blood is sourcing human blood samples. In this study, only eight samples satisfied the

conditions to be included (size of the sample and availability of blood counts). The small number of samples limits the scope and generalisability of this study.

The blood was sourced from oncology patients. These patients, by the nature of their illness and treatment, may exhibit altered blood composition, which could potentially influence the electrical conductivity measurements, thus limiting the generalisability of the findings.

Despite the inherent differences in blood composition between oncology patients and healthy individuals, this study may still serve as a valuable preliminary step for future investigations. The electrical conductivity measurements identified in this study could provide a basis for the design and execution of more focused studies with more diverse and representative samples, including healthy individuals.

Another limitation of this study is the impact of electrode polarisation on conductivity measurements. Although a custom four-electrode probe design was employed to mitigate this issue, the polarisation effect across the entire frequency range was not entirely eliminated. As a result, the functional operating frequency range of the probe was limited to 100 Hz–100 kHz. This limited frequency range also limited the ability to explore the broader spectrum of electrical conductivity in human blood samples. Future studies aiming to overcome this limitation could consider optimising the electrode design.

4.5 Conclusion

In this chapter, electrical impedance measurements were performed in order to help inform the selection of appropriate energy delivery parameters for ablation at low frequencies (e.g. PF and RF ablation). The electrical conductivity of blood was extracted for frequencies of 100 Hz–100 kHz. This data collection addressed the gap of lack of data over the frequency range in the literature.

The conductivity of whole human blood was measured at two temperatures (at 25 °C and at 37 °C), enabling a comparison between the room and body temperature. The four-electrode technique was used to mitigate the problem of electrode polarisation and allowed for accurate conductivity measurements over the 100 Hz–100 kHz frequency range. The results of the study provide

valuable information for the design of numerical models for radiofrequency and pulsed electric field ablation treatments, as well as other medical electromagnetic applications.

While the four-electrode probe employed in our previous studies was suitable for measuring the conductivity of 6 ml blood samples, the application of the probe to cardiac tissue is hindered by its invasiveness, size, and large sensing volume, which are not compatible with the delicate nature of cardiac tissues. Recognising this limitation, the subsequent chapter will not focus on characterising cardiac tissue per se, but rather on developing a specialised probe designed for this purpose. The new probe will feature a planar design with a smaller sensing volume to accommodate the unique requirements of cardiac tissue measurement, thereby advancing the methodologies previously described.

5

Miniaturised Four-electrode Probe for the Measurement of Conductivity of Cardiac Tissue

5.1 Introduction

In *Chapter 2*, limitations in existing literature concerning the conductivity of cardiac tissue at frequencies below 1 MHz are highlighted. Beyond the issue of electrode polarisation, which *Chapter 4* tackled by employing the four-electrode method, another persistent challenge arises: the problem of sensing volume. This issue is particularly prevalent in studies that focus on measuring conductivity at frequencies below 1 MHz. Larger sensing volumes can introduce discrepancies, particularly when dealing with limited or small biological samples, such as those from cardiac tissues [2, 294–296].

This chapter revolves around the development of a miniaturised four-electrode

This chapter is based on published conference papers [292] N. Ištuk et al., "Reducing Sensing Volume Confounding Effects in Conductivity Measurements: The Use of a Miniaturised Four-Electrode Probe," in ICECOM 2023, Dubrovnik, Croatia: IEEE, Sep. 2023, p. 4. and [293] N. Ištuk, R. Matta, H. Benchakroun, J.M. Baena-Montes, L. Quinlan, D. Moreau, R. O'Connor, E. Dunne, A. M. Elahi, M. O'Halloran, "Miniaturised Four-Electrode Conductivity Probe with PEDOT:PSS Coating," in URSI GASS 2023, Sapporo, Japan: URSI GASS 2023, Aug. 2023. For consistency with the rest of this thesis, parts of the content are modified, and equations, figures, references, and tables are updated.

probe designed for the precise assessment of biological tissue conductivity. The primary targeted application of the probe is the measurement of the conductivity of cardiac tissue at low frequencies.

This chapter answers the question: What are the design features and capabilities of a miniaturised four-electrode probe for measuring the conductivity of soft biological tissues such as cardiac tissue? Specifically, the probe is designed to measure the conductivity of small-size biological tissue samples. In addition, the design of the probe aims to minimise the electrode polarisation effect. The polarisation is mitigated by both using the four-electrode approach and by adopting a poly(3,4-ethylenedioxythiophene) polystyrene sulfonate (PEDOT:PSS) electrode coating. PEDOT:PSS is known for reducing electrode impedance and effectively pushing the polarisation effect beyond the target frequency range [297, 298].

To assess the performance of the miniaturised design, the conductivity measurements from two distinct probes are compared. The probes were: the larger, conventional probe (8 mm in width) that was used in *Chapter 4* study, and the miniaturised (900 µm in width) probe designed for this study. The objective was to examine if the miniaturised probe, with the inherent small sensing volume, provides consistent conductivity measurements across varying sample dimensions. If confirmed, this study proposes the miniaturised probe as a potential tool for accurately measuring the conductivity of biological tissues, addressing challenges like tissue heterogeneity and conductivity underestimation in small samples.

The measurement setup and the impedance spectroscopy techniques used for data collection are outlined in *Section 5.3*. The results, along with an in-depth discussion that includes challenges encountered and the performance of the probe analysis, are covered in *Section 5.4*. Finally, the chapter rounds off with key findings and suggestions for future research in *Section 5.5*.

5.2 Design and Fabrication of the Miniaturised Four-Electrode Probe

The conductivity probe was designed as a miniaturised four-electrode, planar-type probe, with PEDOT:PSS coating. In the following sections, the reasons

behind the design choices and the design and microfabrication of the probe are delineated.

5.2.1 Probe Typology

The probe is designed as a miniaturised four-electrode, planar-type probe. As discussed in previous chapters (*Chapter 2* and *Chapter 4*), a four-electrode design is crucial in mitigating the electrode polarisation effect. While this configuration does not entirely eliminate the EP, the configuration significantly reduces the impact. By passing the current through the outer, CC electrodes and measuring the voltage across the inner PU electrodes, this configuration diminishes the influence of electrode impedance and allows for a more accurate representation of the intrinsic properties of the sample.

The planar-type probe design was chosen primarily because of the non-invasive nature of planar probes. Different types of conductivity probes have been proposed, generally categorised as either a needle-type [225, 226] or a planar-type probes [227–230]. Although needle-type probes are suitable for liquid sample measurements, they have also been applied in soft tissue conductivity assessments [225, 226]. However, the invasiveness of such probes raises questions about potential tissue damage that could skew the results. Given these concerns, planar-type probes are considered more appropriate for soft tissue conductivity measurements. Therefore the planar-type design of the probe was chosen for this particular study instead of the needle-type probe design employed in the *Chapter 4* study.

Within the scope of this study, particular attention was paid to the evaluation of different planar probe typologies, notably influenced by the 2023 study conducted by Benchakroun *et al.* [299]. In their analysis, three distinct planar probe configurations were tested on bovine heart samples: a) the large colinear probe, b) the small colinear probe, and c) the polar probe. The findings from this study reveal the small colinear probe demonstrated superior performance compared to its counterparts, achieving a correlation coefficient ($R = 0.99$) and a coefficient of variation ($CV = 1\%$). This contrasts with the results for the other probes, where the highest correlation coefficient reached was $R = 0.95$, accompanied by

a CV ranging from 1% to 5%. This study advocates for the efficacy of the small colinear probe, further reinforcing the decision to pursue a planar-type design for the probe, which aligns with the non-invasive nature preferred for soft tissue conductivity measurements.

Due to the need for carrying current, the CC electrodes are larger in order to distribute the applied current more uniformly across the sample and to decrease the current density at the electrodes. High current density can lead to issues like electrode delamination, increased heat, or even tissue damage in biological applications [300, 301]. Since voltage PU electrodes draw less current due to the high impedance of the voltage measuring circuitry, the PU electrodes can be of smaller size.

5.2.2 Miniaturisation of the Probe

The primary motivation behind the miniaturisation of the probe stems from the need for increased precision in conductivity measurements, especially in smaller, heterogeneous biological samples. Miniaturised probes offer a reduced sensing volume, which mitigates potential discrepancies arising from limited sample sizes. By minimising the dimensions of the probe, the accuracy and reliability of the readings are only representative of the small region in the vicinity of the probe, and the interference from surrounding regions not of immediate interest is reduced.

However, the process of miniaturisation introduces its own set of challenges, particularly concerning the capacity of the electrodes. As the electrodes become smaller, their capacity decreases, which can adversely affect the ability of the probe to mitigate EP. The capacity of an electrode is a critical factor in determining the onset frequency of EP; the higher the capacity, the lower the onset frequency. This relationship is paramount because the onset frequency of EP delineates the lower end of the operational frequency range of the probe. In essence, a lower capacity resulting from miniaturisation elevates the onset frequency of EP, potentially restricting the effective operational range of the probe. This underscores the necessity of balancing the benefits of miniaturisation with its impact on the functional characteristics of the probe.

To address this issue and further reduce electrode polarisation, a PEDOT:PSS coating was applied. The coating enhances the capacity of the electrodes, thereby aiming to lower the onset frequency of EP to expand the operational range of the probe. This adaptation illustrates the intricate balance required in probe design—optimising for precision and measurement accuracy while mitigating the inherent limitations introduced by miniaturisation.

5.2.3 Coating of the probe

To enhance the performance of the probe and mitigate the electrode polarisation effect, the electrodes are coated with Poly(3,4-ethylenedioxythiophene) doped with polystyrene sulfonate (PEDOT:PSS). This conducting polymer is known for excellent conductive properties and biocompatibility, making it highly suitable for use in biomedical devices [297, 298]. An advantage of applying PEDOT:PSS is the significant increase in the capacity of the electrodes, which leads to a reduction in their impedance [297, 298]. Increased capacity leads to lowering the onset frequency of EP, therefore expanding the operational range of the probe.

The electrode coating process involves stacking multiple spin-coated layers of PEDOT:PSS (i.e. four layers). This method provides precise control over the thickness of the coating without introducing electronic or ionic blocking elements between the layers. The volumetric capacitance of PEDOT:PSS implies that each additional layer contributes to an increase in the overall capacity of the electrodes. This enhancement in capacity is crucial for reducing the effects of polarisation by improving polymer-electrolyte interactions. Furthermore, thicker coatings can sustain higher voltages without loss of performance, which enhances the lifetime of the electrodes [297, 298].

This approach to the electrode coating process highlights the balance between achieving optimal conductivity and ensuring biocompatibility, which is essential for applications involving biological samples. The strategic use of PEDOT:PSS, particularly through stacking spin-coated layers, reflects a sophisticated method to boost electrode performance while effectively addressing the challenges of electrode polarisation in precise measurements.

By keeping in mind all the design considerations, the planar typology design shown in Fig. 5.1 was chosen.

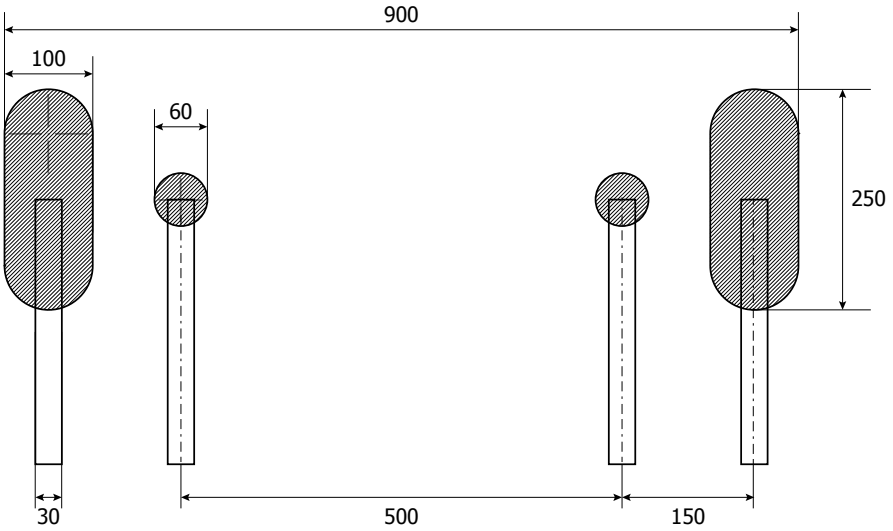

Figure 5.1: The design of the smaller probe. The smaller, miniaturised probe has a width of 900 µm.

The subsequent section will detail the fabrication process of the probe, discussing the steps undertaken to actualise this design.

5.2.4 Microfabrication of the Miniaturised Four-electrode Probe

The probe was made using the microfabrication procedure. Firstly, glass slides were cleaned using solvents followed by an oxygen plasma treatment. Metallic electrodes were then obtained by lift-off with photolithographically patterned AZ nLOF 2070 photoresist (Microchemicals GmbH, Ulm, Germany) using a SUSS MJB4 contact aligner (SÜSS MicroTec SE, Garching, Germany), followed by the deposition of 150 nm gold using a thermal evaporator (BOC Edwards, Burgess Hill, UK). PEDOT:PSS coatings were patterned and deposited as follows: A 3 µm sacrificial layer of parylene C (Specialty Coatin Systems, Inc., Indianapolis, IN, USA) was deposited using an SCS Labcoater 2 (Specialty Coatin Systems, Inc., Indianapolis, IN, USA), and a positive photoresist AZ9260 (AZ Electronic Materials, Luxembourg) was then spin-coated and photolithographically patterned.

The parylene C layer was then etched using a Plasmalab 80 (Oxford Instruments, Abingdon, UK), followed by peel-off of the remaining photoresist.

Four layers of PEDOT:PSS were applied to increase the capacity of the four-electrode probe. The mixture of Clevios PH1000 aqueous PEDOT:PSS dispersion (Heraeus, Hanau, Germany), glycerol, dodecyl benzene sulfonic acid, and (3-glycidyloxypropyl) trimethoxysilane [302] was used. The process involved spin-coating the mixture, baking at 110°C, and cooling down before spin-coating the next layer. This process was repeated until four layers were applied.

PEDOT:PSS is sensitive to harsh solvents and to high-energy processes which are necessary for conventional patterning methods that rely almost exclusively on lift-off or plasma etching techniques [303]. The fabrication of the devices was based on an adapted version of a previously published protocol by Sessolo *et al.* [303]. The critical step is a mechanical peel-off which does not involve the use of chemical or ion etching of the active layer, making the process compatible with any sensitive conducting materials [303].

Finally, the substrate was baked at 140°C for 1 hour and rinsed with deionised water. After the final bake at 140°C for 1 hour, the devices were immersed in deionised water and the sacrificial parylene C layer was peeled off, leaving the four-electrode probe with four PEDOT:PSS layers.

The schematic of the section of the glass wafer containing the tip of the probe is shown in Fig. 5.2.

5.3 Measurement Setup and Impedance Spectroscopy

The experimental setup involved linking the miniaturised probe to a PGSTAT204 potentiostat/galvanostat (Metrohm Autolab B.V. Utrecht, The Netherlands). The pads of the probe were connected using a Zero Insertion Force (ZIF) flex cable (Molex, LLC, Lisle, IL, USA). This connection was further secured with Z-Axis Anisotropic Conductive Tape (3M Company, Maplewood, MN, USA). The glass wafer, carrying the probe and the flex cable, was clamped together, with the anisotropic tape sandwiched between the probe and the flex cable to ensure

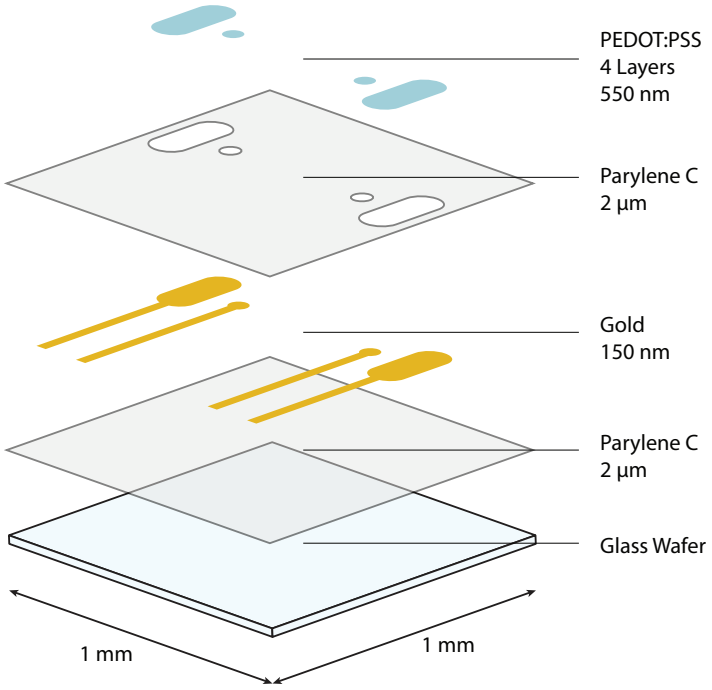

Figure 5.2: A schematic representation of the section of the glass wafer containing the tip of the probe, illustrating the fabrication process. The procedure involves cleaning glass slides, patterning metallic electrodes, and applying four layers of PEDOT:PSS, followed by baking and rinsing. The process results in a four-electrode probe with four PEDOT:PSS layers. The combined thickness of the four layers of PEDOT:PSS is 550 nm. The PEDOT:PSS layers serve to increase the capacitance and decrease the impedance of the electrodes.

optimal contact. The opposite end of the flex cable was attached to a Flexible Printed Circuit/Flexible Flat Cable (FPC/FFC) adapter board (FXI Electronics Co., Ltd., Shenzhen, China). The adapter board converts the 1.0 mm pitch of the flex cable to 2.54 mm pitch pins, which were then connected to the PGSTAT204 using standard cabling.

A variable volume pipette, specifically the Fisherbrand Elite Adjustable-Volume Pipettes with a 1-10 µl range (Fisher Scientific, UK), was employed to measure and transfer the sample volumes onto the surface of the probe. Due to the small sample sizes of 10 µl and 20 µl, direct temperature measurements were impractical. Instead, room temperature was recorded as a proxy. The assumption was that the sample and room temperatures would be equivalent, based on the rationale that the small sample sizes would quickly reach thermal equilibrium with the ambient environment.

The setup is shown in Fig. 5.3.

The PGSTAT204 potentiostat/galvanostat was used to measure impedance in a galvanostatic mode. The measured impedance was then converted to conductivity by dividing the conductance by the respective cell constant from the equation 4.1.

5.3.1 Cell Constant and Size Considerations

In order to compare the performance of the miniaturised four-electrode probe with the more conventional larger four-electrode probe, both probes were characterised within this study. Each probe has a corresponding cell constant, which is the factor that relates measured conductance to the conductivity of the sample [191].

The larger probe (Fig. 4.1) is identical to the probe used in *Chapter 4* and the cell constant of the probe was already determined as $k = 2.80 \times 10^{-2}$ m.

The miniaturised four-electrode probe, which has been micro-fabricated and is displayed in Fig. 5.4, has a width of 900 µm.

In this study, the cell constant was determined by using 0.01, 0.05, and 0.1 mol/l aqueous NaCl solutions at room temperature (23°) as standard liquids. Fig. 5.5b shows the measured conductance (from the measured impedance) on these three standard liquids. The cell constant of the probe is $k = 6.94 \times 10^{-4}$ m.

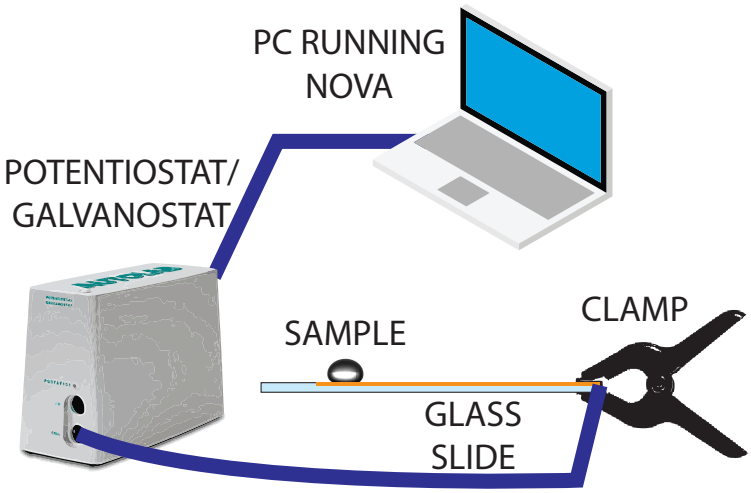

(a)

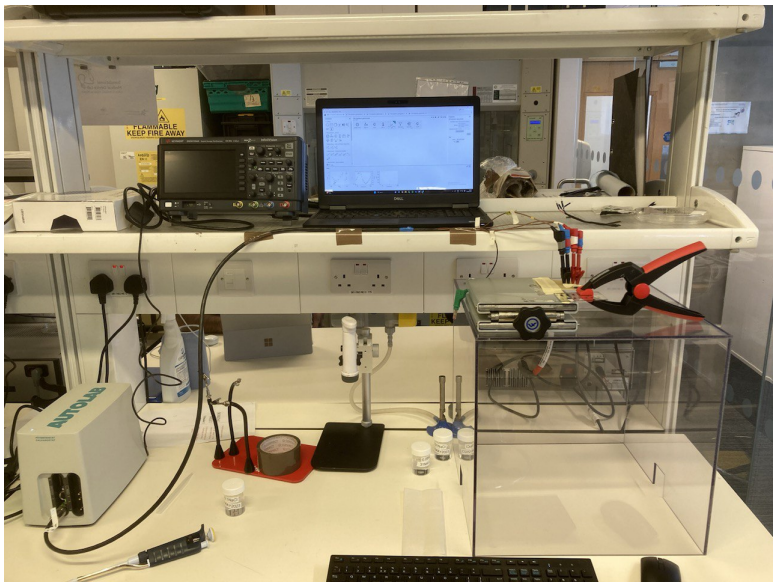

(b)

Figure 5.3: Measurement setup a) schematic and b) photo. The sample in the form of a droplet is placed onto the miniaturised probe. The probe and the measurement setup are in a four-electrode configuration in order to mitigate the effect of electrode polarisation.

An error analysis, carried out in a manner analogous to that detailed in *Chapter 4*, provides values for both random and systematic errors and are summarised in Table 5.1. The combined uncertainty for 0.05 mol/l saline, which has a conductivity closest to that of human blood, is calculated to be 6.51% using equation 4.2.

Table 5.1 summarises the mean measured conductivities, standard deviations, and the percent differences between the measured values and the values from the literature. These discrepancies are particularly notable at lower concentrations, where the high error is attributed to the elevated impedance of low-conductivity samples and the effects of parasitic capacitances. Such factors compromise measurement accuracy outside the optimal dynamic range of the probe.

Table 5.1: Mean conductivity [S/m], standard deviation [S/m], standard deviation as a percentage of the mean [%], reference conductivity [S/m] [268] and the percentage difference between the mean measured conductivity and reference values [%].

NaCl [mol/l]	σ [S/m] average	SD (σ) [S/m]	SD (σ) [%]	σ [S/m] literature [268]	Error [%]
0.01	0.126	1.35×10^{-3}	1.07	0.104	21.15
0.05	0.550	9.73×10^{-3}	1.77	0.518	6.17
0.1	0.968	2.75×10^{-2}	2.84	1.029	-5.93

5.3.2 Small Size Sample Conductivity Measurement Capabilities

To showcase that the miniaturised probe remains consistent in measurements irrespective of the sample size – too as low sample sizes as 10 µl – an experiment was conducted. In this study, both the conventional and miniaturised probes were used to measure the conductivity of 0.1 mol/l NaCl samples. For the conventional probe, the sample volumes tested were 2 ml, 4 ml, and 6 ml, with ten separate measurements for each volume. On the other hand, the miniaturised probe was employed to test sample sizes of 20 µl and 10 µl, also with ten measurements each. The frequency range for these tests was between 10 Hz and 100 kHz for the miniaturised probe, and from 100 Hz to 100 kHz for the conventional probe,

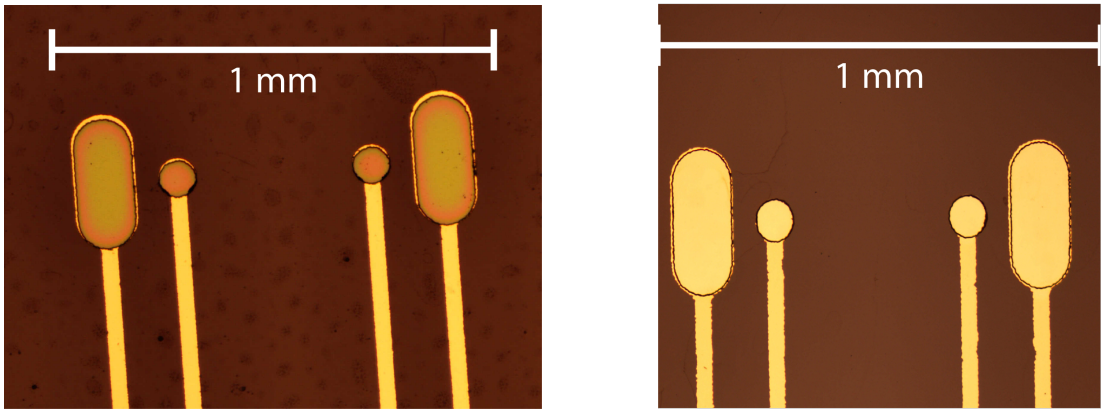

(a) (b)

Figure 5.4: The microscopy image of the miniaturised probe a) with PEDOT:PSS and b) without PEDOT:PSS. The miniaturised probes have a width of 900 µm, which makes the probe suitable for the measurement of conductivity of small samples.

using ten points per decade. The current applied with the conventional probe was 10 mA RMS, which is equivalent to the current applied in the previous study covered in *Chapter 4*. The miniaturised probe has a smaller electrode surface area. Applying the same current levels as a conventional probe would increase the current density, which might lead to issues like electrode delamination, increased heat, or even tissue damage in biological applications [300, 301]. The current applied with the miniaturised probe was therefore limited to 100 µA RMS.

5.3.3 Eliminating the Electrode Polarisation Effect by Using the PEDOT:PSS Coating

A second part of the study focused on understanding the impact of PEDOT:PSS on electrode polarisation. Two versions of the miniaturised probe were compared: one that had four layers of PEDOT:PSS and another without the PEDOT:PSS coating. The conductance of the 20 µl samples was measured across a frequency range of 10 Hz to 100 kHz (10 points per decade). The applied current for this part of the experiment was consistent at 100 µA RMS. The findings from these various tests are analysed and discussed in the results section.

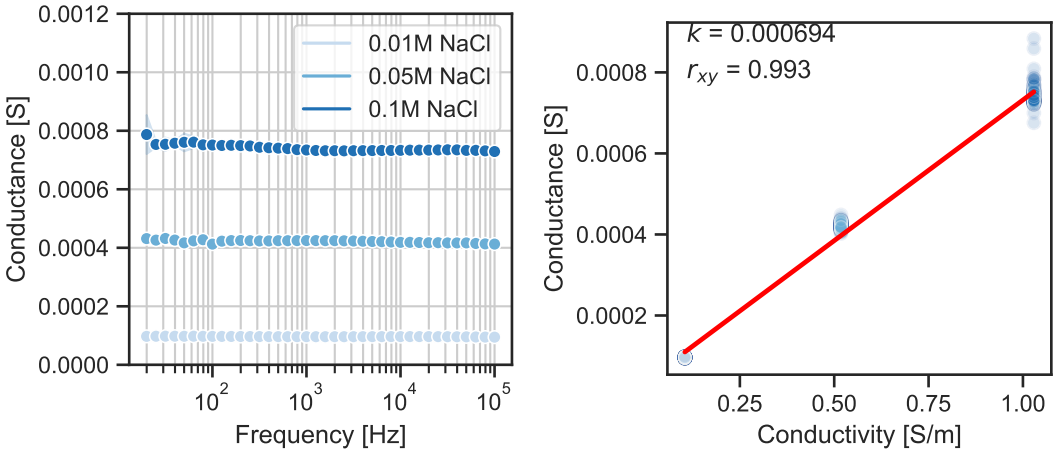

Figure 5.5: Measured a) conductance and b) correlation with reference conductivity. The cell constant, k, relates conductance to conductivity, and r_{xy} represents the Pearson correlation coefficient. The conductance over frequency plot displays a flat pattern, in agreement with the expected behaviour of ionic aqueous solutions at frequencies below 1 MHz [191]. The standard deviation, depicted by the shaded area, is small, indicating a high degree of measurement repeatability. The high value of r_{xy} indicates a strong linear relationship between the measured conductances and reference conductivities.

5.4 Results and Discussion

The results from the first part of the study, which compares the miniaturised probe with the larger conventional probe, are visually summarised in Fig. 5.6. Fig. 5.6 shows boxplots representing the distribution of conductivity measurements obtained from the larger probe (labelled as "Probe 1") and the smaller, miniaturised probe (labelled as "Probe 2"). The boxplots allow for a qualitative comparison of the conductivity measurements conducted with two distinctly sized probes on various sample sizes.

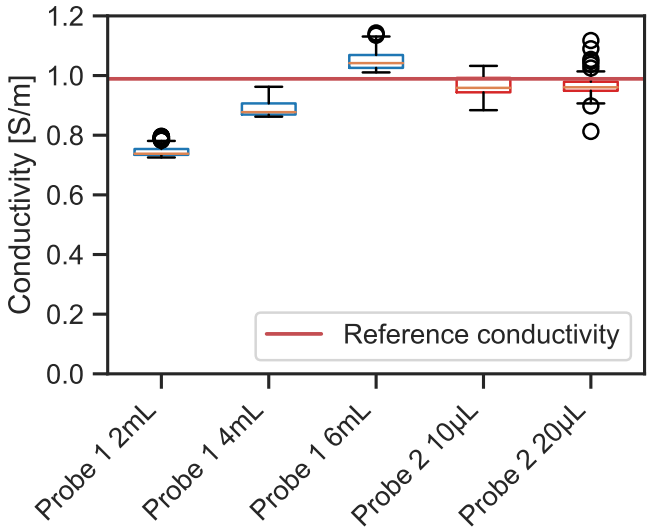

Figure 5.6: Conductivity measurements obtained from the larger probe (Probe 1, blue boxes) and the smaller, miniaturised probe (Probe 2, red boxes). The boxplots allow for a qualitative comparison of the conductivity measurements conducted with two distinctly sized probes on various sample sizes. The conductivity measurements with the larger probe (Probe 1) change for different sample sizes. The conductivity measurement for samples of different sizes measured with the smaller probe (Probe 2) is more consistent.

In the case of the larger probe, the results demonstrate that the mean conductivity varies noticeably with changes in the sample size. Specifically, smaller samples tended to exhibit a lower apparent conductivity. This variation can be attributed to the relatively larger sensing volume of the probe, which leads to a

decrease in the available volume for the electrical current to flow through when the sample size is reduced. Consequently, smaller samples may appear to have lower conductivity than they truly possess, highlighting the confounding impact of the sensing volume on the conductivity measurements.

On the contrary, the measurements obtained from the miniaturised probe presented a significantly different pattern. Notably, the mean conductivity measured by the miniaturised probe remained relatively consistent across the two different sample sizes, irrespective of the reduced sample volumes. This consistency is reflective of the reduced sensing volume of the miniaturised probe. Due to the smaller size of the miniaturised probe, the electrical current flows through a much more confined space around the probe. As such, even with reduced sample sizes, these samples appear semi-infinite from the perspective of the probe, minimising the confounding effect of the sensing volume.

For the larger probe, pairwise Student's t-tests [291] were conducted to compare the conductivity measurements among three different sample volumes: 2 ml, 4 ml, and 6 ml. The tests yielded statistically significant differences in conductivity measurements among all pairs of sample volumes, as confirmed by the extremely low p-values in all comparisons. Similarly, a Student's t-test [291] was conducted to compare the conductivity measurements between 10 µl and 20 µl samples using the miniaturised probe, which did not yield a statistically significant difference as the p-value was above the alpha level of 0.05.

Table 5.2: Summary of t-test Results

	Sample Volume 1	Sample Volume 2	t-Statistic	p-value
Larger Probe	2 ml	4 ml	-79.932	< 0.001
	2 ml	6 ml	-150.219	< 0.001
	4 ml	6 ml	-68.155	< 0.001
Miniaturised Probe	10 µl	20 µl	0.651	0.516

In Fig. 5.7 the effectiveness of PEDOT:PSS coating on the mitigation of electrode polarisation effect can be seen. The conductance of the 20 µl 0.1 mol/l NaCl solution samples measured with the miniaturised probe with PEDOT:PSS coating shows consistent value across the 10 Hz–100 kHz frequency range. The conductance of the same sample measured with the miniaturised probe without

PEDOT:PSS coating shows lower conductance at the low end of the frequency range. This can be explained by the electrode polarisation having a blocking effect at lower frequencies.

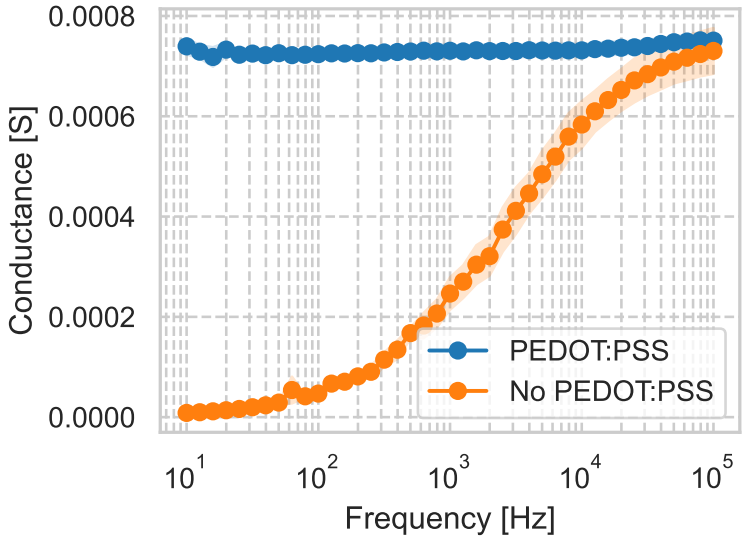

Figure 5.7: Comparison between the miniaturised probe with PEDOT:PSS and without PEDOT:PSS. The probe without PEDOT:PSS failed to eliminate the EP effect across the 10 Hz–100 kHz frequency range. The probe with PEDOT:PSS completely shifts the EP outside of the 10 Hz–100 kHz frequency range.

5.5 Conclusion and Future Work

In *Chapter 5*, the focus was on developing a miniaturised four-electrode probe specifically designed for measuring the conductivity of biological tissues, including cardiac tissues. This innovation aimed to address the issue of sensing volume, especially for studies conducted at 10 Hz–100 kHz frequency range.

This chapter stands as a significant technical contribution, detailing the design, development, and performance evaluation of a miniaturised four-electrode probe. The ability to make accurate measurements of small samples makes the miniaturised probe a potential tool for measuring the conductivity of biological tissues, addressing challenges like tissue heterogeneity and conductivity underestimation in small samples.

The chapter presents valuable insights into the challenges and solutions associated with miniaturisation. It demonstrates the ability of the probe to reduce sensing volume confounding effects, thereby enhancing the accuracy of conductivity measurements. Techniques like coating the electrodes with PEDOT:PSS, a conductive polymer, were explored to optimise the performance of the probe in regard to electrode polarisation.

This study highlighted the importance of electrode size and geometry, and consequently, the sensing volume, when conducting conductivity measurements in the context of small samples. The investigation revealed the inherent challenges and potential inaccuracies that may arise when utilising a larger probe on small sample sizes, due to the relative size discrepancy between the sensing volume and the sample volume. This confounding effect can result in lower apparent conductivity measurements, and therefore, potentially misleading data interpretation.

However, the study demonstrated that these challenges can be effectively mitigated using a miniaturised four-electrode probe. The results of the study suggest that the miniaturised probe can deliver relatively consistent conductivity measurements across two different sample sizes, exhibiting minimal influence of the sensing volume on the obtained results. This consistency could be attributed to the smaller sensing volume of the miniaturised probe. Due to the smaller dimensions of the probe and small sensing volume, even the small 10 µl sample is effectively semi-infinite from the perspective of the probe, which helps mitigate the volume limitation challenges experienced by the larger probe.

The positive implications of this study extend beyond the realm of conductivity measurements of aqueous NaCl solutions. This probe has the potential to reliably measure conductivity in the context of biological tissue analysis, where sample sizes are often limited, and sample heterogeneity can confound measurement results. The miniaturised probe could greatly enhance the accuracy of conductivity-based diagnosis or monitoring of various health conditions using impedance-based sensors.

Future work should focus on testing and improving the durability and resilience of the miniaturised probe to enhance the applicability of the probe in biological and other research fields. Moreover, conducting additional studies to

further validate the effectiveness of the miniaturised probe in different experimental setups and various sample types would be beneficial to more fully realise the potential of the probe.

In conclusion, this study provides a good indication of the potential of miniaturised four-electrode probes in overcoming sensing volume confounding effects in conductivity measurements, paving the way for more accurate, reliable, tissue property measurement and potentially, use of the technology in the medical device applications.

6

Conclusions and Future Work

In this chapter, a summary of the research objectives and a summary of the key findings are presented. Then, potential future research directions are laid out that could further build upon and extend the findings of this thesis.

6.1 Summary

Atrial fibrillation is a widespread cardiac arrhythmia that necessitates precise and effective treatment modalities like cardiac ablation. The success of such treatments is intricately tied to the accurate understanding of dielectric properties within the heart, namely blood and cardiac tissue. Inaccuracies or lack of clarity in these properties can compromise treatment outcomes, leading to both health risks and financial burdens. The existing gaps and limitations in the understanding of these dielectric properties were critically discussed in *Chapter 2*. These shortcomings underscored the pressing need for advancements in the field, which in turn required the development of specialised tools such as the miniaturised four-electrode probe for more accurate conductivity measurements.

Chapter 2 laid the foundation by delving into AF, a widespread medical condition that necessitates targeted management. The chapter underscored the role of dielectric properties in cardiac ablation, a treatment for AF. It highlighted key gaps in current research, especially the lack of studies acknowledging the heterogeneous nature of the heart and the limitations of the studies on low-frequency (below 1 MHz) conductivity of blood and cardiac tissue. The importance of

accurate impedance and dielectric property measurements was emphasised, as inaccuracies could result in suboptimal treatment outcomes.

The chapter highlighted the pressing need for precise dielectric measurements, a requirement made more urgent by existing gaps in the understanding. These shortcomings included the complexities of measuring conductivity at lower frequencies (below 1 MHz) and the absence of comprehensive studies that address challenges like electrode polarisation and the importance of human sample measurements. The chapter called for a nuanced approach to consider the heterogeneity of the heart and advocated for the development of specialised tools, such as a miniaturised four-electrode probe with a small sensing volume, tailored for cardiac tissue conductivity measurement.

Gaps in the literature were identified, particularly in the knowledge of the dielectric properties of cardiac tissue at MW frequencies (500 MHz to 20 GHz) and the conductivity of both blood and cardiac tissue at frequencies below 1 MHz. These identified gaps motivated the research questions posed in this thesis. Given these gaps, *Chapter 3* aimed to delve deeper into the dielectric properties of cardiac tissue at MW frequencies, taking the initial steps to address these research voids.

In *Chapter 3*, the lack of comprehensive examination (as discussed in *Chapter 2*) of the dielectric properties of the heart as a heterogeneous organ at the microwave frequency range was addressed. Measurements were conducted on six different regions of the heart at room temperature for four ovine heart samples. The data was compared with a model and data from Gabriel *et al.* [273], which serve as a basis for two widely used literature databases on the dielectric properties of tissues [276, 277]. The observed differences between the multiple sets of data were attributed to variations between different parts of the organ.

Furthermore, the study investigated the impact of tissue dehydration on measurement results and discovered no noticeable trend in changes in dielectric properties with respect to time from excision. Relative permittivity and conductivity for each part of the heart were reported at frequencies of 915 MHz and 2.45 GHz, which are commonly used for MW thermal ablation. The results indicated that the dielectric properties are not uniform across all regions of the heart.

For the purpose of supporting computer modelling, a broadband three-pole Debye model was fitted to the mean of the measurement data, with parameters determined from the measurements on the four ovine heart samples. The fit error between the measurement data and the model was calculated to be low, suggesting a good fit.

The conclusion is that for accurate dielectric characterisation, a heterogeneous approach to modelling the heart may be necessary. These models can potentially be used to construct an anatomically accurate model of the heart, thereby improving patient outcomes in cardiac MW ablation treatment.

In order to address the gaps in the literature in the knowledge of the conductivity of blood and cardiac tissue for RF and PF ablation, the research was shifted towards frequencies more relevant to these two ablation modalities.

Chapter 4 focused on the electrical conductivity measurements of human blood, addressing the gap found in the literature. These shortcomings included the complexities of measuring conductivity at lower frequencies (below 1 MHz) and the absence of comprehensive studies that address challenges like electrode polarisation and the importance of human sample measurements. The analysis covers the conductivity of whole human blood measured at two different temperatures (25°C and 37°C), enabling a comparison between room and body temperature conditions. These measurements spanned a frequency range from 100 Hz to 100 kHz.

To mitigate the problem of electrode polarisation and to enable accurate conductivity measurements over this frequency range, a custom four-electrode probe was used. However, despite this mitigation strategy, the polarisation effect was not entirely eliminated across the entire frequency range, which limited the functional operating frequency range of the probe.

The study employed blood samples from oncology patients, introducing potential variations in blood composition due to their illness and treatment. This factor could have potentially influenced the electrical conductivity measurements and thus posed a limitation on the generalisability of the findings. Nonetheless, these results could serve as a basis for future investigations with more diverse and representative samples. The study demonstrated a good agreement between the measured conductivity and existing data from the literature and the data

contributes to the understanding of the conductivity of human blood at body temperature, measured over 100 Hz–100 kHz frequency range.

The four-electrode probe that was used in the study is suitable for accurately measuring the conductivity of 6 ml blood samples, but the probe may not be suitable for measuring the conductivity of soft tissues, such as cardiac tissue, due to constraints related to invasiveness, probe size, and sensing volume. For cardiac tissue, a smaller planar typology probe with a smaller sensing volume may be more appropriate.

This finding created the need for developing a probe design for accurately measuring the conductivity of cardiac tissue.

Chapter 5 focused on the development of a miniaturised four-electrode probe designed to measure the conductivity of biological tissues, particularly cardiac tissues. A probe was designed to address the issue of sensing volume when measuring conductivity, especially among studies performed at frequency ranges below 1 MHz. Larger sensing volumes can introduce discrepancies, particularly when dealing with limited or small biological samples, such as those from cardiac tissues.

The chapter also addressed the challenges associated with miniaturisation. One significant issue is the reduction of the capacity of the electrodes. The limited capacity of the probe can impede the electrical current, and this limitation could have affected the measurements. To mitigate this problem, the chapter introduced the innovative approach of coating the electrodes with PEDOT:PSS, a conductive polymer. This coating served to increase the capacity of the electrodes, and in turn, reduced the electrode polarisation effects. The chapter concluded by underscoring the potential impact of this technology on medical diagnostics and treatment.

Overall, this thesis contributed to the advancements in the knowledge of dielectric properties of blood and cardiac tissue, thereby filling crucial gaps in the existing literature that are of relevance to cardiac ablation. For the next steps in this line of research, the design refinements, validation studies, and potential clinical applications are outlined in the following section.

6.2 Future Work

To further develop the miniaturised four-electrode probe, a redesign is needed. While the probe overcame the limitations of sensing volume and tissue heterogeneity, the probe had limitations of lack of robustness and durability. To increase robustness and durability, areas of material selection, electrode configuration, and miniaturisation techniques will be scrutinised. Special attention is also required to formalise the analysis of the sensing volume of the probe to further support the finding that the probe has overcome the sensing volume challenges. Future work could incorporate computational modelling and experimental validation to ensure optimal results.

Once the redesigned probe has been developed, the next step is to test it on ex vivo tissue samples. This initial testing phase will provide essential data on the reliability, accuracy, and efficacy of the probe in a controlled environment that mimics physiological conditions. Following successful ex vivo testing, the research will then be extended to include in vivo studies and human cardiac tissue samples from a diverse demographic. These further studies will validate the clinical applicability of the probe and pave the way for its use in characterising the conductivity of cardiac tissue for cardiac ablation procedures.

By focusing on these sequential steps, from design refinement to clinical application, the research aims to contribute towards advancing catheter cardiac ablation, helping to improve treatment outcomes and patient safety.

References

[1] K. R. Foster and H. P. Schwan, "Dielectric properties of tissues and biological materials: a critical review," *Critical Reviews in Biomedical Engineering*, vol. 17, no. 1, pp. 25–104, 1989.

[2] A. La Gioia, E. Porter, I. Merunka, A. Shahzad, S. Salahuddin, M. Jones, and M. O'Halloran, "Open-Ended Coaxial Probe Technique for Dielectric Measurement of Biological Tissues : Challenges and Common Practices," *Diagnostics*, vol. 8, no. 40, pp. 1– 38, 2018.

[3] Q. Castellví, B. Mercadal, and A. Ivorra, "Assessment of Electroporation by Electrical Impedance Methods," in *Handbook of Electroporation* (D. Miklavcic, ed.), pp. 1–20, Cham: Springer International Publishing, 2016.

[4] M. Wang, R. Scapaticci, M. Cavagnaro, and L. Crocco, "Towards a Microwave Imaging System for Continuous Monitoring of Liver Tumor Ablation: Design and In Silico Validation of an Experimental Setup," *Diagnostics*, vol. 11, p. 866, May 2021.

[5] M. Thiriet, "Cardiac Pump: An Introduction," in *PanVascular Medicine* (P. Lanzer, ed.), pp. 345–412, Berlin, Heidelberg: Springer, 2015.

[6] Gray, *Elsevier: Gray's Anatomy, 41st Edition: Standring.* Elsevier Scientific Pub. Co, 2016.

[7] M. H. Ross and W. Pawlina, *Histology: a text and atlas: with correlated cell and molecular biology.* Philadelphia: Wolters Kluwer, eighth edition ed., 2020.

[8] H. Calkins et al., "2017 HRS/EHRA/ECAS/APHRS/SOLAECE expert consensus statement on catheter and surgical ablation of atrial fibrillation: executive summary," *Journal of Interventional Cardiac Electrophysiology*, vol. 50, pp. 1–55, Oct. 2017.

[9] T. G. Laske and P. A. Iaizzo, "The Cardiac Conduction System," in *Handbook of Cardiac Anatomy, Physiology, and Devices* (P. A. Iaizzo, ed.), pp. 123–136, Totowa, NJ: Humana Press, 2005.

[10] C. Antzelevitch and A. Burashnikov, "Overview of Basic Mechanisms of Cardiac Arrhythmia," *Cardiac electrophysiology clinics*, vol. 3, pp. 23–45, Mar. 2011.

[11] J. Billette and R. Tadros, "An integrated overview of AV node physiology," *Pacing and clinical electrophysiology: PACE*, vol. 42, pp. 805–820, July 2019.

[12] G. H. von Knorre, "The 125th anniversary of the His bundle discovery," *Herzschrittmachertherapie + Elektrophysiologie*, vol. 29, pp. 116–121, Mar. 2018.

[13] W. Dun and P. A. Boyden, "The Purkinje cell; 2008 style," *Journal of Molecular and Cellular Cardiology*, vol. 45, pp. 617–624, Nov. 2008.

[14] J. W. Mason, D. J. Ramseth, D. O. Chanter, T. E. Moon, D. B. Goodman, and B. Mendzelevski, "Electrocardiographic reference ranges derived from 79,743 ambulatory subjects," *Journal of Electrocardiology*, vol. 40, pp. 228–234.e8, May 2007.

[15] D.-g. Fu, "Cardiac Arrhythmias: Diagnosis, Symptoms, and Treatments," *Cell Biochemistry and Biophysics*, vol. 73, pp. 291–296, Nov. 2015.

[16] A. S. Go, E. M. Hylek, K. A. Phillips, Y. Chang, L. E. Henault, J. V. Selby, and D. E. Singer, "Prevalence of Diagnosed Atrial Fibrillation in Adults: National Implications for Rhythm Management and Stroke Prevention: the AnTicoagulation and Risk Factors In Atrial Fibrillation (ATRIA) Study," *JAMA*, vol. 285, p. 2370, May 2001.

[17] R. H. Falk, "Atrial fibrillation," *The New England Journal of Medicine*, vol. 344, pp. 1067–1078, Apr. 2001.

[18] S. Nattel, "New ideas about atrial fibrillation 50 years on," *Nature*, vol. 415, pp. 219–226, Jan. 2002.

[19] E. Anter, M. Jessup, and D. J. Callans, "Atrial Fibrillation and Heart Failure," *Circulation*, vol. 119, pp. 2516–2525, May 2009. Publisher: American Heart Association.

[20] S. Bordignon, M. Chiara Corti, and C. Bilato, "Atrial Fibrillation Associated with Heart Failure, Stroke and Mortality," *Journal of Atrial Fibrillation*, vol. 5, p. 467, June 2012.

[21] J. L. Anderson, J. L. Halperin, N. M. Albert, B. Bozkurt, R. G. Brindis, L. H. Curtis, D. DeMets, R. A. Guyton, J. S. Hochman, R. J. Kovacs, E. M. Ohman, S. J. Pressler, F. W. Sellke, and W.-K. Shen, "Management of Patients With Atrial Fibrillation (Compilation of 2006 ACCF/AHA/ESC and 2011 ACCF/AHA/HRS Recommendations): A Report of the American College of Cardiology/American Heart Association Task Force on Practice Guidelines," *Journal of the American College of Cardiology*, vol. 61, pp. 1935–1944, May 2013.

[22] M. M. Society, "A Comparison of Rate Control and Rhythm Control in Patients with Atrial Fibrillation," *The New England Journal of Medicine*, 2002.

[23] L. The National Heart, "Atrial fibrillation: Current understandings and research imperatives," *Journal of the American College of Cardiology*, vol. 22, pp. 1830–1834, Dec. 1993. Publisher: Journal of the American College of Cardiology Section: Clinical study.

[24] A. L. Waldo, "Management of atrial fibrillation: the need for AFFIRMative action. AFFIRM investigators. Atrial Fibrillation Follow-up Investigation of Rhythm Management," *The American Journal of Cardiology*, vol. 84, pp. 698–700, Sept. 1999.

[25] C. Narasimhan, Z. Blanck, and M. Akhtar, "Atrioventricular nodal modification and atrioventricular junctional ablation for control of ventricular rate in atrial fibrillation," *Journal of Cardiovascular Electrophysiology*, vol. 9, pp. S146–150, Aug. 1998.

[26] V. Markides and R. J. Schilling, "Atrial fibrillation: classification, pathophysiology, mechanisms and drug treatment," *Heart*, vol. 89, pp. 939–943, Aug. 2003.

[27] C. T. January, L. S. Wann, J. S. Alpert, H. Calkins, J. E. Cigarroa, J. C. Cleveland, J. B. Conti, P. T. Ellinor, M. D. Ezekowitz, M. E. Field, K. T. Murray, R. L. Sacco, W. G. Stevenson, P. J. Tchou, C. M. Tracy, C. W. Yancy, and American College of Cardiology/American Heart Association Task Force on Practice Guidelines, "2014 AHA/ACC/HRS guideline for the management of patients

with atrial fibrillation: a report of the American College of Cardiology/American Heart Association Task Force on Practice Guidelines and the Heart Rhythm Society," *Journal of the American College of Cardiology*, vol. 64, pp. e1–76, Dec. 2014.

[28] P. Jaïs, M. Haïssaguerre, D. C. Shah, S. Chouairi, L. Gencel, M. Hocini, and J. Clémenty, "A focal source of atrial fibrillation treated by discrete radiofrequency ablation," *Circulation*, vol. 95, pp. 572–576, Feb. 1997.

[29] M. Haïssaguerre, P. Jaïs, D. C. Shah, A. Takahashi, M. Hocini, G. Quiniou, S. Garrigue, A. Le Mouroux, P. Le Métayer, and J. Clémenty, "Spontaneous initiation of atrial fibrillation by ectopic beats originating in the pulmonary veins," *The New England Journal of Medicine*, vol. 339, pp. 659–666, Sept. 1998.

[30] O. Selfridge, "Studies on flutter and fibrillation; some notes on the theory of flutter," *Archivos Del Instituto De Cardiologia De Mexico*, vol. 18, pp. 177–187, Apr. 1948.

[31] G. K. Moe and J. A. Abildskov, "Atrial fibrillation as a self-sustaining arrhythmia independent of focal discharge," *American Heart Journal*, vol. 58, pp. 59–70, July 1959.

[32] L. Staerk, J. A. Sherer, D. Ko, E. J. Benjamin, and R. H. Helm, "Atrial Fibrillation: Epidemiology, Pathophysiology, and Clinical Outcomes," *Circulation research*, vol. 120, pp. 1501–1517, Apr. 2017.

[33] C. A. Morillo, G. J. Klein, D. L. Jones, and C. M. Guiraudon, "Chronic rapid atrial pacing. Structural, functional, and electrophysiological characteristics of a new model of sustained atrial fibrillation," *Circulation*, vol. 91, pp. 1588–1595, Mar. 1995.

[34] S. S. Chugh, R. Havmoeller, K. Narayanan, D. Singh, M. Rienstra, E. J. Benjamin, R. F. Gillum, Y.-H. Kim, J. H. McAnulty, Z.-J. Zheng, M. H. Forouzanfar, M. Naghavi, G. A. Mensah, M. Ezzati, and C. J. Murray, "Worldwide Epidemiology of Atrial Fibrillation: A Global Burden of Disease 2010 Study," *Circulation*, vol. 129, pp. 837–847, Feb. 2014.

[35] H. Zulkifly, G. Y. H. Lip, and D. A. Lane, "Epidemiology of atrial fibrillation," *International Journal of Clinical Practice*, vol. 72, p. e13070, Mar. 2018.

[36] F. Pistoia, S. Sacco, C. Tiseo, D. Degan, R. Ornello, and A. Carolei, "The Epidemiology of Atrial Fibrillation and Stroke," *Cardiology Clinics*, vol. 34, pp. 255–268, May 2016.

[37] H. Stefansdottir, T. Aspelund, V. Gudnason, and D. O. Arnar, "Trends in the incidence and prevalence of atrial fibrillation in Iceland and future projections," *EP Europace*, vol. 13, pp. 1110–1117, Aug. 2011.

[38] D. A. Lane, F. Skjøth, G. Y. H. Lip, T. B. Larsen, and D. Kotecha, "Temporal Trends in Incidence, Prevalence, and Mortality of Atrial Fibrillation in Primary Care," *Journal of the American Heart Association*, vol. 6, no. 5, p. e005155, 2017. Publisher: American Heart Association.

[39] S. Colilla, A. Crow, W. Petkun, D. E. Singer, T. Simon, and X. Liu, "Estimates of Current and Future Incidence and Prevalence of Atrial Fibrillation in the U.S. Adult Population," *The American Journal of Cardiology*, vol. 112, pp. 1142–1147, Oct. 2013.

[40] "Cardiovascular Health Study (CHS) | NHLBI, NIH."

[41] L. P. Fried, N. O. Borhani, P. Enright, C. D. Furberg, J. M. Gardin, R. A. Kronmal, L. H. Kuller, T. A. Manolio, M. B. Mittelmark, and A. Newman, "The Cardiovascular Health Study: design and rationale," *Annals of Epidemiology*, vol. 1, pp. 263–276, Feb. 1991.

[42] L. Y. Chen and W.-K. Shen, "Epidemiology of atrial fibrillation: A current perspective," *Heart Rhythm*, vol. 4, pp. S1–S6, Mar. 2007.

[43] W. M. Feinberg, J. L. Blackshear, A. Laupacis, R. Kronmal, and R. G. Hart, "Prevalence, age distribution, and gender of patients with atrial fibrillation. Analysis and implications," *Archives of Internal Medicine*, vol. 155, pp. 469–473, Mar. 1995.

[44] M. A. Allessie, K. Konings, C. J. Kirchhof, and M. Wijffels, "Electrophysiologic mechanisms of perpetuation of atrial fibrillation," *The American Journal of Cardiology*, vol. 77, pp. 10A–23A, Jan. 1996.

[45] D. M. Lloyd-Jones, T. J. Wang, E. P. Leip, M. G. Larson, D. Levy, R. S. Vasan, R. B. D'Agostino, J. M. Massaro, A. Beiser, P. A. Wolf, and E. J. Benjamin, "Lifetime risk for development of atrial fibrillation: the Framingham Heart Study," *Circulation*, vol. 110, pp. 1042–1046, Aug. 2004.

[46] G. Tse, "Mechanisms of cardiac arrhythmias," *Journal of Arrhythmia*, vol. 32, pp. 75–81, Apr. 2016.

[47] A. M. Pertsov, J. M. Davidenko, R. Salomonsz, W. T. Baxter, and J. Jalife, "Spiral waves of excitation underlie reentrant activity in isolated cardiac muscle.," *Circulation Research*, vol. 72, pp. 631–650, Mar. 1993. Publisher: American Heart Association.

[48] C. H. Roney, A. L. Wit, and N. S. Peters, "Challenges Associated with Interpreting Mechanisms of AF," *Arrhythmia & Electrophysiology Review*, vol. 8, pp. 273–284, Dec. 2019.

[49] C.-H. Xu, F. Xiong, W.-F. Jiang, X. Liu, T. Liu, and M. Qin, "Rotor mechanism and its mapping in atrial fibrillation," *Europace*, vol. 25, pp. 783–792, Feb. 2023.

[50] J. L. Cox, T. E. Canavan, R. B. Schuessler, M. E. Cain, B. D. Lindsay, C. Stone, P. K. Smith, P. B. Corr, and J. P. Boineau, "The surgical treatment of atrial fibrillation," *The Journal of Thoracic and Cardiovascular Surgery*, vol. 101, pp. 406–426, Mar. 1991.

[51] V. Fuster, L. E. Rydén, R. W. Asinger, D. S. Cannom, H. J. Crijns, R. L. Frye, J. L. Halperin, G. N. Kay, W. W. Klein, S. Lévy, R. L. McNamara, E. N. Prystowsky, L. S. Wann, D. G. Wyse, R. J. Gibbons, E. M. Antman, J. S. Alpert, D. P. Faxon, V. Fuster, G. Gregoratos, L. F. Hiratzka, A. K. Jacobs, R. O. Russell, S. C. Smith, W. W. Klein, A. Alonso-Garcia, C. Blomström-Lundqvist, G. de Backer, M. Flather, J. Hradec, A. Oto, A. Parkhomenko, S. Silber, A. Torbicki, American College of Cardiology/American Heart Association Task Force on Practice Guidelines, European Society of Cardiology Committee for Practice Guidelines and Policy Conferences (Committee to Develop Guidelines for the Management of Patients With Atrial Fibrillation), and North American Society of Pacing and Electrophysiology, "ACC/AHA/ESC Guidelines for the Management of Patients With Atrial Fibrillation: Executive Summary A Report of the American College of Cardiology/American Heart Association Task Force on Practice Guidelines and the European Society of Cardiology Committee for Practice Guidelines and Policy Conferences (Committee to Develop Guidelines for the Management of Patients With Atrial Fibrillation) Developed in Collaboration With the North American Society of Pacing and Electrophysiology," *Circulation*, vol. 104, pp. 2118–2150, Oct. 2001.

[52] M. Sucu, V. Davutoglu, and O. Ozer, "Electrical cardioversion," *Annals of Saudi Medicine*, vol. 29, no. 3, pp. 201–206, 2009.

[53] A. D. Krahn, J. Manfreda, R. B. Tate, F. A. Mathewson, and T. E. Cuddy, "The natural history of atrial fibrillation: incidence, risk factors, and prognosis in the Manitoba Follow-Up Study," *The American Journal of Medicine*, vol. 98, pp. 476–484, May 1995.

[54] K. M. Flegel, M. J. Shipley, and G. Rose, "Risk of stroke in non-rheumatic atrial fibrillation," *Lancet (London, England)*, vol. 1, pp. 526–529, Mar. 1987.

[55] E. J. Benjamin, P. A. Wolf, R. B. D'Agostino, H. Silbershatz, W. B. Kannel, and D. Levy, "Impact of atrial fibrillation on the risk of death: the Framingham Heart Study," *Circulation*, vol. 98, pp. 946–952, Sept. 1998.

[56] O. M. Wazni, N. F. Marrouche, D. O. Martin, A. Verma, M. Bhargava, W. Saliba, D. Bash, R. Schweikert, J. Brachmann, J. Gunther, K. Gutleben, E. Pisano, D. Potenza, R. Fanelli, A. Raviele, S. Themistoclakis, A. Rossillo, A. Bonso, and A. Natale, "Radiofrequency Ablation vs Antiarrhythmic Drugs as First-line Treatment of Symptomatic Atrial Fibrillation: A Randomized Trial," *JAMA*, vol. 293, p. 2634, June 2005.

[57] M. A. Brodsky, B. J. Allen, C. J. Walker, T. P. Casey, C. R. Luckett, and W. L. Henry, "Amiodarone for maintenance of sinus rhythm after conversion of atrial fibrillation in the setting of a dilated left atrium," *The American Journal of Cardiology*, vol. 60, pp. 572–575, Sept. 1987.

[58] I. C. Van Gelder, H. J. Crijns, R. G. Tieleman, J. Brügemann, P. J. De Kam, A. T. Gosselink, F. W. Verheugt, and K. I. Lie, "Chronic atrial fibrillation. Success of serial cardioversion therapy and safety of oral anticoagulation," *Archives of Internal Medicine*, vol. 156, pp. 2585–2592, Dec. 1996.

[59] H. J. Crijns, I. C. Van Gelder, W. H. Van Gilst, H. Hillege, A. M. Gosselink, and K. I. Lie, "Serial antiarrhythmic drug treatment to maintain sinus rhythm after electrical cardioversion for chronic atrial fibrillation or atrial flutter," *The American Journal of Cardiology*, vol. 68, pp. 335–341, Aug. 1991.

[60] E. J. Benjamin, D. Levy, S. M. Vaziri, R. B. D'Agostino, A. J. Belanger, and P. A. Wolf, "Independent risk factors for atrial fibrillation in a population-based cohort. The Framingham Heart Study," *JAMA*, vol. 271, pp. 840–844, Mar. 1994.

[61] J. L. Cox, R. B. Schuessler, D. G. Lappas, and J. P. Boineau, "An 8 1/2-year clinical experience with surgery for atrial fibrillation," *Annals of Surgery*, vol. 224, pp. 267–273; discussion 273–275, Sept. 1996.

[62] J. L. Cox, "Cardiac surgery for arrhythmias," *Journal of Cardiovascular Electrophysiology*, vol. 15, pp. 250–262, Feb. 2004.

[63] T. Weimar, M. S. Bailey, Y. Watanabe, D. Marin, H. S. Maniar, R. B. Schuessler, and R. J. Damiano, "The Cox-maze IV procedure for lone atrial fibrillation: a single center experience in 100 consecutive patients," *Journal of interventional cardiac electrophysiology : an international journal of arrhythmias and pacing*, vol. 31, pp. 47–54, June 2011.

[64] N. Viola, M. R. Williams, M. C. Oz, and N. Ad, "The technology in use for the surgical ablation of atrial fibrillation," *Seminars in Thoracic and Cardiovascular Surgery*, vol. 14, pp. 198–205, July 2002.

[65] J. E. Cummings, A. Pacifico, J. L. Drago, F. Kilicaslan, and A. Natale, "Alternative Energy Sources for the Ablation of Arrhythmias," *Pacing and Clinical Electrophysiology*, vol. 28, pp. 434–443, May 2005. Publisher: John Wiley & Sons, Ltd.

[66] K. Khargi, B. A. Hutten, B. Lemke, and T. Deneke, "Surgical treatment of atrial fibrillation; a systematic review," *European Journal of Cardio-Thoracic Surgery: Official Journal of the European Association for Cardio-Thoracic Surgery*, vol. 27, pp. 258–265, Feb. 2005.

[67] M. R. Williams, M. Garrido, M. C. Oz, and M. Argenziano, "Alternative energy sources for surgical atrial ablation," *Journal of Cardiac Surgery*, vol. 19, pp. 201–206, June 2004.

[68] E. P. Gerstenfeld, P. Guerra, P. B. Sparks, K. Hattori, and M. D. Lesh, "Clinical outcome after radiofrequency catheter ablation of focal atrial fibrillation triggers," *Journal of Cardiovascular Electrophysiology*, vol. 12, pp. 900–908, Aug. 2001.

[69] H. Oral, B. P. Knight, H. Tada, M. Ozaydin, A. Chugh, S. Hassan, C. Scharf, S. W. K. Lai, R. Greenstein, F. Pelosi, S. A. Strickberger, and F. Morady, "Pulmonary vein isolation for paroxysmal and persistent atrial fibrillation," *Circulation*, vol. 105, pp. 1077–1081, Mar. 2002.

[70] European Heart Rhythm Association (EHRA), European Cardiac Arrhythmia Scoiety (ECAS), American College of Cardiology (ACC), American Heart Association (AHA), Society of Thoracic Surgeons (STS), H. Calkins, J. Brugada, D. L. Packer, R. Cappato, S.-A. Chen, H. J. G. Crijns, R. J. Damiano, D. W. Davies, D. E. Haines, M. Haissaguerre, Y. Iesaka, W. Jackman, P. Jais, H. Kottkamp, K. H. Kuck, B. D. Lindsay, F. E. Marchlinski, P. M. McCarthy, J. L. Mont, F. Morady, K. Nademanee, A. Natale, C. Pappone, E. Prystowsky, A. Raviele, J. N. Ruskin, and R. J. Shemin, "HRS/EHRA/ECAS expert Consensus Statement on catheter and surgical ablation of atrial fibrillation: recommendations for personnel, policy, procedures and follow-up. A report of the Heart Rhythm Society (HRS) Task Force on catheter and surgical ablation of atrial fibrillation," *Heart Rhythm*, vol. 4, pp. 816–861, June 2007.

[71] A. J. Camm, P. Kirchhof, G. Y. H. Lip, U. Schotten, I. Savelieva, S. Ernst, I. C. Van Gelder, N. Al-Attar, G. Hindricks, B. Prendergast, H. Heidbuchel, O. Alfieri, A. Angelini, D. Atar, P. Colonna, R. De Caterina, J. De Sutter, A. Goette, B. Gorenek, M. Heldal, S. H. Hohloser, P. Kolh, J.-Y. Le Heuzey, P. Ponikowski, F. H. Rutten, and ESC Committee for Practice Guidelines, "Guidelines for the management of atrial fibrillation: the Task Force for the Management of Atrial Fibrillation of the European Society of Cardiology (ESC)," *Europace: European Pacing, Arrhythmias, and Cardiac Electrophysiology: Journal of the Working Groups on Cardiac Pacing, Arrhythmias, and Cardiac Cellular Electrophysiology of the European Society of Cardiology*, vol. 12, pp. 1360–1420, Oct. 2010.

[72] V. Fuster, L. E. Rydén, D. S. Cannom, H. J. Crijns, A. B. Curtis, K. A. Ellenbogen, J. L. Halperin, G. N. Kay, J.-Y. Le Huezey, J. E. Lowe, S. B. Olsson, E. N. Prystowsky, J. L. Tamargo, and L. S. Wann, "2011 ACCF/AHA/HRS focused updates incorporated into the ACC/AHA/ESC 2006 Guidelines for the management of patients with atrial fibrillation: a report of the American College of Cardiology Foundation/American Heart Association Task Force on Practice Guidelines developed in partnership with the European Society of Cardiology and in collaboration with the European Heart Rhythm Association and the Heart Rhythm Society," *Journal of the American College of Cardiology*, vol. 57, pp. e101–198, Mar. 2011.

[73] L. B. Mitchell and CCS Atrial Fibrillation Guidelines Committee, "Canadian Cardiovascular Society atrial fibrillation guidelines 2010: prevention and treat-

ment of atrial fibrillation following cardiac surgery," *The Canadian Journal of Cardiology*, vol. 27, no. 1, pp. 91–97, 2011.

[74] T. Wonnell, P. Stauffer, and J. Langberg, "Evaluation of microwave and radio frequency catheter ablation in a myocardium-equivalent phantom model," *IEEE Transactions on Biomedical Engineering*, vol. 39, pp. 1086–1095, Oct. 1992.

[75] P. Kirchhof, S. Benussi, D. Kotecha, A. Ahlsson, D. Atar, B. Casadei, M. Castella, H.-C. Diener, H. Heidbuchel, J. Hendriks, G. Hindricks, A. S. Manolis, J. Oldgren, B. A. Popescu, U. Schotten, B. Van Putte, P. Vardas, S. Agewall, J. Camm, G. Baron Esquivias, W. Budts, S. Carerj, F. Casselman, A. Coca, R. De Caterina, S. Deftereos, D. Dobrev, J. M. Ferro, G. Filippatos, D. Fitzsimons, B. Gorenek, M. Guenoun, S. H. Hohnloser, P. Kolh, G. Y. H. Lip, A. Manolis, J. McMurray, P. Ponikowski, R. Rosenhek, F. Ruschitzka, I. Savelieva, S. Sharma, P. Suwalski, J. L. Tamargo, C. J. Taylor, I. C. Van Gelder, A. A. Voors, S. Windecker, J. L. Zamorano, and K. Zeppenfeld, "2016 ESC Guidelines for the management of atrial fibrillation developed in collaboration with EACTS," *European Journal of Cardio-Thoracic Surgery*, vol. 50, pp. e1–e88, Nov. 2016.

[76] I. Sheikh, D. Krum, R. Cooley, A. Dhala, Z. Blanck, A. Bhatia, V. Nangia, M. Akhtar, and J. Sra, "Pulmonary vein isolation and linear lesions in atrial fibrillation ablation," *Journal of Interventional Cardiac Electrophysiology*, vol. 17, pp. 103–109, Nov. 2006.

[77] P. Santangeli, L. Di Biase, D. J. Burkhardt, R. Horton, J. Sanchez, R. Bai, A. Pump, M. Perez, P. J. Wang, A. Natale, and A. Al-Ahmad, "Catheter ablation of atrial fibrillation: state-of-the-art techniques and future perspectives," *Journal of Cardiovascular Medicine*, vol. 13, pp. 108–124, Feb. 2012.

[78] H. Oral, C. Scharf, A. Chugh, B. Hall, P. Cheung, E. Good, S. Veerareddy, F. Pelosi, and F. Morady, "Catheter Ablation for Paroxysmal Atrial Fibrillation: Segmental Pulmonary Vein Ostial Ablation Versus Left Atrial Ablation," *Circulation*, vol. 108, pp. 2355–2360, Nov. 2003.

[79] K. Benali, V. Barre, A. Hermida, A. Milhem, S. Philibert, S. Boveda, C. Bars, F. Anselme, B. Maille, C. André, A. Behaghel, G. Moubarak, N. Clémenty, A. Da Costa, M. Arnaud, S. Venier, F. Sebag, L. Jesel, L. Macle, and R. Martins, "Atrial fibrillation recurrences despite durable pulmonary vein isolation:

Characteristics, management and outcomes, the PARTY-PVI study," *Archives of Cardiovascular Diseases Supplements*, vol. 15, pp. 92–93, Jan. 2023.

[80] M. Lycke, M. Kyriakopoulou, M. El Haddad, J.-Y. Wielandts, G. Hilfiker, A. Almorad, T. Strisciuglio, J. De Pooter, M. Wolf, P. Unger, Y. Vandekerckhove, R. Tavernier, J.-B. E. P. de Waroux, M. Duytschaever, and S. Knecht, "Predictors of recurrence after durable pulmonary vein isolation for paroxysmal atrial fibrillation," *Europace: European Pacing, Arrhythmias, and Cardiac Electrophysiology: Journal of the Working Groups on Cardiac Pacing, Arrhythmias, and Cardiac Cellular Electrophysiology of the European Society of Cardiology*, vol. 23, pp. 861–867, June 2021.

[81] M. Yano, Y. Egami, K. Yanagawa, Y. Matsuhiro, H. Nakamura, K. Yasumoto, N. Okamoto, A. Tanaka, Y. Matsunaga-Lee, D. Nakamura, M. Yamato, R. Shutta, M. Nishino, and J. Tanouchi, "Predictors of recurrence after pulmonary vein isolation in patients with normal left atrial diameter," *Journal of Arrhythmia*, vol. 36, pp. 75–81, Sept. 2019.

[82] K. Benali, V. Barré, A. Hermida, V. Galand, A. Milhem, S. Philibert, S. Boveda, C. Bars, F. Anselme, B. Maille, C. André, A. Behaghel, G. Moubarak, N. Clémenty, A. Da Costa, M. Arnaud, S. Venier, F. Sebag, L. Jésel-Morel, A. Sagnard, L. Champ-Rigot, D. Dang, B. Guy-Moyat, S. Abbey, R. Garcia, O. Césari, N. Badenco, A. Lepillier, S. Ninni, S. Boulé, P. Maury, V. Algalarrondo, B. Bakouboula, J. Mansourati, F. Lesaffre, P. Lagrange, A. Bouzeman, L. Muresan, R. Bacquelin, A. Bortone, S.-S. Bun, D. Pavin, L. Macle, and R. P. Martins, "Recurrences of Atrial Fibrillation Despite Durable Pulmonary Vein Isolation: The PARTY-PVI Study," *Circulation: Arrhythmia and Electrophysiology*, vol. 16, p. e011354, Mar. 2023. Publisher: American Heart Association.

[83] G. Katritsis and H. Calkins, "Catheter Ablation of Atrial Fibrillation – Techniques and Technology," *Arrhythmia & Electrophysiology Review*, vol. 1, pp. 29–33, Sept. 2012.

[84] D. J. Wilber, C. Pappone, P. Neuzil, A. De Paola, F. Marchlinski, A. Natale, L. Macle, E. G. Daoud, H. Calkins, B. Hall, V. Reddy, G. Augello, M. R. Reynolds, C. Vinekar, C. Y. Liu, S. M. Berry, D. A. Berry, and ThermoCool AF Trial Investigators, "Comparison of antiarrhythmic drug therapy and radiofrequency catheter ablation in patients with paroxysmal atrial fibrillation: a randomized controlled trial," *JAMA*, vol. 303, pp. 333–340, Jan. 2010.

[85] P. Jaïs, B. Cauchemez, L. Macle, E. Daoud, P. Khairy, R. Subbiah, M. Hocini, F. Extramiana, F. Sacher, P. Bordachar, G. Klein, R. Weerasooriya, J. Clémenty, and M. Haïssaguerre, "Catheter ablation versus antiarrhythmic drugs for atrial fibrillation: the A4 study," *Circulation*, vol. 118, pp. 2498–2505, Dec. 2008.

[86] H. Calkins, M. R. Reynolds, P. Spector, M. Sondhi, Y. Xu, A. Martin, C. J. Williams, and I. Sledge, "Treatment of atrial fibrillation with antiarrhythmic drugs or radiofrequency ablation: two systematic literature reviews and meta-analyses," *Circulation. Arrhythmia and Electrophysiology*, vol. 2, pp. 349–361, Aug. 2009.

[87] D. L. Packer, S. Asirvatham, and T. M. Munger, "Progress in Non-pharmacologic Therapy of Atrial Fibrillation," *Journal of Cardiovascular Electrophysiology*, vol. 14, no. s12, pp. S296–S309, 2003. _eprint: https://onlinelibrary.wiley.com/doi/pdf/10.1046/j.1540-8167.2003.90403.x.

[88] D. E. Haines, "The biophysics of radiofrequency catheter ablation in the heart: the importance of temperature monitoring," *Pacing and clinical electrophysiology: PACE*, vol. 16, pp. 586–591, Mar. 1993.

[89] D. Haines, "Biophysics of Ablation:. Application to Technology," *Journal of Cardiovascular Electrophysiology*, vol. 15, pp. S2–S11, Oct. 2004.

[90] M. R. Williams, M. Knaut, D. Bérubé, and M. C. Oz, "Application of microwave energy in cardiac tissue ablation: from in vitro analyses to clinical use," *The Annals of Thoracic Surgery*, vol. 74, pp. 1500–1505, Nov. 2002.

[91] C. J. Bradley and D. E. Haines, "Pulsed field ablation for pulmonary vein isolation in the treatment of atrial fibrillation," *Journal of Cardiovascular Electrophysiology*, vol. 31, no. 8, pp. 2136–2147, 2020. _eprint: https://onlinelibrary.wiley.com/doi/pdf/10.1111/jce.14414.

[92] S. McBride, S. Avazzadeh, A. M. Wheatley, B. O'Brien, K. Coffey, A. Elahi, M. O'Halloran, and L. R. Quinlan, "Ablation Modalities for Therapeutic Intervention in Arrhythmia-Related Cardiovascular Disease: Focus on Electroporation," *Journal of Clinical Medicine*, vol. 10, p. 2657, June 2021.

[93] A. Verma, C.-y. Jiang, T. R. Betts, J. Chen, I. Deisenhofer, R. Mantovan, L. Macle, C. A. Morillo, W. Haverkamp, R. Weerasooriya, J.-P. Albenque,

S. Nardi, E. Menardi, P. Novak, and P. Sanders, "Approaches to Catheter Ablation for Persistent Atrial Fibrillation," *New England Journal of Medicine*, vol. 372, pp. 1812–1822, May 2015.

[94] V. Y. Reddy, P. Neuzil, J. S. Koruth, J. Petru, M. Funosako, H. Cochet, L. Sediva, M. Chovanec, S. R. Dukkipati, and P. Jais, "Pulsed Field Ablation for Pulmonary Vein Isolation in Atrial Fibrillation," *Journal of the American College of Cardiology*, vol. 74, pp. 315–326, July 2019.

[95] S. K. Huang, S. Bharati, A. R. Graham, M. Lev, F. I. Marcus, and R. C. Odell, "Closed chest catheter desiccation of the atrioventricular junction using radiofrequency energy—A new method of catheter ablation," *Journal of the American College of Cardiology*, vol. 9, pp. 349–358, Feb. 1987. Publisher: American College of Cardiology Foundation.

[96] J. E. Marine, "Catheter Ablation Therapy for Supraventricular Arrhythmias," *JAMA*, vol. 298, p. 2768, Dec. 2007.

[97] S. Nath, J. P. DiMarco, and D. E. Haines, "Basic aspects of radiofrequency catheter ablation," *Journal of Cardiovascular Electrophysiology*, vol. 5, pp. 863–876, Oct. 1994.

[98] M. Ahmed, C. L. Brace, F. T. Lee, and S. N. Goldberg, "Principles of and Advances in Percutaneous Ablation," *Radiology*, vol. 258, pp. 351–369, Feb. 2011.

[99] S. Curto, M. Taj-Eldin, D. Fairchild, and P. Prakash, "Microwave ablation at 915 MHz vs 2.45 GHz: A theoretical and experimental investigation," *Medical Physics*, vol. 42, pp. 6152–6161, Nov. 2015.

[100] A. Bottiglieri, G. Ruvio, M. O'Halloran, and L. Farina, "Exploiting Tissue Dielectric Properties to Shape Microwave Thermal Ablation Zones," *Sensors*, vol. 20, p. 3960, Jan. 2020. Number: 14 Publisher: Multidisciplinary Digital Publishing Institute.

[101] S. Saksena, R. J. Damiano, N. A. M. Estes, and F. E. Marchlinski, eds., *Interventional cardiac electrophysiology: a multidisciplinary approach*. Minneapolis, Minnesota: Cardiotext Publishing, 2015. OCLC: 908374143.

[102] J. G. Whayne, S. Nath, and D. E. Haines, "Microwave catheter ablation of myocardium in vitro. Assessment of the characteristics of tissue heating and injury," *Circulation*, vol. 89, pp. 2390–2395, May 1994.

[103] A. M. Gillinov, P. M. Mccarthy, N. Marrouche, and A. Natale, "Contemporary Surgical Treatment for Atrial Fibrillation," *Pacing and Clinical Electrophysiology*, vol. 26, no. 7p2, pp. 1641–1644, 2003. _eprint: https://onlinelibrary.wiley.com/doi/pdf/10.1046/j.1460-9592.2003.t01-1-00245.x.

[104] M. R. Williams, M. Argenziano, and M. C. Oz, "Microwave ablation for surgical treatment of atrial fibrillation," *Seminars in Thoracic and Cardiovascular Surgery*, vol. 14, pp. 232–237, July 2002.

[105] O. Seror, "Ablative therapies: Advantages and disadvantages of radiofrequency, cryotherapy, microwave and electroporation methods, or how to choose the right method for an individual patient?," *Diagnostic and Interventional Imaging*, vol. 96, pp. 617–624, June 2015.

[106] A. Di Monaco, N. Vitulano, F. Troisi, F. Quadrini, I. Romanazzi, V. Calvi, and M. Grimaldi, "Pulsed Field Ablation to Treat Atrial Fibrillation: A Review of the Literature," *Journal of Cardiovascular Development and Disease*, vol. 9, p. 94, Mar. 2022.

[107] B. C. du Pré, V. J. van Driel, H. van Wessel, P. Loh, P. A. Doevendans, R. Goldschmeding, F. H. Wittkampf, and A. Vink, "Minimal coronary artery damage by myocardial electroporation ablation," *EP Europace*, vol. 15, pp. 144–149, Jan. 2013.

[108] K. Neven, V. van Driel, H. van Wessel, R. van Es, B. du Pré, P. A. Doevendans, and F. Wittkampf, "Safety and Feasibility of Closed Chest Epicardial Catheter Ablation Using Electroporation," *Circulation: Arrhythmia and Electrophysiology*, vol. 7, pp. 913–919, Oct. 2014. Publisher: American Heart Association.

[109] A. Sugrue, V. R. Vaidya, C. Livia, D. Padmanabhan, A. Abudan, A. Isath, T. Witt, C. V. DeSimone, P. Stalboerger, S. Kapa, S. J. Asirvatham, and C. J. McLeod, "Feasibility of selective cardiac ventricular electroporation," *PLOS ONE*, vol. 15, no. 2, p. e0229214, 2020. Publisher: Public Library of Science.

[110] V. Y. Reddy, J. Koruth, P. Jais, J. Petru, F. Timko, I. Skalsky, R. Hebeler, L. Labrousse, L. Barandon, S. Kralovec, M. Funosako, B. B. Mannuva, L. Sediva, and P. Neuzil, "Ablation of Atrial Fibrillation With Pulsed Electric Fields: An Ultra-Rapid, Tissue-Selective Modality for Cardiac Ablation," *JACC: Clinical Electrophysiology*, vol. 4, no. 8, pp. 987–995, 2018.

[111] W. Krassowska, "Effects of Electroporation on Transmembrane Potential Induced by Defibrillation Shocks," *Pacing and Clinical Electrophysiology*, vol. 18, no. 9, pp. 1644–1660, 1995. _eprint: https://onlinelibrary.wiley.com/doi/pdf/10.1111/j.1540-8159.1995.tb06986.x.

[112] I. Kaminska, M. Kotulska, A. Stecka, J. Saczko, M. Drag-Zalesinska, T. Wysocka, A. Choromanska, N. Skolucka, R. Nowicki, J. Marczak, and J. Kulbacka, "Electroporation-induced changes in normal immature rat myoblasts (H9C2)," *General physiology and biophysics*, vol. 31, no. 01, pp. 19–25, 2012.

[113] L. S. Poulou, E. Botsa, I. Thanou, P. D. Ziakas, and L. Thanos, "Percutaneous microwave ablation vs radiofrequency ablation in the treatment of hepatocellular carcinoma," *World Journal of Hepatology*, vol. 7, pp. 1054–1063, May 2015.

[114] E. Neumann and K. Rosenheck, "Permeability changes induced by electric impulses in vesicular membranes," *The Journal of Membrane Biology*, vol. 10, pp. 279–290, Dec. 1972.

[115] V. J. H. M. van Driel, K. Neven, H. van Wessel, A. Vink, P. A. F. M. Doevendans, and F. H. M. Wittkampf, "Low vulnerability of the right phrenic nerve to electroporation ablation," *Heart Rhythm*, vol. 12, pp. 1838–1844, Aug. 2015.

[116] C. M. Witt, A. Sugrue, D. Padmanabhan, V. Vaidya, S. Gruba, J. Rohl, C. V. DeSimone, A. M. Killu, N. Naksuk, J. Pederson, S. Suddendorf, D. J. Ladewig, E. Maor, D. R. Holmes, S. Kapa, and S. J. Asirvatham, "Intrapulmonary Vein Ablation Without Stenosis: A Novel Balloon-Based Direct Current Electroporation Approach," *Journal of the American Heart Association*, vol. 7, p. e009575, July 2018. Publisher: American Heart Association.

[117] K. Neven, R. van Es, V. van Driel, H. van Wessel, H. Fidder, A. Vink, P. Doevendans, and F. Wittkampf, "Acute and Long-Term Effects of Full-Power Electroporation Ablation Directly on the Porcine Esophagus," *Circulation: Arrhythmia and Electrophysiology*, vol. 10, p. e004672, May 2017. Publisher: American Heart Association.

[118] F. H. Wittkampf, V. J. Van Driel, H. Van Wessel, A. Vink, I. E. Hof, P. F. Gründeman, R. N. Hauer, and P. Loh, "Feasibility of Electroporation for the Creation of Pulmonary Vein Ostial Lesions," *Journal of Cardiovascular Electrophysiology*, vol. 22, no. 3, pp. 302–309, 2011. _eprint: https://onlinelibrary.wiley.com/doi/pdf/10.1111/j.1540-8167.2010.01863.x.

[119] J. Koruth, K. Kuroki, J. Iwasawa, Y. Enomoto, R. Viswanathan, R. Brose, E. D. Buck, M. Speltz, S. R. Dukkipati, and V. Y. Reddy, "Preclinical Evaluation of Pulsed Field Ablation," *Circulation: Arrhythmia and Electrophysiology*, vol. 12, p. e007781, Dec. 2019. Publisher: American Heart Association.

[120] C. V. DeSimone, E. Ebrille, F. F. Syed, S. B. Mikell, S. H. Suddendorf, D. Wahnschaffe, D. J. Ladewig, E. J. Gilles, A. J. Danielsen, D. R. Holmes, and S. J. Asirvatham, "Novel balloon catheter device with pacing, ablating, electroporation, and drug-eluting capabilities for atrial fibrillation treatment—preliminary efficacy and safety studies in a canine model," *Translational Research*, vol. 164, pp. 508–514, Dec. 2014.

[121] V. J. van Driel, K. G. Neven, H. van Wessel, B. C. du Pré, A. Vink, P. A. Doevendans, and F. H. Wittkampf, "Pulmonary Vein Stenosis After Catheter Ablation," *Circulation: Arrhythmia and Electrophysiology*, vol. 7, pp. 734–738, Aug. 2014. Publisher: American Heart Association.

[122] K. Kuroki, W. Whang, C. Eggert, J. Lam, J. Leavitt, I. Kawamura, A. Reddy, B. Morrow, C. Schneider, J. Petru, M. K. Turagam, J. S. Koruth, M. A. Miller, S. Choudry, B. Ellsworth, S. R. Dukkipati, P. Neuzil, and V. Y. Reddy, "Ostial dimensional changes after pulmonary vein isolation: Pulsed field ablation vs radiofrequency ablation," *Heart Rhythm*, vol. 17, pp. 1528–1535, Sept. 2020.

[123] C. Tutuianu, J. Szilagy, R. Pap, and L. Sághy, "Very Long-Term Results Of Atrial Fibrillation Ablation Confirm That This Therapy Is Really Effective," *Journal of Atrial Fibrillation*, vol. 8, p. 1226, Aug. 2015.

[124] M. Takigawa, A. Takahashi, T. Kuwahara, K. Okubo, Y. Takahashi, Y. Watari, E. Nakashima, J. Nakajima, K. Yamao, K. Takagi, Y. Tanaka, T. Fujino, S. Kimura, H. Hikita, K. Hirao, and M. Isobe, "Long-term outcome after catheter ablation of paroxysmal atrial fibrillation: Impact of different atrial fibrillation foci," *International Journal of Cardiology*, vol. 227, pp. 407–412, Jan. 2017.

[125] A. G. Brooks, M. K. Stiles, J. Laborderie, D. H. Lau, P. Kuklik, N. J. Shipp, L.-F. Hsu, and P. Sanders, "Outcomes of long-standing persistent atrial fibrillation ablation: a systematic review," *Heart Rhythm*, vol. 7, pp. 835–846, June 2010.

[126] R. R. Tilz, K. R. J. Chun, B. Schmidt, A. Fuernkranz, E. Wissner, I. Koester, D. Baensch, S. Boczor, B. Koektuerk, A. Metzner, T. Zerm, S. Ernst, M. Antz,

K.-H. Kuck, and F. Ouyang, "Catheter ablation of long-standing persistent atrial fibrillation: a lesson from circumferential pulmonary vein isolation," *Journal of Cardiovascular Electrophysiology*, vol. 21, pp. 1085–1093, Oct. 2010.

[127] A. N. Ganesan, N. J. Shipp, A. G. Brooks, P. Kuklik, D. H. Lau, H. S. Lim, T. Sullivan, K. C. Roberts-Thomson, and P. Sanders, "Long-term outcomes of catheter ablation of atrial fibrillation: a systematic review and meta-analysis," *Journal of the American Heart Association*, vol. 2, p. e004549, Mar. 2013.

[128] W. S. Tzou, F. E. Marchlinski, E. S. Zado, D. Lin, S. Dixit, D. J. Callans, J. M. Cooper, R. Bala, F. Garcia, M. D. Hutchinson, M. P. Riley, R. Verdino, and E. P. Gerstenfeld, "Long-term outcome after successful catheter ablation of atrial fibrillation," *Circulation. Arrhythmia and Electrophysiology*, vol. 3, pp. 237–242, June 2010.

[129] F. Ouyang, R. Tilz, J. Chun, B. Schmidt, E. Wissner, T. Zerm, K. Neven, B. Köktürk, M. Konstantinidou, A. Metzner, A. Fuernkranz, and K.-H. Kuck, "Long-term results of catheter ablation in paroxysmal atrial fibrillation: lessons from a 5-year follow-up," *Circulation*, vol. 122, pp. 2368–2377, Dec. 2010.

[130] C. Medi, P. B. Sparks, J. B. Morton, P. M. Kistler, K. Halloran, R. Rosso, J. K. Vohra, S. Kumar, and J. M. Kalman, "Pulmonary vein antral isolation for paroxysmal atrial fibrillation: results from long-term follow-up," *Journal of Cardiovascular Electrophysiology*, vol. 22, pp. 137–141, Feb. 2011.

[131] C. R. Kerr, K. H. Humphries, M. Talajic, G. J. Klein, S. J. Connolly, M. Green, J. Boone, R. Sheldon, P. Dorian, and D. Newman, "Progression to chronic atrial fibrillation after the initial diagnosis of paroxysmal atrial fibrillation: results from the Canadian Registry of Atrial Fibrillation," *American Heart Journal*, vol. 149, pp. 489–496, Mar. 2005.

[132] C. B. de Vos, R. Pisters, R. Nieuwlaat, M. H. Prins, R. G. Tieleman, R.-J. S. Coelen, A. C. van den Heijkant, M. A. Allessie, and H. J. G. M. Crijns, "Progression from paroxysmal to persistent atrial fibrillation clinical correlates and prognosis," *Journal of the American College of Cardiology*, vol. 55, pp. 725–731, Feb. 2010.

[133] J. Caldwell and D. Redfearn, "Ablation of Complex Fractionated Atrial Electrograms in Catheter Ablation for AF; Where have we been and where are we going?," *Current Cardiology Reviews*, vol. 8, pp. 347–353, Nov. 2012.

[134] B. P. Mody, A. Raza, J. Jacobson, S. Iwai, D. Frenkel, R. Rojas, and W. S. Aronow, "Ablation of long-standing persistent atrial fibrillation," *Annals of Translational Medicine*, vol. 5, p. 305, Aug. 2017.

[135] S. Magnani, D. Muser, W. Chik, and P. Santangeli, "Adjunct ablation strategies for persistent atrial fibrillation— beyond pulmonary vein isolation," *Journal of Thoracic Disease*, vol. 7, no. 2, 2015.

[136] K. P. Letsas, M. Efremidis, C. Charalampous, S. Tsikrikas, and A. Sideris, "Current ablation strategies for persistent and long-standing persistent atrial fibrillation," *Cardiology Research and Practice*, vol. 2011, p. 376969, Mar. 2011.

[137] M. D. O'Neill, P. Jaïs, M. Hocini, F. Sacher, G. J. Klein, J. Clémenty, and M. Haïssaguerre, "Catheter Ablation for Atrial Fibrillation," *Circulation*, vol. 116, pp. 1515–1523, Sept. 2007. Publisher: American Heart Association.

[138] M. C. E. F. Wijffels, C. J. H. J. Kirchhof, R. B. Dorland, and M. A. Allessie, "Atrial Fibrillation Begets Atrial Fibrillation: A Study in Awake Chronically Instrumented Goats," *Circulation*, vol. 92, pp. 1954–1968, Oct. 1995.

[139] A. W. Teh, P. M. Kistler, G. Lee, C. Medi, P. M. Heck, S. J. Spence, J. B. Morton, P. Sanders, and J. M. Kalman, "Long-term effects of catheter ablation for lone atrial fibrillation: Progressive atrial electroanatomic substrate remodeling despite successful ablation," *Heart Rhythm*, vol. 9, pp. 473–480, Apr. 2012.

[140] A. Deshmukh, N. J. Patel, S. Pant, N. Shah, A. Chothani, K. Mehta, P. Grover, V. Singh, S. Vallurupalli, G. T. Savani, A. Badheka, T. Tuliani, K. Dabhadkar, G. Dibu, Y. M. Reddy, A. Sewani, M. Kowalski, R. Mitrani, H. Paydak, and J. F. Viles-Gonzalez, "In-Hospital Complications Associated With Catheter Ablation of Atrial Fibrillation in the United States Between 2000 and 2010: Analysis of 93 801 Procedures," *Circulation*, vol. 128, pp. 2104–2112, Nov. 2013.

[141] V. Velagic, I. Prepolec, V. Pasara, M. Puljevic, D. Puljevic, I. Planinc, J. Samardzic, and D. Milicic, "Learning curves in atrial fibrillation ablation – A comparison between second generation cryoballoon and contact force sensing radiofrequency catheters," *Indian Pacing and Electrophysiology Journal*, vol. 20, pp. 273–280, Sept. 2020.

[142] A. E. Darby, "Recurrent Atrial Fibrillation After Catheter Ablation: Considerations For Repeat Ablation And Strategies To Optimize Success," *Journal of Atrial Fibrillation*, vol. 9, p. 1427, June 2016.

[143] D. Lin, P. Santangeli, E. S. Zado, R. Bala, M. D. Hutchinson, M. P. Riley, D. S. Frankel, F. Garcia, S. Dixit, D. J. Callans, and F. E. Marchlinski, "Electrophysiologic findings and long-term outcomes in patients undergoing third or more catheter ablation procedures for atrial fibrillation," *Journal of Cardiovascular Electrophysiology*, vol. 26, pp. 371–377, Apr. 2015.

[144] C.-I. Park, H. Lehrmann, C. Keyl, R. Weber, J. Schiebeling, J. Allgeier, P. Schurr, A. Shah, F.-J. Neumann, T. Arentz, and A. S. Jadidi, "Mechanisms of Pulmonary Vein Reconnection After Radiofrequency Ablation of Atrial Fibrillation: The Deterministic Role of Contact Force and Interlesion Distance: Mechanisms of Pulmonary Vein Reconnection After Radiofrequency Ablation of Atrial Fibrillation," *Journal of Cardiovascular Electrophysiology*, vol. 25, pp. 701–708, July 2014.

[145] Z. Li, S. Wang, T. H. Hidru, Y. Sun, L. Gao, X. Yang, and Y. Xia, "Long Atrial Fibrillation Duration and Early Recurrence Are Reliable Predictors of Late Recurrence After Radiofrequency Catheter Ablation," *Frontiers in Cardiovascular Medicine*, vol. 9, 2022.

[146] "Late recurrence of atrial fibrillation 5 years after catheter ablation: predictors and outcome | EP Europace | Oxford Academic."

[147] A. J. Shah, M. Hocini, Y. Komatsu, M. Daly, S. Zellerhoff, L. Jesel, S. Amaroui, K. Ramoul, A. Denis, N. Derval, F. Sacher, P. Jais, and M. Haissaguerre, "The Progressive Nature of Atrial Fibrillation:A Rationale for Early Restoration and Maintenance of Sinus Rhythm," *Journal of Atrial Fibrillation*, vol. 6, p. 849, Aug. 2013.

[148] N. Mujović, M. Marinković, R. Lenarczyk, R. Tilz, and T. S. Potpara, "Catheter Ablation of Atrial Fibrillation: An Overview for Clinicians," *Advances in Therapy*, vol. 34, no. 8, pp. 1897–1917, 2017.

[149] L. O'Neill, J.-Y. Wielandts, K. Gillis, G. Hilfiker, J.-B. Le Polain De Waroux, R. Tavernier, M. Duytschaever, and S. Knecht, "Catheter Ablation in Persistent AF, the Evolution towards a More Pragmatic Strategy," *Journal of Clinical Medicine*, vol. 10, p. 4060, Sept. 2021.

[150] E. Charitakis, S. Metelli, L. O. Karlsson, A. P. Antoniadis, K. D. Rizas, I. Liuba, H. Almroth, A. Hassel Jönsson, J. Schwieler, D. Tsartsalis, S. Sideris, E. Dragioti, N. Fragakis, and A. Chaimani, "Comparing efficacy and safety in catheter ablation strategies for atrial fibrillation: a network meta-analysis," *BMC Medicine*, vol. 20, p. 193, May 2022.

[151] P. K. Arora, J. C. Hansen, A. D. Price, J. Koblish, and B. Avitall, "An Update on the Energy Sources and Catheter Technology for the Ablation of Atrial Fibrillation," *Journal of Atrial Fibrillation*, vol. 2, p. 233, Mar. 2010.

[152] A. V. Brick and D. M. Braile, "Surgical Ablation of Atrial Fibrillation Using Energy Sources," *Brazilian Journal of Cardiovascular Surgery*, vol. 30, no. 6, pp. 636–643, 2015.

[153] J. O. Robertson, C. P. Lawrance, H. S. Maniar, and R. J. Damiano Jr, "Surgical Techniques Used for the Treatment of Atrial Fibrillation," *Circulation Journal*, vol. 77, no. 8, pp. 1941–1951, 2013.

[154] N. Ad and S. D. Holmes, "Early Stable Sinus Rhythm Associated With Greater Success 5 Years After Surgical Ablation," *The Annals of Thoracic Surgery*, vol. 105, pp. 1370–1376, May 2018.

[155] A. Cluckey, A. C. Perino, F. N. Yunus, G. C. Leef, M. Askari, P. A. Heidenreich, S. M. Narayan, P. J. Wang, and M. P. Turakhia, "Efficacy of Ablation Lesion Sets in Addition to Pulmonary Vein Isolation for Paroxysmal Atrial Fibrillation: Findings From the SMASH-AF Meta-Analysis Study Cohort," *Journal of the American Heart Association*, vol. 8, p. e009976, Jan. 2019.

[156] C.-C. Chen, P.-T. Lee, V. Van Ba, C.-M. Chuang, Y.-J. Lin, L.-W. Lo, Y.-F. Hu, F.-P. Chung, C.-Y. Lin, T.-Y. Chang, J. J. Vicera, T.-C. Huang, C.-M. Liu, C.-I. Wu, I. C. Lugtu, A. Jain, S.-L. Chang, and S.-A. Chen, "Comparison of lesion characteristics between conventional and high-power short-duration ablation using contact force-sensing catheter in patients with paroxysmal atrial fibrillation," *BMC Cardiovascular Disorders*, vol. 21, p. 387, Dec. 2021.

[157] L. W. M. Leung, Z. Akhtar, A. Elbatran, A. Bajpai, A. Li, M. Norman, R. Kaba, M. Sohal, Z. Zuberi, M. M. Gallagher, and on behalf of the IMPACT Study Group, "Effect of esophageal cooling on ablation lesion formation in the left atrium: Insights from Ablation Index data in the IMPACT trial and clinical

outcomes," *Journal of Cardiovascular Electrophysiology*, vol. 33, pp. 2546–2557, Dec. 2022.

[158] P. Sanders, O. Berenfeld, M. Hocini, P. Jaïs, R. Vaidyanathan, L.-F. Hsu, S. Garrigue, Y. Takahashi, M. Rotter, F. Sacher, C. Scavée, R. Ploutz-Snyder, J. Jalife, and M. Haïssaguerre, "Spectral Analysis Identifies Sites of High-Frequency Activity Maintaining Atrial Fibrillation in Humans," *Circulation*, vol. 112, pp. 789–797, Aug. 2005.

[159] M. G. Bongiorni' and F. Menichetti', "Paroxysmal tachycardias - Imaging modalities and their integration into electrophysiology, described – Fourth in series.." Issue: 25 Volume: 13.

[160] "Mapping Technologies for Catheter Ablation of AF - Expert Reviews."

[161] H. Mizuno, G. Maccabelli, and P. D. Bella, "Possibility of contact force monitoring during catheter ablation of ventricular tachycardia," *Interventional Cardiology*, vol. 4, pp. 701–708, Dec. 2012.

[162] G. L. Rosa, J. G. Quintanilla, R. Salgado, J. J. González-Ferrer, V. Cañadas-Godoy, J. Pérez-Villacastín, N. Pérez-Castellano, J. Jalife, and D. Filgueiras-Rama, "Mapping Technologies for Catheter Ablation of Atrial Fibrillation Beyond Pulmonary Vein Isolation," *European Cardiology Review*, vol. 16, p. e21, May 2021.

[163] J. Dong, D. Dalal, D. Scherr, A. Cheema, S. Nazarian, K. Bilchick, I. Almasry, A. Cheng, C. A. Henrikson, D. Spragg, J. E. Marine, R. D. Berger, and H. Calkins, "Impact of heart rhythm status on registration accuracy of the left atrium for catheter ablation of atrial fibrillation," *Journal of Cardiovascular Electrophysiology*, vol. 18, pp. 1269–1276, Dec. 2007.

[164] M. R. Turchioe, S. Mangal, J. S. Ancker, J. Gwyn, P. Varosy, and D. Slotwiner, ""Replace uncertainty with information": Shared decision-making and decision quality surrounding catheter ablation for atrial fibrillation," *European journal of cardiovascular nursing*, vol. 22, pp. 430–440, May 2023.

[165] C. H. Roney, I. Sim, J. Yu, M. Beach, A. Mehta, J. Alonso Solis-Lemus, I. Kotadia, J. Whitaker, C. Corrado, O. Razeghi, E. Vigmond, S. M. Narayan, M. O'Neill, S. E. Williams, and S. A. Niederer, "Predicting Atrial Fibrillation Recurrence by Combining Population Data and Virtual Cohorts of Patient-Specific

Left Atrial Models," *Circulation: Arrhythmia and Electrophysiology*, vol. 15, p. e010253, Feb. 2022. Publisher: American Heart Association.

[166] G. R. Mirams, P. Pathmanathan, R. A. Gray, P. Challenor, and R. H. Clayton, "Uncertainty and variability in computational and mathematical models of cardiac physiology," *The Journal of Physiology*, vol. 594, no. 23, pp. 6833–6847, 2016. _eprint: https://onlinelibrary.wiley.com/doi/pdf/10.1113/JP271671.

[167] J. C. Maxwell, "VIII. A dynamical theory of the electromagnetic field," *Philosophical Transactions of the Royal Society of London*, vol. 155, pp. 459–512, Dec. 1865.

[168] D. M. Pozar, *Microwave engineering.* Hoboken, NJ: Wiley, 4th ed ed., 2012. OCLC: ocn714728044.

[169] K. C. Kao, "Electrical Conduction and Photoconduction," in *Dielectric Phenomena in Solids*, pp. 381–514, Elsevier, 2004.

[170] E. Baer and L. Zhu, "*50th Anniversary Perspective* : Dielectric Phenomena in Polymers and Multilayered Dielectric Films," *Macromolecules*, vol. 50, pp. 2239–2256, Mar. 2017.

[171] N. Nasir and M. Al Ahmad, "Cells Electrical Characterization: Dielectric Properties, Mixture, and Modeling Theories," *Journal of Engineering*, vol. 2020, pp. 1–17, Jan. 2020.

[172] E. Hirota, "On the Infrared Frequency Shift in the Liquid State and its Relation to the Atomic Polarization," *Bulletin of the Chemical Society of Japan*, vol. 26, pp. 397–400, July 1953.

[173] R. Smith, S. Lee, H. Komori, and K. Arai, "Relative permittivity and dielectric relaxation in aqueous alcohol solutions," *Fluid Phase Equilibria*, vol. 144, pp. 315–322, Feb. 1998.

[174] W. J. Ellison, "Permittivity of Pure Water, at Standard Atmospheric Pressure, over the Frequency Range 0–25THz and the Temperature Range 0–100°C," *Journal of Physical and Chemical Reference Data*, vol. 36, pp. 1–18, Mar. 2007.

[175] V. Shilov, A. Delgado, F. González-Caballero, J. Horno, J. López-García, and C. Grosse, "Polarization of the Electrical Double Layer. Time Evolution after Application of an Electric Field," *Journal of Colloid and Interface Science*, vol. 232, pp. 141–148, Dec. 2000.

[176] G. Perrier and A. Bergeret, "Maxwell–Wagner–Sillars relaxations in polystyrene–glass-bead composites," *Journal of Applied Physics*, vol. 77, pp. 2651–2658, Mar. 1995.

[177] G. M. Tsangaris, G. C. Psarras, and G. M. Tsangaris, "Electric modulus and interfacial polarization in composite polymeric systems," *Journal of Materials Science*, vol. 33, pp. 2027–2037, Apr. 1998.

[178] A. Delgado, F. González-Caballero, R. Hunter, L. Koopal, and J. Lyklema, "Measurement and interpretation of electrokinetic phenomena," *Journal of Colloid and Interface Science*, vol. 309, pp. 194–224, May 2007.

[179] C.-Y. Hou, J. Qian, and D. E. Freed, "Low-frequency dielectric response of a periodic array of charged spheres in an electrolyte solution: The simple cubic lattice," *Physical Review E*, vol. 99, p. 032604, Mar. 2019.

[180] H. Schwan and K. Foster, "RF-field interactions with biological systems: Electrical properties and biophysical mechanisms," *Proceedings of the IEEE*, vol. 68, no. 1, pp. 104–113, 1980.

[181] S. Gabriel, R. W. Lau, and C. Gabriel, "The dielectric properties of biological tissues: III. Parametric models for the dielectric spectrum of tissues," *Physics in Medicine and Biology*, vol. 41, pp. 2271–2293, Nov. 1996.

[182] M. Lazebnik, D. Popovic, L. McCartney, C. B. Watkins, M. J. Lindstrom, J. Harter, S. Sewall, T. Ogilvie, A. Magliocco, T. M. Breslin, W. Temple, D. Mew, J. H. Booske, M. Okoniewski, and S. C. Hagness, "A large-scale study of the ultrawideband microwave dielectric properties of normal, benign and malignant breast tissues obtained from cancer surgeries," *Physics in Medicine and Biology*, vol. 52, pp. 6093–6115, Oct. 2007. Publisher: IOP Publishing.

[183] A. P. Gregory, R. N. Clarke, T. E. Hodgetts, and G. T. Symm, "RF and microwave dielectric measurements upon layered materials using coaxial sensors.," Feb. 2008. ISSN: 1754-2979.

[184] R. Gulich, M. Köhler, P. Lunkenheimer, and A. Loidl, "Dielectric spectroscopy on aqueous electrolytic solutions," *Radiation and Environmental Biophysics*, vol. 48, pp. 107–114, Feb. 2009.

[185] K. S. Cole and R. H. Cole, "Dispersion and Absorption in Dielectrics I. Alternating Current Characteristics," *The Journal of Chemical Physics*, vol. 9, pp. 341–351, Apr. 1941.

[186] M. Lazebnik, M. C. Converse, J. H. Booske, and S. C. Hagness, "Ultrawideband temperature-dependent dielectric properties of animal liver tissue in the microwave frequency range," *Physics in Medicine and Biology*, vol. 51, pp. 1941–1955, Apr. 2006.

[187] W. D. Hurt, "Multiterm Debye Dispersion Relations for Permittivity of Muscle," *IEEE Transactions on Biomedical Engineering*, vol. BME-32, pp. 60–64, Jan. 1985.

[188] S. Grimnes, *Bioimpedance and bioelectricity basics*. Boston, MA: Elsevier, 2014.

[189] C. Littwitz, T. Ragheb, and L. A. Geddes, "Cell constant of the tetrapolar conductivity cell," *Medical & Biological Engineering & Computing*, vol. 28, pp. 587–590, Nov. 1990.

[190] H. Ma, Y. Su, and A. Nathan, "Cell constant studies of bipolar and tetrapolar electrode systems for impedance measurement," *Sensors and Actuators, B: Chemical*, vol. 221, pp. 1264–1270, 2015.

[191] C. Gabriel, A. Peyman, and E. H. Grant, "Electrical conductivity of tissue at frequencies below 1 MHz.," *Physics in medicine and biology*, vol. 54, no. 16, pp. 4863–4878, 2009. ISBN: 0031-9155.

[192] W. Kuang and S. O. Nelson, "LOW-FREQUENCY DIELECTRIC PROPERTIES OF BIOLOGICAL TISSUES: A REVIEWWITH SOME NEW INSIGHTS," *Transactions of the ASAE*, vol. 41, no. 1, pp. 173–184, 1998.

[193] A. Ivorra and B. Rubinsky, "In vivo electrical impedance measurements during and after electroporation of rat liver," *Bioelectrochemistry*, vol. 70, pp. 287–295, May 2007.

[194] U. Pliquett, "Bioimpedance: A Review for Food Processing," *Food Engineering Reviews*, vol. 2, pp. 74–94, June 2010.

[195] P. B. Ishai, M. S. Talary, A. Caduff, E. Levy, and Y. Feldman, "Electrode polarization in dielectric measurements: A review," *Measurement Science and Technology*, vol. 24, no. 102001, 2013. ISBN: 0957-0233.

[196] H. P. Schwan, "Electrode polarization impedance and measurements in biological materials," *Annals of the New York Academy of Sciences*, vol. 148, pp. 191–209, Feb. 1968.

[197] J. Lyklema, *Fundamentals of interface and colloid science*. San Diego: Academic Press, 2000.

[198] J. O. Bockris, A. K. N. Reddy, and M. E. Gamboa-Aldeco, *Modern electrochemistry*. New York: Plenum Press, 2nd ed ed., 1998.

[199] C. W. Finkl, *The Encyclopedia of Field and General Geology*. New York, NY: Springer, 2006. OCLC: 1066194049.

[200] P. J. W. P. J. W. Debye, *Polar molecules*. Dover Publications, 1929.

[201] Keysight, "Application Note 5950:3000 - Impedance Measurement Handbook: A Guide to Measurement Technology and Techniques, 6th Edition," 2020.

[202] A. La Gioia, *Accurate dielectric characterisation of biological tissues in the microwave range using the open-ended coaxial probe technique*. Doctoral Dissertation, NUI Galway, Dec. 2019. Accepted: 2020-01-02T10:39:44Z.

[203] P. De Langhe, K. Blomme, L. Martens, and D. De Zutter, "Measurement of low-permittivity materials based on a spectral-domain analysis for the open-ended coaxial probe," *IEEE Transactions on Instrumentation and Measurement*, vol. 42, pp. 879–886, Oct. 1993. Conference Name: IEEE Transactions on Instrumentation and Measurement.

[204] D. Misra, "A Quasi-Static Analysis of Open-Ended Coaxial Lines (Short Paper)," *IEEE Transactions on Microwave Theory and Techniques*, vol. 35, pp. 925–928, Oct. 1987. Conference Name: IEEE Transactions on Microwave Theory and Techniques.

[205] E. C. Burdette, F. L. Cain, and J. Seals, "In Vivo Probe Measurement Technique for Determining Dielectric Properties at VHF through Microwave Frequencies," *IEEE Transactions on Microwave Theory and Techniques*, vol. 28, pp. 414–427,

Apr. 1980. Conference Name: IEEE Transactions on Microwave Theory and Techniques.

[206] A. Kraszewski, M. A. Stuchly, S. S. Stuchly, and A. M. Smith, "In vivo and in vitro dielectric properties of animal tissues at radio frequencies," *Bioelectromagnetics*, vol. 3, no. 4, pp. 421–432, 1982. _eprint: https://onlinelibrary.wiley.com/doi/pdf/10.1002/bem.2250030405.

[207] S. Gabriel, R. W. Lau, and C. Gabriel, "The dielectric properties of biological tissues: II. Measurements in the frequency range 10 Hz to 20 GHz," *Physics in Medicine and Biology*, vol. 41, pp. 2251–2269, Nov. 1996.

[208] A. Gregory and R. Clarke, "A review of RF and microwave techniques for dielectric measurements on polar liquids," *IEEE Transactions on Dielectrics and Electrical Insulation*, vol. 13, pp. 727–743, Aug. 2006. Conference Name: IEEE Transactions on Dielectrics and Electrical Insulation.

[209] K. R. Foster, J. L. Schepps, R. D. Stoy, and H. P. Schwan, "Dielectric properties of brain tissue between 0.01 and 10 GHz," *Physics in Medicine and Biology*, vol. 24, pp. 1177–1187, Nov. 1979.

[210] T. W. Athey, M. A. Stuchly, and S. S. Stuchly, "Measurement of Radio Frequency Permittivity of Biological Tissues with an Open-Ended Coaxial Line: Part I," *IEEE Transactions on Microwave Theory and Techniques*, vol. 30, pp. 82–86, Jan. 1982.

[211] C. Gabriel, E. H. Grant, and I. R. Young, "Use of time domain spectroscopy for measuring dielectric properties with a coaxial probe," *Journal of Physics E: Scientific Instruments*, vol. 19, pp. 843–846, Oct. 1986. Publisher: IOP Publishing.

[212] D. Popovic, L. McCartney, C. Beasley, M. Lazebnik, M. Okoniewski, S. C. Hagness, and J. H. Booske, "Precision open-ended coaxial probes for in vivo and ex vivo dielectric spectroscopy of biological tissues at microwave frequencies," *IEEE Transactions on Microwave Theory and Techniques*, vol. 53, pp. 1713–1722, May 2005. Conference Name: IEEE Transactions on Microwave Theory and Techniques.

[213] C. Gabriel, T. Y. Chan, and E. H. Grant, "Admittance models for open ended coaxial probes and their place in dielectric spectroscopy," *Physics in Medicine and Biology*, vol. 39, pp. 2183–2200, Dec. 1994.

[214] D. Misra, "On the measurement of the complex permittivity of materials by an open-ended coaxial probe," *IEEE Microwave and Guided Wave Letters*, vol. 5, pp. 161–163, May 1995. Conference Name: IEEE Microwave and Guided Wave Letters.

[215] D. Berube, F. Ghannouchi, and P. Savard, "A comparative study of four open-ended coaxial probe models for permittivity measurements of lossy dielectric/biological materials at microwave frequencies," *IEEE Transactions on Microwave Theory and Techniques*, vol. 44, pp. 1928–1934, Oct. 1996.

[216] J. P. Grant, R. N. Clarke, G. T. Symm, and N. M. Spyrou, "A critical study of the open-ended coaxial line sensor technique for RF and microwave complex permittivity measurements," *Journal of Physics E: Scientific Instruments*, vol. 22, p. 757, Sept. 1989.

[217] D. Blackham and R. Pollard, "An improved technique for permittivity measurements using a coaxial probe," *IEEE Transactions on Instrumentation and Measurement*, vol. 46, pp. 1093–1099, Oct. 1997. Conference Name: IEEE Transactions on Instrumentation and Measurement.

[218] T. Sugitani, S.-i. Kubota, S.-i. Kuroki, K. Sogo, K. Arihiro, M. Okada, T. Kadoya, M. Hide, M. Oda, and T. Kikkawa, "Complex permittivities of breast tumor tissues obtained from cancer surgeries," *Applied Physics Letters*, vol. 104, p. 253702, June 2014. Publisher: American Institute of Physics.

[219] A. Martellosio, M. Pasian, M. Bozzi, L. Perregrini, A. Mazzanti, F. Svelto, P. E. Summers, G. Renne, L. Preda, and M. Bellomi, "Dielectric Properties Characterization From 0.5 to 50 GHz of Breast Cancer Tissues," *IEEE Transactions on Microwave Theory and Techniques*, vol. 65, pp. 998–1011, Mar. 2017. Conference Name: IEEE Transactions on Microwave Theory and Techniques.

[220] L. Abdilla, C. Sammut, and L. Z. Mangion, "Dielectric properties of muscle and liver from 500 MHz-40 GHz," *Electromagnetic Biology and Medicine*, vol. 32, pp. 244–252, June 2013.

[221] A. Sabouni, C. Hahn, S. Noghanian, E. Sauter, and T. Weiland, "Study of the Effects of Changing Physiological Conditions on Dielectric Properties of Breast Tissues," *International Scholarly Research Notices*, vol. 2013, p. e894153, July 2013. Publisher: Hindawi.

[222] T. Karacolak, R. Cooper, E. S. Unlu, and E. Topsakal, "Dielectric Properties of Porcine Skin Tissue and In Vivo Testing of Implantable Antennas Using Pigs as Model Animals," *IEEE Antennas and Wireless Propagation Letters*, vol. 11, pp. 1686–1689, 2012. Conference Name: IEEE Antennas and Wireless Propagation Letters.

[223] Keysight, "Technical Overview 5992:0263 - N1500A Materials Measurement Suite," 2023.

[224] M. Grossi and B. Riccò, "Electrical impedance spectroscopy (EIS) for biological analysis and food characterization: a review," *Journal of Sensors and Sensor Systems*, vol. 6, pp. 303–325, Aug. 2017.

[225] S. Laufer, A. Ivorra, V. E. Reuter, B. Rubinsky, and S. B. Solomon, "Electrical impedance characterization of normal and cancerous human hepatic tissue," *Physiological Measurement*, vol. 31, no. 7, pp. 995–1009, 2010.

[226] O. Casas, R. Bragós, P. J. Riu, J. Rosell, M. Tresànchez, M. Warren, A. Rodriguez-Sinovas, A. Carreño, and J. Cinca, "In vivo and in situ ischemic tissue characterization using electrical impedance spectroscopy," in *Annals of the New York Academy of Sciences*, vol. 873, pp. 51–58, 1999. ISSN: 00778923.

[227] L. D. Suits, T. C. Sheahan, J. H. Kim, H.-K. Yoon, S.-H. Cho, Y. S. Kim, and J.-S. Lee, "Four Electrode Resistivity Probe for Porosity Evaluation," *Geotechnical Testing Journal*, vol. 34, no. 6, p. 102866, 2011.

[228] M. Ibrahim, J. Claudel, D. Kourtiche, and M. Nadi, "Geometric parameters optimization of planar interdigitated electrodes for bioimpedance spectroscopy," *Journal of Electrical Bioimpedance*, vol. 4, pp. 13–22, Mar. 2013.

[229] R. Shima, Z. Jiang, S. Y. Fen, A.-A. Monnavar, and K. Ali, "Development and Evaluation of a Novel Four-Electrode Device System for Monitoring Skin Impedance," *African Journal of Traditional, Complementary, and Alternative Medicines*, vol. 9, pp. 599–606, July 2012.

[230] B. J. Lanterman, A. A. Riet, N. S. Gates, J. D. Flygare, A. D. Cutler, J. E. Vogel, D. R. Wheeler, and B. A. Mazzeo, "Micro-Four-Line Probe to Measure Electronic Conductivity and Contact Resistance of Thin-Film Battery Electrodes," *Journal of The Electrochemical Society*, vol. 162, p. A2145, Aug. 2015. Publisher: IOP Publishing.

[231] H. P. Schwan, "Electrical Properties of Tissue and Cell Suspensions* *This work was supported in part by grants from the United States Public Health Service, H-1253(c2-4) and in part by the Office of Naval Research, 119–289.," in *Advances in Biological and Medical Physics* (J. H. Lawrence and C. A. Tobias, eds.), vol. 5, pp. 147–209, Elsevier, 1957.

[232] M. A. Fallert, M. S. Mirotznik, S. W. Downing, E. B. Savage, K. R. Foster, M. E. Josephson, and D. K. Bogen, "Myocardial electrical impedance mapping of ischemic sheep hearts and healing aneurysms," *Circulation*, vol. 87, no. 1, pp. 199–207, 1993.

[233] M. I. Ellenby, K. W. Small, R. M. Wells, D. J. Hoyt, and J. E. Lowe, "On-line Detection of Reversible Myocardial Ischemic Injury by Measurement of Myocardial Electrical Impedance," *The Annals of Thoracic Surgery*, vol. 44, pp. 587–597, Dec. 1987.

[234] Cinca Juan, Warren Mark, Carreño Ana, Tresànchez Màrius, Armadans Lluís, Gómez Pilar, and Soler-Soler J., "Changes in Myocardial Electrical Impedance Induced by Coronary Artery Occlusion in Pigs With and Without Preconditioning," *Circulation*, vol. 96, pp. 3079–3086, Nov. 1997. Publisher: American Heart Association.

[235] J. Z. Tsai, J. A. Will, S. H. V. Stelle, H. Cao, S. Tungjitkusolmun, Y. B. Choy, D. Haemmerich, V. R. Vorperian, and J. G. Webster, "In-vivo measurement of swine myocardial resistivity," *IEEE Transactions on Biomedical Engineering*, vol. 49, no. 5, pp. 472–483, 2002.

[236] C. Gabriel, S. Gabriel, and E. Corthout, "The dielectric properties of biological tissues: I. Literature survey," *Physics in Medicine and Biology*, vol. 41, pp. 2231–2249, Nov. 1996.

[237] J.-L. Schwartz and G. A. R. Mealing, "Dielectric properties of frog tissues in vivo and in vitro," *Physics in Medicine and Biology*, vol. 30, pp. 117–124, Feb. 1985. Publisher: IOP Publishing.

[238] D. Xu, L. Liu, and Z. Jiang, "Measurement of the Dielectric Properties of Biological Substances Using an Improved Open-Ended Coaxial Line Resonator Method," *IEEE Transactions on Microwave Theory and Techniques*, vol. 35, pp. 1424–1428, Dec. 1987. Conference Name: IEEE Transactions on Microwave Theory and Techniques.

[239] A. Fornes-Leal, N. Cardona, M. Frasson, S. Castelló-Palacios, A. Nevárez, V. P. Beltrán, and C. Garcia-Pardo, "Dielectric Characterization of In Vivo Abdominal and Thoracic Tissues in the 0.5–26.5 GHz Frequency Band for Wireless Body Area Networks," *IEEE Access*, vol. 7, pp. 31854–31864, 2019.

[240] S. Salahuddin, A. La Gioia, A. Shahzad, M. Elahi, A. Kumar, D. Kilroy, E. Porter, and M. O'Halloran, "Demonstration of dielectric heterogeneity of previously assumed homogeneous tissues: examination of the Heart," in *12th European Conference on Antennas and Propagation (EuCAP 2018)*, (London, UK), pp. 407 (5 pp.)–407 (5 pp.), Institution of Engineering and Technology, 2018.

[241] E. Porter, S. Salahuddin, A. L. Gioia, M. A. Elahi, A. Shahzad, A. Kumar, D. Kilroy, and M. O'Halloran, "Characterization of the Dielectric Properties of the Bladder Over the Microwave Range," *IEEE Journal of Electromagnetics, RF and Microwaves in Medicine and Biology*, vol. 2, pp. 208–215, Sept. 2018. Conference Name: IEEE Journal of Electromagnetics, RF and Microwaves in Medicine and Biology.

[242] J. M. Alison and R. J. Sheppard, "Dielectric properties of human blood at microwave frequencies," *Physics in Medicine and Biology*, vol. 38, pp. 971–978, July 1993.

[243] M. Wolf, R. Gulich, P. Lunkenheimer, and A. Loidl, "Broadband dielectric spectroscopy on human blood," *Biochimica et Biophysica Acta (BBA) - General Subjects*, vol. 1810, pp. 727–740, Aug. 2011.

[244] A. Santorelli, B. Abbasi, M. Lyons, A. Hayat, S. Gupta, M. O'Halloran, and A. Gupta, "Investigation of Anemia and the Dielectric Properties of Human Blood at Microwave Frequencies," *IEEE Access*, vol. 6, pp. 56885–56892, 2018.

[245] S. Salahuddin, L. Farrugia, C. V. Sammut, M. O'Halloran, and E. Porter, "Dielectric properties of fresh human blood," in *2017 International Conference on Electromagnetics in Advanced Applications (ICEAA)*, (Verona, Italy), pp. 356–359, IEEE, Sept. 2017.

[246] H. Fricke and S. Morse, "THE ELECTRIC RESISTANCE AND CAPACITY OF BLOOD FOR FREQUENCIES BETWEEN 800 AND $4\frac{1}{2}$ MILLION CYCLES," *Journal of General Physiology*, vol. 9, pp. 153–167, Nov. 1925.

[247] H. Fricke, "THE ELECTRIC CAPACITY OF SUSPENSIONS WITH SPECIAL REFERENCE TO BLOOD," *Journal of General Physiology*, vol. 9, pp. 137–152, Nov. 1925.

[248] F. G. Hirsch, E. C. Texter, L. A. Wood, W. C. Ballard, F. E. Horan, and I. S. Wright, "THE ELECTRICAL CONDUCTIVITY OF BLOOD: I. Relationship to Erythrocyte Concentration," *Blood*, vol. 5, pp. 1017–1035, Nov. 1950.

[249] E. C. Texter, F. G. Hirsch, F. E. Horan, L. A. Wood, W. C. Ballard, and I. S. Wright, "THE ELECTRICAL CONDUCTIVITY OF BLOOD: II. Relation to Red Cell Count," *Blood*, vol. 5, pp. 1036–1048, Nov. 1950.

[250] L. A. Geddes and C. P. D. Costa, "The Specific Resistance of Canine Blood at Body Temperature," *IEEE Transactions on Biomedical Engineering*, vol. BME-20, pp. 51–53, Jan. 1973. Conference Name: IEEE Transactions on Biomedical Engineering.

[251] S. N. Mohapatra and D. W. Hill, "The changes in blood resistivity with haematocrit and temperature," *European journal of intensive care medicine*, vol. 1, pp. 153–162, Dec. 1975.

[252] H. Beving, L. E. G. Eriksson, C. L. Davey, and D. B. Kell, "Dielectric properties of human blood and erythrocytes at radio frequencies (0.2–10 MHz); dependence on cell volume fraction and medium composition," *European Biophysics Journal*, vol. 23, pp. 207–215, May 1994.

[253] T. Chelidze, "Dielectric spectroscopy of blood," *Journal of Non-Crystalline Solids*, vol. 305, pp. 285–294, July 2002.

[254] F. Jaspard, M. Nadi, and A. Rouane, "Dielectric properties of blood: an investigation of haematocrit dependence," *Physiological Measurement*, vol. 24, pp. 137–147, Feb. 2003.

[255] Z. Y. Chang, G. A. Pop, and G. C. Meijer, "A comparison of two- and four-electrode techniques to characterize blood impedance for the frequency range of 100 Hz to 100 MHz," *IEEE Transactions on Biomedical Engineering*, vol. 55, no. 3, pp. 1247–1249, 2008.

[256] L. Constantinou, I. F. Triantis, M. Hickey, and P. A. Kyriacou, "On the Merits of Tetrapolar Impedance Spectroscopy for Monitoring Lithium Concentration Variations in Human Blood Plasma," *IEEE Transactions on Biomedical Engineering*, vol. 64, no. 3, pp. 601–609, 2017.

[257] N. Ištuk, E. Porter, D. O'Loughlin, B. McDermott, A. Santorelli, S. Abedi, N. Joachimowicz, H. Roussel, and M. O'Halloran, "Dielectric Properties of Ovine Heart at Microwave Frequencies," *Diagnostics*, vol. 11, p. 531, Mar. 2021.

[258] Keysight, "Technical Overview 5909:0222 - Keysight 85070E Dielectric Probe Kit 200 MHz to 50 GHz," Dec. 2017.

[259] V. Teppati, A. Ferrero, and M. Sayed, eds., *Modern RF and Microwave Measurement Techniques*. Cambridge University Press, 1 ed., June 2013.

[260] S. Salahuddin, E. Porter, P. M. Meaney, and M. O'Halloran, "Effect of logarithmic and linear frequency scales on parametric modelling of tissue dielectric data," *Biomedical Physics & Engineering Express*, vol. 3, p. 015020, Feb. 2017.

[261] C. L. Brace, "Microwave Tissue Ablation: Biophysics, Technology, and Applications," *Critical Reviews™ in Biomedical Engineering*, vol. 38, no. 1, pp. 65–78, 2010.

[262] D. Keane, "New catheter ablation techniques for the treatment of cardiac arrhythmias," *Cardiac Electrophysiology Review*, vol. 6, no. 4, pp. 341–348, 2002.

[263] L. Farrugia, P. S. Wismayer, L. Z. Mangion, and C. V. Sammut, "Accurate in vivo dielectric properties of liver from 500 MHz to 40 GHz and their correlation to ex vivo measurements," *Electromagnetic Biology and Medicine*, vol. 35, pp. 365–373, Oct. 2016. Publisher: Taylor & Francis _eprint: https://doi.org/10.3109/15368378.2015.1120221.

[264] E. Porter, A. L. Gioia, A. Santorelli, and M. O'Halloran, "Modeling of the dielectric properties of biological tissues within the histology region," *IEEE Transactions on Dielectrics and Electrical Insulation*, vol. 24, pp. 3290–3301, Oct. 2017.

[265] J. Wilde, L. Reindl, and C. Stewart, "Testing, Calibration and Compensation," in *Comprehensive Microsystems*, pp. 495–538, Elsevier, 2008.

[266] E. Porter, A. La Gioia, S. Salahuddin, S. Decker, A. Shahzad, M. A. Elahi, M. O'Halloran, and O. Beyan, "Minimum information for dielectric measurements of biological tissues (MINDER): A framework for repeatable and reusable data," *International Journal of RF and Microwave Computer-Aided Engineering*, vol. 28, p. e21201, Mar. 2018.

[267] S. Salahuddin, M. O'Halloran, E. Porter, L. Farrugia, J. Bonello, C. V. Sammut, and P. S. Wismayer, "Effects of standard coagulant agents on the dielectric properties of fresh human blood," *IEEE Transactions on Dielectrics and Electrical Insulation*, vol. 24, pp. 3283–3289, Oct. 2017.

[268] A. Peyman, C. Gabriel, and E. Grant, "Complex permittivity of sodium chloride solutions at microwave frequencies," *Bioelectromagnetics*, vol. 28, pp. 264–274, May 2007.

[269] W. C. Vieira de Castro, "The 3Rs and Good Scientific Practice," in *Animal Ethics in Animal Research* (H. Röcklinsberg, I. A. S. Olsson, and M. Gjerris, eds.), pp. 15–40, Cambridge: Cambridge University Press, 2017.

[270] E. Commission, "H2020 Programme: Guidelines on FAIR Data Management in Horizon 2020 Version 3.0.," 2016. Medium: 12pp Publisher: European Commission, Directorate-General for Research & Innovation.

[271] N. Istuk, B. McDermott, E. Porter, A. Santorelli, S. Abedi, M. O'Halloran, N. Joachimowicz, and H. Roussel, "Dielectric Measurements of Ovine Heart," Apr. 2020.

[272] S. Salahuddin, E. Porter, F. Krewer, and M. O' Halloran, "Optimised analytical models of the dielectric properties of biological tissue," *Medical Engineering & Physics*, vol. 43, pp. 103–111, May 2017.

[273] C. Gabriel, "Compilation of the Dielectric Properties of Body Tissues at RF and Microwave Frequencies.," *Occupational and environmental health directorate, Radiofrequency Radiation Division, Brooks Air Force Base, Texas (USA)*, 1996.

[274] S. Cruciani, V. D. Santis, M. Feliziani, and F. Maradei, "Cole-Cole vs Debye models for the assessment of electromagnetic fields inside biological tissues produced by wideband EMF sources," in *2012 Asia-Pacific Symposium on Electromagnetic Compatibility*, pp. 685–688, May 2012. ISSN: 2162-7673.

[275] R. G. Brereton, "ANOVA tables and statistical significance of models," *Journal of Chemometrics*, vol. 33, no. 3, p. e3019, 2019. _eprint: https://onlinelibrary.wiley.com/doi/pdf/10.1002/cem.3019.

[276] IFAC, "Dielectric Properties of Body Tissues: Home page," 2000.

[277] I. Foundation, "Tissue Properties Database V4.0," 2018. Medium: .h5, .xml, .txt.

[278] G. Maenhout, *Dielectric Detection and Ablation Techniques for Endoscopic Cancer Theranostics*. PhD thesis, KU Leuven, 2022.

[279] C. Rossmann and D. Haemmerich, "Review of temperature dependence of thermal properties, dielectric properties, and perfusion of biological tissues at hyperthermic and ablation temperatures," *Critical reviews in biomedical engineering*, vol. 42, no. 6, pp. 467–492, 2014.

[280] C. L. Brace, "Temperature-dependent dielectric properties of liver tissue measured during thermal ablation: toward an improved numerical model," *Annual International Conference of the IEEE Engineering in Medicine and Biology Society. IEEE Engineering in Medicine and Biology Society. Annual International Conference*, vol. 2008, pp. 230–233, 2008.

[281] V. Lopresto, R. Pinto, G. A. Lovisolo, and M. Cavagnaro, "Changes in the dielectric properties of ex vivo bovine liver during microwave thermal ablation at 2.45 GHz.," *Physics in Medicine and Biology*, vol. 57, pp. 2309–2327, Mar. 2012.

[282] A. Shahzad, S. Khan, M. Jones, R. M. Dwyer, and M. O'Halloran, "Investigation of the effect of dehydration on tissue dielectric properties in ex vivo measurements," *Biomedical Physics & Engineering Express*, vol. 3, p. 045001, June 2017. Publisher: IOP Publishing.

[283] N. Istuk, A. L. Gioia, H. Benchakroun, A. Lowery, B. McDermott, and M. O'Halloran, "Relationship Between the Conductivity of Human Blood and Blood Counts," *IEEE Journal of Electromagnetics, RF and Microwaves in Medicine and Biology*, vol. 6, pp. 184–190, June 2022.

[284] A. Zhbanov and S. Yang, "Effects of Aggregation on Blood Sedimentation and Conductivity," *PloS One*, vol. 10, no. 6, p. e0129337, 2015.

[285] JCGM, "Evaluation of measurement data — Guide to the expression of uncertainty in measurement," Sept. 2008. JCGM 100:2008 GUM 1995 with minor corrections.

[286] NIST, "Guidelines for Evaluating and Expressing the Uncertainty of NIST Measurement Results," 1994.

[287] curtis.suplee@nist.gov, "NIST Technical Note 1297," July 2009. Last Modified: 2019-11-25T09:41-05:00.

[288] C. Gabriel and A. Peyman, "Dielectric measurement: error analysis and assessment of uncertainty," *Physics in Medicine and Biology*, vol. 51, pp. 6033–6046, Dec. 2006.

[289] R. L. Rosenthal and C. W. Tobias, "Measurement of the electric resistance of human blood; use in coagulation studies and cell volume determinations," *The Journal of Laboratory and Clinical Medicine*, vol. 33, pp. 1110–1122, Sept. 1948.

[290] S. Abdalla, S. S. Al-ameer, and S. H. Al-Magaishi, "Electrical properties with relaxation through human blood," *Biomicrofluidics*, vol. 4, July 2010.

[291] Student, "The probable error of a mean," *Biometrika*, vol. 6, pp. 1–25, 1908.

[292] N. Ištuk, H. Benchakroun, A. Elahi, M. O'Halloran, R. Matta, D. Moreau, R. O'Connor, and E. Dunne, "Reducing Sensing Volume Confounding Effects in Conductivity Measurements: The Use of a Miniaturised Four-Electrode Probe," in *24th International Conference on Applied Electromagnetics and Communications*, (Dubrovnik, Croatia), p. 4, IEEE, Sept. 2023.

[293] N. Ištuk, R. Matta, H. Benchakroun, J. M. Baena-Montes, L. Quinlan, D. Moreau, R. O'Connor, E. Dunne, A. M. Elahi, and M. O'Halloran, "Miniaturised Four-Electrode Conductivity Probe with PEDOT:PSS Coating," in *URSI GASS 2023*, (Sapporo, Japan), URSI GASS 2023, Aug. 2023.

[294] Y. Wang, P. Schimpf, D. Haynor, and Y. Kim, "Geometric effects on resistivity measurements with four-electrode probes in isotropic and anisotropic tissues," *IEEE Transactions on Biomedical Engineering*, vol. 45, pp. 877–884, July 1998. Conference Name: IEEE Transactions on Biomedical Engineering.

[295] N. Istuk, C. DeCaro, H. Benchakroun, E. Dunne, A. Elahi, and M. O'Halloran, "Eliminating the Geometric Error in Tissue Conductivity Measurements by Increasing the Sample Size," in *BioEM2022*, (Nagoya, Japan), p. 3, June 2022.

[296] A. L. Gioia, E. Porter, S. Salahuddin, and M. O'Halloran, "Impact of Radial Heterogeneities of Biological Tissues on Dielectric Measurements," in *2017 International Conference on Electromagnetics in Advanced Applications (ICEAA)*, pp. 421–424, Sept. 2017.

[297] G. Dijk, A. L. Rutz, and G. G. Malliaras, "Stability of PEDOT:PSS-Coated Gold Electrodes in Cell Culture Conditions," *Advanced Materials Technologies*, vol. 5, p. 1900662, Mar. 2020.

[298] G. Dijk, H. J. Ruigrok, and R. P. O'Connor, "Influence of PEDOT:PSS Coating Thickness on the Performance of Stimulation Electrodes," *Advanced Materials Interfaces*, vol. 7, no. 16, p. 2000675, 2020. _eprint: https://onlinelibrary.wiley.com/doi/pdf/10.1002/admi.202000675.

[299] H. Benchakroun, N. Ištuk, E. Dunne, A. Elahi, T. O'Halloran, M. O'Halloran, and D. O'Loughlin, "Design of a Tetrapolar Probe for Electrical Characterization of the Left Atrial Appendage From 0.1 Hz to 100 kHz," *IEEE Sensors Journal*, vol. 23, pp. 741–749, Jan. 2023. Conference Name: IEEE Sensors Journal.

[300] Changsup Ryu, Kee-Won Kwon, A. Loke, V. Dubin, R. Kavari, G. Ray, and S. Wong, "Electromigration of submicron Damascene copper interconnects," in *1998 Symposium on VLSI Technology Digest of Technical Papers (Cat. No.98CH36216)*, (Honolulu, HI, USA), pp. 156–157, IEEE, 1998.

[301] S. Kilgore, *Electromigration in Gold Interconnects*. PhD thesis, Arizona State University, Nov. 2013.

[302] S. Zhang, P. Kumar, A. S. Nouas, L. Fontaine, H. Tang, and F. Cicoira, "Solvent-induced changes in PEDOT:PSS films for organic electrochemical transistors," *APL Materials*, vol. 3, p. 014911, Jan. 2015.

[303] M. Sessolo, D. Khodagholy, J. Rivnay, F. Maddalena, M. Gleyzes, E. Steidl, B. Buisson, and G. G. Malliaras, "Easy-to-Fabricate Conducting Polymer Microelectrode Arrays," *Advanced Materials*, vol. 25, pp. 2135–2139, Apr. 2013.